RUNOFF GENERATION AND WATER EROSION IN THE UPLANDS OF THE LOWER FRASER VALLEY

By

Sandra J. Brown

B. Sc. (Physical Geography) University of British Columbia

A THESIS SUBMITTED IN PARTIAL FULFILLMENT OF

THE REQUIREMENTS FOR THE DEGREE OF

MASTER OF SCIENCE

in

THE FACULTY OF GRADUATE STUDIES

SOIL SCIENCE

We accept this thesis as conforming

to the required standard

THE UNIVERSITY OF BRITISH COLUMBIA

April 1990

© Sandra J. Brown, 1990

In presenting this thesis in partial fulfilment of the requirements for an advanced degree at the University of British Columbia, I agree that the Library shall make it freely available for reference and study. I further agree that permission for extensive copying of this thesis for scholarly purposes may be granted by the head of my department or by his or her representatives. It is understood that copying or publication of this thesis for financial gain shall not be allowed without my written permission.

Department of SOIL SCIENCE

The University of British Columbia
Vancouver, Canada

Date April 26, 1990

ABSTRACT

An understanding of runoff generation is a requirement for efficient erosion control and land management practices. This research is designed to investigate the processes by which runoff occurs on a Whatcom soil at an upland site in the Lower Fraser Valley. The objectives of this study are to summarize water erosion measurements, to determine soil hydraulic properties, to predict infiltration for typical rainstorms and to determine the mechanism of runoff generation.

Rill, interrill and rainsplash measurements, and previous erosion measurements made at the study site are used to qualitatively assess the magnitude of water erosion. Soil loss is dominated by rill erosion and erosion rates are greatest from November to January. Runoff coefficients are relatively low ($<26\%$), but erosion rates are anticipated to be in excess of 35–45 t ha^{-1}yr^{-1}.

Soil hydraulic properties are measured using a low tension absorption technique described by Clothier and White (1981). The sorptivity tube device provides a simple method for obtaining S, λ^* and K_{-2}. Measured values of i and x^* depend on $t^{1/2}$ as expected from the constant-concentration absorption theory. Soil hydraulic variables and constant-concentration absorption theory are used to determine the soil-water diffusivity characteristics. Measured $D(\theta)$ functions for the field varied widely in a and b, especially for the lower horizons. The Van Genuchten (1980) $\theta(h)$ expression provides a good fit to the water retention data. $D(\theta)$ functions predicted from the soil-water retention curves and the conductivity at satiation are at least 1–2 orders of magnitude greater than the measured functions. Hysteresis effects may account for a 1 order of magnitude increase in $D(\theta)$, but the predictions are poor without matching at $D(\theta_s)$.

ii

The measured hydraulic properties are used to predict infiltration, runoff and drainage. Constant-flux infiltration theory is used to model soil moisture profiles for various rainfall events. High field moisture contents necessitate the inclusion of gravity effects during infiltration. Rainfall, runoff and soil loss measurements at the Mahal farm indicate that rainfall intensities <10 mm h^{-1} cause considerable runoff and erosion. For rainfall intensities known to cause runoff and erosion, runoff is not predicted for most A$_p$ horizon cores. Infiltration may be restricted at some sites by the lower horizon but runoff is not predicted at many sites. To evaluated soil moisture conditions between rainfall events, drainage is estimated from a unit gradient model. A rapid decrease in θ between rainfall events predicted by the unit gradient model, but θ measured at the Mahal farm suggests limited drainage between rainfall events. Rainfall, runoff and soil loss measurements suggest that factors other than those measured are contributing to the runoff observed in the field. Compaction, surface sealing and subsurface seepage may be factors influencing runoff and moisture conditions in the field. The high moisture contents observed in the field suggest the water table is perching on a layer of lower conductivity which in consistent with Dunne runoff. However, the measured infiltrabilities suggest Hortonian runoff and the resultes of the thesis are not conclusive with respect to the mechanism of runoff generation.

Table of Contents

iv

List of Tables

List of Figures

Acknowledgement

INTRODUCTION

Soil erosion in Canada is recognized as an important agricultural issue. In British Columbia, water erosion is a major soil degradation problem. Water erosion is particularly severe in the uplands of the Lower Fraser Valley due to many row crops being grown in this region (Sparrow, 1984). In the late 1970's and early 1980's, high market prices for fruits and vegetables induced the cropping of land traditionally in pasture. Land was converted to perennial row crops such as strawberries and raspberries, and annual cole crops such as cauliflower. After the crops are harvested, the soil is often left unprotected through the heavy rains of fall and winter. As a result, there are higher than tolerable soil losses by surface water erosion (Wood, 1983; 1984). The predominance of erodible soils, steep complex topography, and the lack of adequate crop cover (due to poor farm management) are considered the major factors that have led to this soil degradation.

An understanding of runoff generation is a requirement for efficient erosion control and land management practices. Runoff occurs when the soil becomes saturated at the surface or when the rainfall rate exceeds the infiltrability of the soil. This thesis mainly investigates the rainfall infiltration process for a Whatcom soil on an upland site in the Lower Fraser Valley. There are three specific objectives to this work:

1. To summarize rill and interrill erosion measurements.

2. To determine the soil hydraulic properties of the surface and lower horizons.

3. To use these properties to predict infiltration rates for typical rain storms and

1

determine the mechanism of runoff generation.

Chapter 1 describes water erosion on a typical Whatcom soil in the uplands of the lower Fraser Valley. Introductory rill, interrill and rainsplash measurements are presented along with previous erosion measurements made at the study site. The magnitude of water erosion is qualitatively assessed from these data. Chapter 2 describes the theory and methods used to measure the basic soil properties of the surface and lower horizons. Soil hydraulic diffusivity functions, water retention functions and saturated hydraulic conductivities are presented. Chapter 3 uses the soil hydraulic properties determined in Chapter 2 to model soil moisture profiles for various rainfall events. Rainfall intensities, durations and return periods required to generate runoff are compared to typical storms measured at the study site. Drainage rates are estimated from a unit gradient model to evaluate soil moisture conditions between rainfall events.

Chapter 1

SURFACE WATER EROSION AT THE MAHAL FARM

1.1 INTRODUCTION

Water erosion for a typical soil in the uplands of the Lower Fraser Valley was qualitatively assessed at the Mahal farm, located in the Matsqui region (Fig. 1.1). The study area was under pasture for 22 years prior to cultivation in 1981. Erosion problems developed during the first year of cultivation, when strawberries were planted up-and-down the slope. Sediment eroded from the site was washed into a tributary of the Fraser River. Sedimentation of salmon spawning habitat below the farm prompted a fisheries concern and the British Columbia Ministry of Agriculture and Food began a series of erosion plot studies on the farm.

The soil is the Whatcom series (Luttmerding, 1980) disturbed by clearing and cultivation. Typically 15–30 cm SiL aeolian material, with a weak fine granular structure, and less than 5% organic matter, overlies variably permeable, weakly stratified SiCL glaciomarine material (Wood, 1983). The soil classification is Luvisolic Humo-Ferric Podzol (Luttmerding, 1981). Rainfall accumulation from October to April is approximately 1200 mm (Wood, 1983). The average duration storm is 4.5 h, with a 12 day return period and a 2.0 mm h^{-1} intensity (AES, 1987).

The study site is approximately 3.2 ha in area. In the spring of 1985, the study site was cultivated across the slope and cauliflower was planted with an approximately 1 m spacing between row centres. Tillage was not along the contour and slight gradients
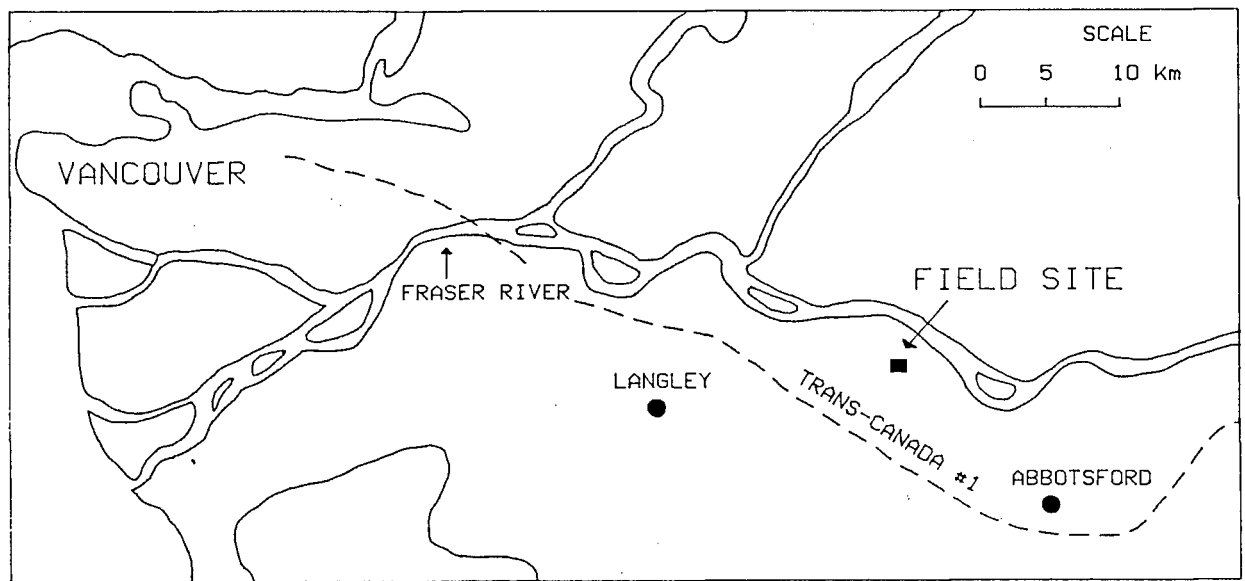
Figure 1.1: Location of the Mahal farm site, Matsqui, British Columbia.

existed along rows and interrows. Non-harvested cauliflower plants were left in the field to rot over winter. Water erosion occurs over much of the study area in winter (Fig. 1.2). Introductory measurements of rill, interrill and splash erosion are compared to previous erosion measurements made at the study site. The magnitude of water erosion at the Mahal farm is assessed qualitatively using this data.

1.2 METHODS

Soil erosion was monitored at the Mahal farm from January to May, 1986. The methods used in the erosion measurements are outlined for rill, interrill and rainsplash erosion.

Rill erosion was measured using a portable photographically-recording rill meter (Fig. 1.3) (McCool et al., 1981). On January 11, 1986, 1 m lengths of 1.6 cm diameter rebar were driven approximately 0.9 m into the soil to mark the locations of rill cross sections. Pairs of rebar were placed 2.3 m apart at 6 randomly spaced locations along the 2 most dominant rills (Fig. 1.4). The rills were identified as left and right and

Figure 1.2: Rill erosion at the Mahal farm, April, 1985.

Figure 1.3:   The portable photographically recording rill meter.

cross section sites were labelled 1–6 indicating the location along each rill. The rill meter was placed across the rill, between each rebar pair and levelled by adjusting the legs and tripod. A series of equally spaced pins were lowered to conform with the topography. A photograph was taken from the tripod of the pins against a graph paper background. Projection of the resulting slides allowed the determination of the cross section areas using a planimeter (McCool et al., 1981). The rill meter is capable of measuring depths up to 0.5 m. For cross sections deeper than 0.5 m the depth below the rill meter pins was estimated using a metric tape.

Before rill measurements were taken, 2 cross section locations on the right rill were relocated. Site 1 was moved upslope due to lateral expansion of the rill beyond the width of the rill meter, and site 4 was shifted laterally due to undercutting of the rill bank. Rill meter measurements were taken over the winter on January 18, February 13, and April 18, 1986. The approximate distances between cross sections were measured from aerial

NORTH

P4

P5

P6

P3

■
SPLASH PAN

P7

P2

R6

L6
L5
L4

R5
R4
R3
R2
R1

P8

L3
L2
L1

P1

L = LEFT RILL	
R = RIGHT RILL	
P = EROSION PIN	
■ = SPLASH PAN	
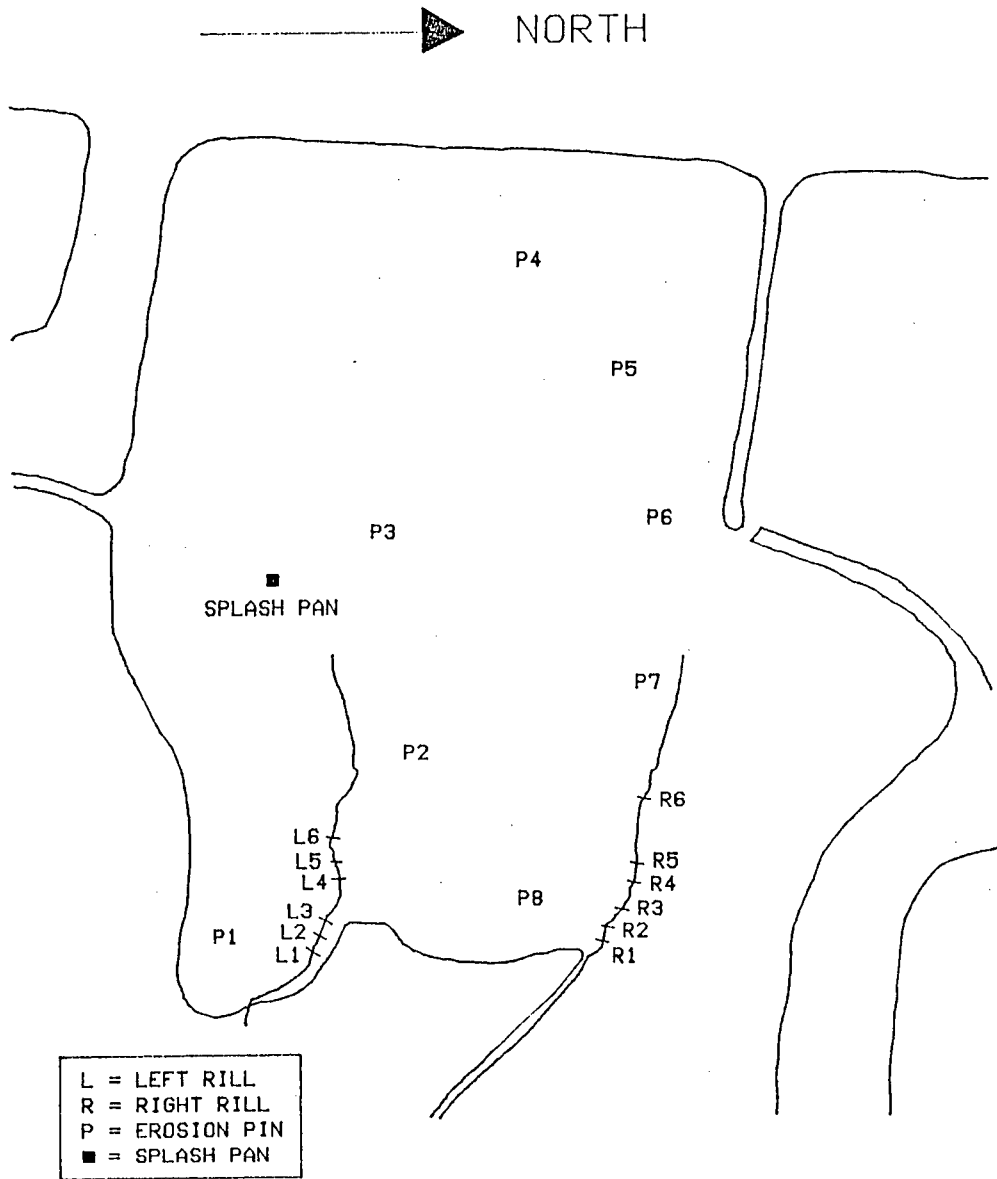
Figure 1.4: Rill, interrill and rainsplash sampling schemes.

photographs taken on April 7, 1986. The volume of the rill between 2 sites was estimated by multiplying the average cross section area of the 2 sites by the distance between the sites.

Erosion pins were utilized to measure net interrill erosion. On January 25, 1986, pairs of steel rods, placed approximately 15 cm apart, were pushed into the soil to mark the locations of the interrill erosion sites. Eight interrill erosion sites were randomly scattered over the study area (Fig. 1.4). The rods were placed parallel to the rows and along both rows and interrows. To avoid frost heave, 1 mm diameter, 0.7 m lengths of rod were pushed approximately 0.6 m into the soil. The rods were notched near the top and a flexible wire was strung tightly between the notches (Fig. 1.5). Measurements were taken below 2 marks on the wire on February 1, March 9 and May 4, 1986. The distance to the soil surface was measured to the nearest mm using a metric tape.

Figure 1.5: Erosion pins.

Rainsplash erosion was qualitatively assessed with a splash pan apparatus (Fig. 1.6). The apparatus consisted of an aluminum box 40 by 40 by 25 cm in size, with one open side. Four removable trays, 1600 cm^2 in area, were stacked 10 cm above each other. The splash pan apparatus was placed facing upslope parallel to the rows with the open side between 2 rows. The splash pan apparatus was tied to the ground with stakes to avoid being blown over by the wind and was left in the field from February 13 to May 7, 1986. The trays were dried and weighed, then cleaned, dried and re-weighed; the difference being the weight of the soil retained. Time constraints prevented the construction of more splash pans, so the results are a very preliminary and exploratory assessment.

Figure 1.6: Splash pan apparatus.

1.3 EROSION MEASUREMENTS

Projections of rill cross sections determined with the photographically-recording rill meter provide rill size and shape. Projections of cross sections down a rill on a given date

display the irregularity of rill shape. Fig. 1.7 shows channel splitting due to a more resistant section, in this instance a decaying cauliflower plant. Projections of a cross section versus time display channel enlargement. Fig. 1.8 shows cross section 1 of the left rill in January, February and April of 1986.
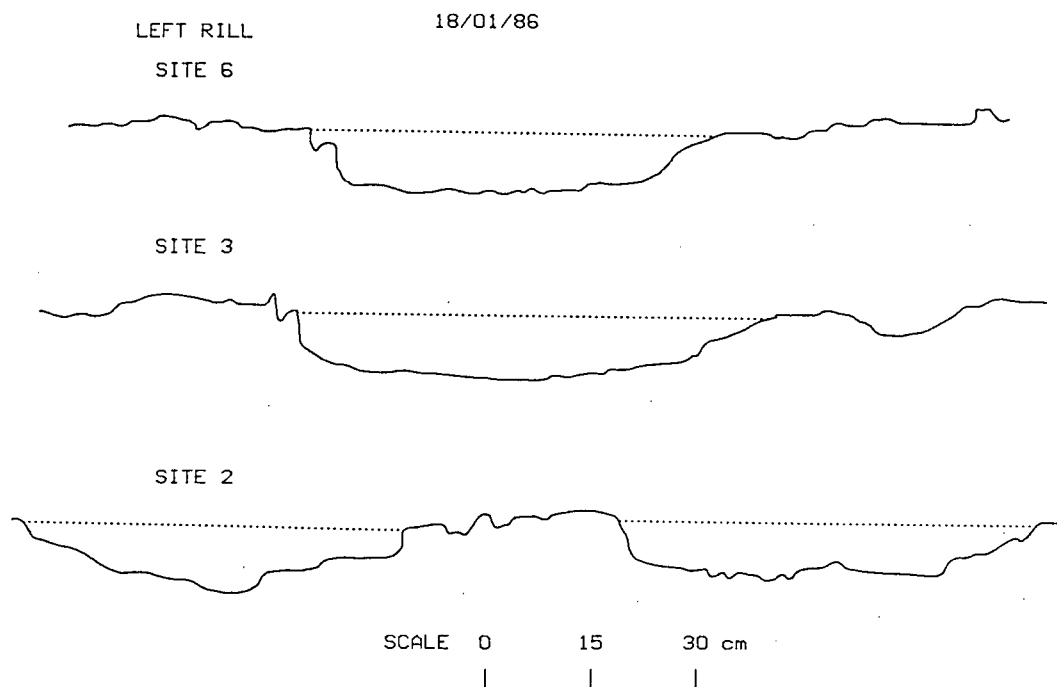
Figure 1.7: Irregularity of cross sections down a rill in January, 1986.

Rill cross section areas and volumes are given in Tables 1.1 and 1.2 respectively. The rill cross section areas and volumes measured in January and February, relative to those measured in April, 1986, indicate that the majority of rill erosion occurs prior to January. The volume of the right rill is substantially greater than the left rill. The total volumes of soil removed in the formation of the measured portions of the left and right rills were approximately 1 m^3 and 4 m^3 respectively. Rills with cross section areas as large as the right rill were not noted in previous work conducted at the Mahal farm (Crudge, 1987). The accelerated erosion (Fig. 1.9) is assumed due to a blocked culvert above the study area which diverted the flow in a field ditch into the right rill. The blocked culvert was

LEFT RILL SITE 1

18/01/86

13/02/86

18/04/86

SCALE 0   15   30 cm
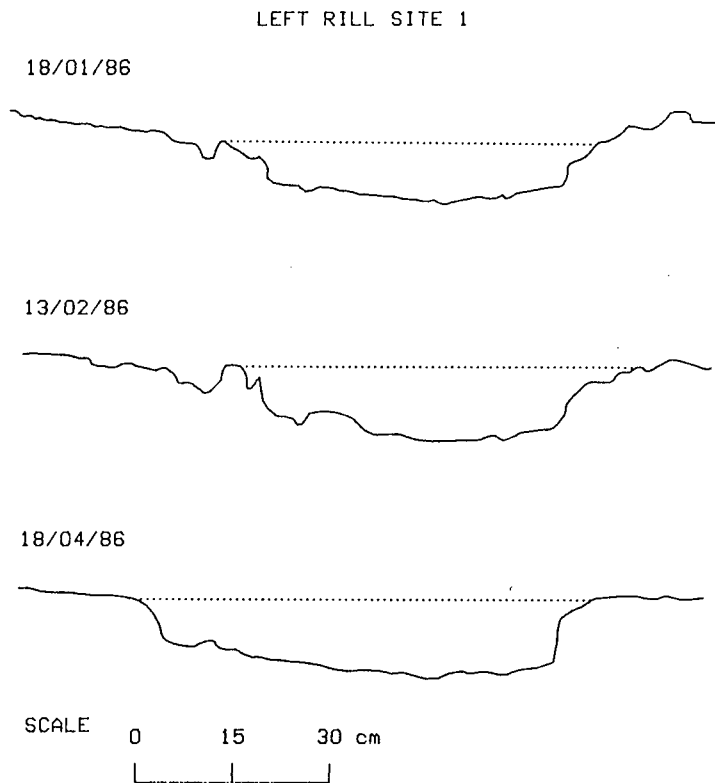
Figure 1.8: Rill cross section projections over time at the left rill, site 1.

noticed on January 25, 1986 but it is speculated that the culvert was blocked earlier as the majority of rill erosion occurred prior to January, 1986.

Not all cross sections enlarge over time due to infilling by upslope material (e.g. site 2 of the right rill shown in Fig. 1.10). Cross sections 4 and 5 of the left rill contained multiple rills which expanded laterally beyond the width of the rill meter in April, 1986. Minimum cross section areas are therefore presented for these 2 sites on the last measurement date. As numerous rills cover the field (Fig. 1.2), the contributing area for the 2 measured rills is unknown. Assuming a contributing area of 3.2 ha (the total area of the study site), the soil loss from the two partial rills alone is 1.6 t $ha^{-1}yr^{-1}$.

Interrill erosion between February 1 and March 9, 1986 was determined by erosion pins. The change in the surface position and the average change over the 8 sites is given in

Table 1.1: Rill meter cross section areas.

Date	Site	Left Rill		Right Rill	
		Area [cm²]	% of Final Area	Area [cm²]	% of Final Area
18-01-86	6	157	73	604	92
	5	241	88	500	63
	4	240	91	754	73
	3	206	70	735	47
	2	287	98	1141	85
	1	124	56	971	76
13-02-86	6	209	98	657	100
	5	275	100	477	60
	4	265	100	809	78
	3	249	84	735	47
	2	291	99	1126	84
	1	173	78	1131	89
18-04-86	6	214	100	655	
	5	> 258		792	100
	4	> 262		1038	100
	3	296	100	1561	100
	2	293	100	1341	100
	1	221	100	1273	100

Table 1.3. Negative values indicate erosion and positive values indicate deposition. The average interrill erosion is less than the measurement error ($\pm$ 1 mm). The negligible interrill erosion suggests that both rain splash and sheet flow erosion are small. The negligible net interrill soil loss was not surprising as crop rows were nearly on the contour and both deposition and erosion were likely to occur throughout the interrill region.

The cumulative downslope rainsplash is given in Table 1.4. The soil collected over 84 days is minimal except in the lower tray. The value for the bottom tray includes an undetermined amount of sheet flow erosion. During rainfall events, the same soil particles are displaced many times by splash, but once they have been collected in the splash trays they cannot move again. The results are, therefore, a cumulative measurement of the

Table 1.2: Calculated rill volumes.

Date	Site	Left Rill			Right Rill		
		Length [m]	Volume [m^3]	% of Final Volume	Length [m]	Volume [m^3]	% of Final Volume
18-01-86	6-5	9.7	0.19	83	18.8	1.04	76
	5-4	5.4	0.13	87	5.4	0.34	69
	4-3	11.3	0.25	78	6.9	0.51	57
	3-2	3.8	0.09	82	5.4	0.51	65
	2-1	6.5	0.13	76	4.9	0.52	81
	total	36.7	0.79	81	41.4	2.92	70
13-02-86	6-5	9.7	0.23	100	18.8	1.07	79
	5-4	5.4	0.15	100	5.4	0.35	71
	4-3	11.3	0.29	91	6.9	0.53	59
	3-2	3.8	0.10	91	5.4	0.50	64
	2-1	6.5	0.15	88	4.9	0.55	86
	total	36.7	0.92	95	41.4	3.00	72
18-04-86	6-5	9.7	>0.23		18.8	1.36	100
	5-4	5.4	>0.14		5.4	0.49	100
	4-3	11.3	>0.32	100	6.9	0.90	100
	3-2	3.8	0.11	100	5.4	0.78	100
	2-1	6.5	0.17	100	4.9	0.64	100
	total	36.7	>0.97	100	41.4	4.17	100

quantities of soil moved downslope and cannot be interpreted as the quantity of soil transported to the bottom of the slope by rainsplash (Bolline, 1978; 1980).

For the rain splash apparatus, the contributing area is unknown and soil loss on a t ha^{-1} basis cannot be calculated. Similar cumulative soil losses due to splash erosion were measured by Bolline (1980) for a loamy soil and low intensity rains. Over 85 days 2.5–12.3 g of soil were collected in 6–15 cm diameter splash funnels. The net annual soil loss was calculated using the method of De Ploey (1969) to account for the percentages of soil projected upslope and downslope. Based on 3 years of data, the net mean annual soil loss was approximately 0.03 t ha^{-1}yr^{-1}. This low value of soil loss and the negligible interrill soil loss suggests that splash erosion at the Mahal farm is also low.

Figure 1.9:   Accelerated rill erosion due to a blocked ditch culvert.
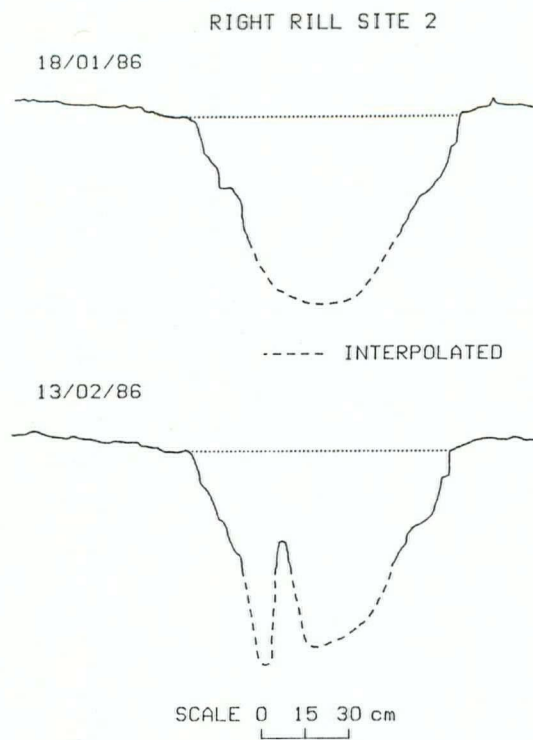
Figure 1.10: Cross section infilling by upslope material at right rill site 2.

Table 1.3: Interrill erosion determined by erosion pins.

Site	Change in Soil Position [mm ± 1]		
	Feb 1-Mar 9	Mar 9-May 5	Feb 1-May 5
1-1	-4	-3	-7
1-2	-8	-10	-18
2-1	1	-3	4
2-2	1	4	3
3-1	3	-3	0
3-2	2	7	9
4-1	2	2	4
4-2	3	-4	-1
5-1	3	-1	2
5-2	0	-4	-4
6-1	2	-2	0
6-2	2	-3	0
7-1	-3	9	6
7-2	0	-4	4
8-1	-1	3	2
8-2	-5	1	-4
Ave	-0.4	-0.7	0
SD	4.8	4.8	6.3

Table 1.4: Cumulative rainsplash erosion.

Tray	Splashed Soil [g] [a]
1 (top)	0.5
2	1.0
3	3.0
4 (btm.)	36.0

[a]Total over 84 days

1.4 PREVIOUS EROSION STUDIES

Previous erosion studies were conducted at the Mahal farm by Crudge (1987) and Wood (1983; 1984). The results of their work are reviewed to augment the introductory measurements of rill, interrill and rainsplash erosion.

Crudge (1987) estimated the net soil loss due to rill erosion from this site for the winter of 1984–1985. In the fall of 1984, the field was ploughed and a cover crop of rye grass was planted. The field was divided into 144 representative units, 32 of which were sampled on a stratified random basis. The rill volume was determined for each sampled unit in April, 1985. The soil loss calculated from the rill volumes was 38 t $ha^{-1}yr^{-1}$.

C. Wood of the BCMAF conducted plot studies at the site from 1982 to 1984. He maintained two 42 m long plots in the south-east corner of the field (Fig. 1.11). The plots were under strawberries planted up-and-down the slope. A Coshocton-type runoff sampler designed to sample 1% of the runoff through a flume was located at the bottom of each plot. Measurement of the sediment content of the sample allowed the determination of the soil loss. The volume of water collected and rain gauge data yield the percentage of the precipitation generating runoff. On one plot, an interceptor type drainage system was installed at a 15.2 m spacing. The drainage system consisted of a 0.75 m trench with a drainage pipe at the bottom, back filled to the surface with gravel.

Table 1.5 and Figs. 1.12 and 1.13 give the results of the plot study by Wood (1983; 1984). Runoff coefficients on the undrained plot are relatively low (19–26 %), but cause considerable erosion. Estimated soil loss ranges from 35–45 t ha^{-1} over one winter. Erosion is initially low in September and October, and most of the soil loss (75–85 %) occurs between mid-November and January. By March, erosion rates have declined even though precipitation rates remain relatively constant. The decline in erosion rates after January are in agreement with the decrease in the rate of growth of rill cross section areas
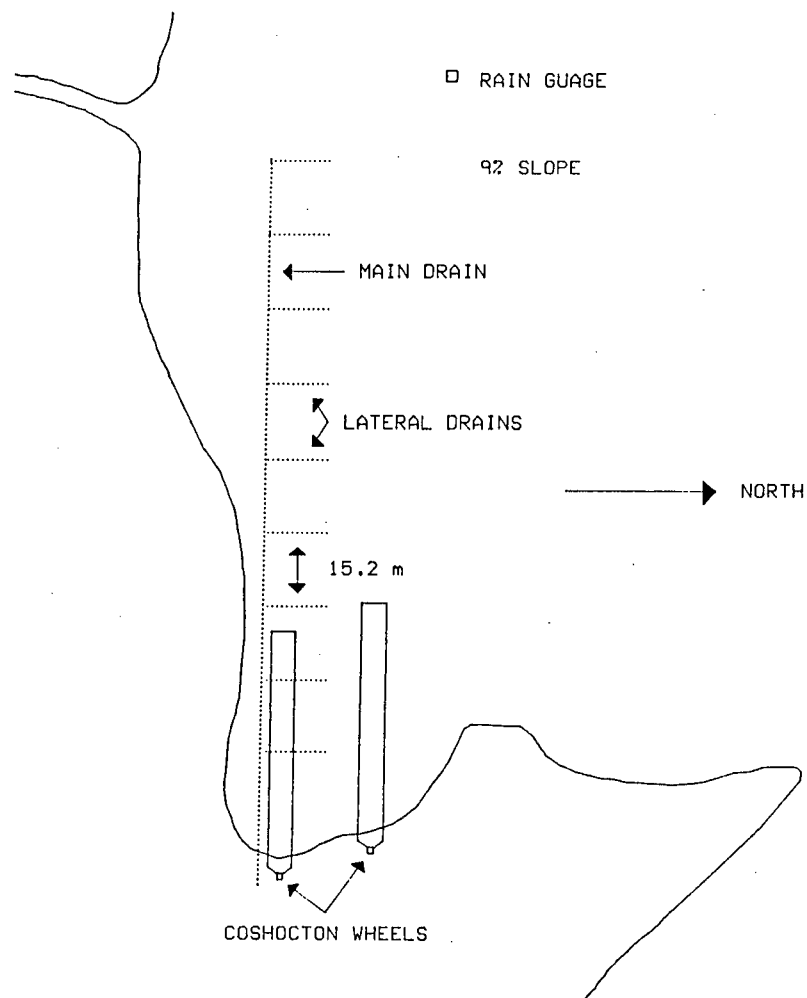
Figure 1.11: BCMAF plot study layout.

reported in section 1.3. The high initial erosion rates likely coincide with the formation of rills, and the decline in erosion with the establishment of equilibrium in rill volume (Novak, 1985).

The interceptor type drainage system is effective in reducing runoff and soil erosion to negligible amounts. Overland and subsurface flow are intercepted and diverted off the field by the drainage system. However, interceptor drains are impractical to maintain on cultivated land (Wood, 1984).

Table 1.5: Soil loss on drained versus undrained plots.

Event	October '82–April '83		September '83–July '84	
	Drained	Undrained	Drained	Undrained
Rainfall Measured	887 mm	887 mm	1623 mm	1623 mm
Runoff events	11	24	6	31
% of Rainfall as Runoff	6%	26%	2%	19%
Soil Loss	0.4 t ha^{-1}	28.7 t ha^{-1a}	0.1 t ha^{-1}	26.7 t ha^{-1b}

[a]Runoff exceeded the collecting tank capacity. Wood (1983) estimates an additional soil loss of 12 t ha^{-1}
[b]Runoff exceeded the collecting tank capacity. Wood (1984) estimates an additional soil loss of 10–20 t ha^{-1}

1.5 COMPARISON OF RESULTS

For this Whatcom soil, the net soil loss due to rainsplash and sheetwash is small compared to rill erosion, even though these mechanisms are a potentially important source of sediment to rills. The soil loss in the development of rills is estimated at 38 t ha^{-1}yr^{-1} (Crudge, 1987). Runoff coefficients are relatively low (<26 %), but soil loss is extensive. Net soil losses based on plot studies (Wood, 1983; 1984) are expected to range from 35–45 t ha^{-1}yr^{-1} and erosion over longer slope lengths is anticipated to be even greater. Most of the erosion occurs from November to January and by March erosion rates have declined even though precipitation rates remain relatively constant.

In soil conservation practice, acceptable rates of erosion for shallow soils are 2–5 t ha^{-1}yr^{-1} (Troeh et al., 1980). Erosion rates at the Mahal farm exceed of these limits. For efficient erosion control and land management practices, an understanding of runoff generation is required. Soil hydraulic properties are necessary to estimate infiltration and drainage, both of which influence runoff. The measurement of the soil hydraulic properties at the Mahal farm is described in Chapter 2.
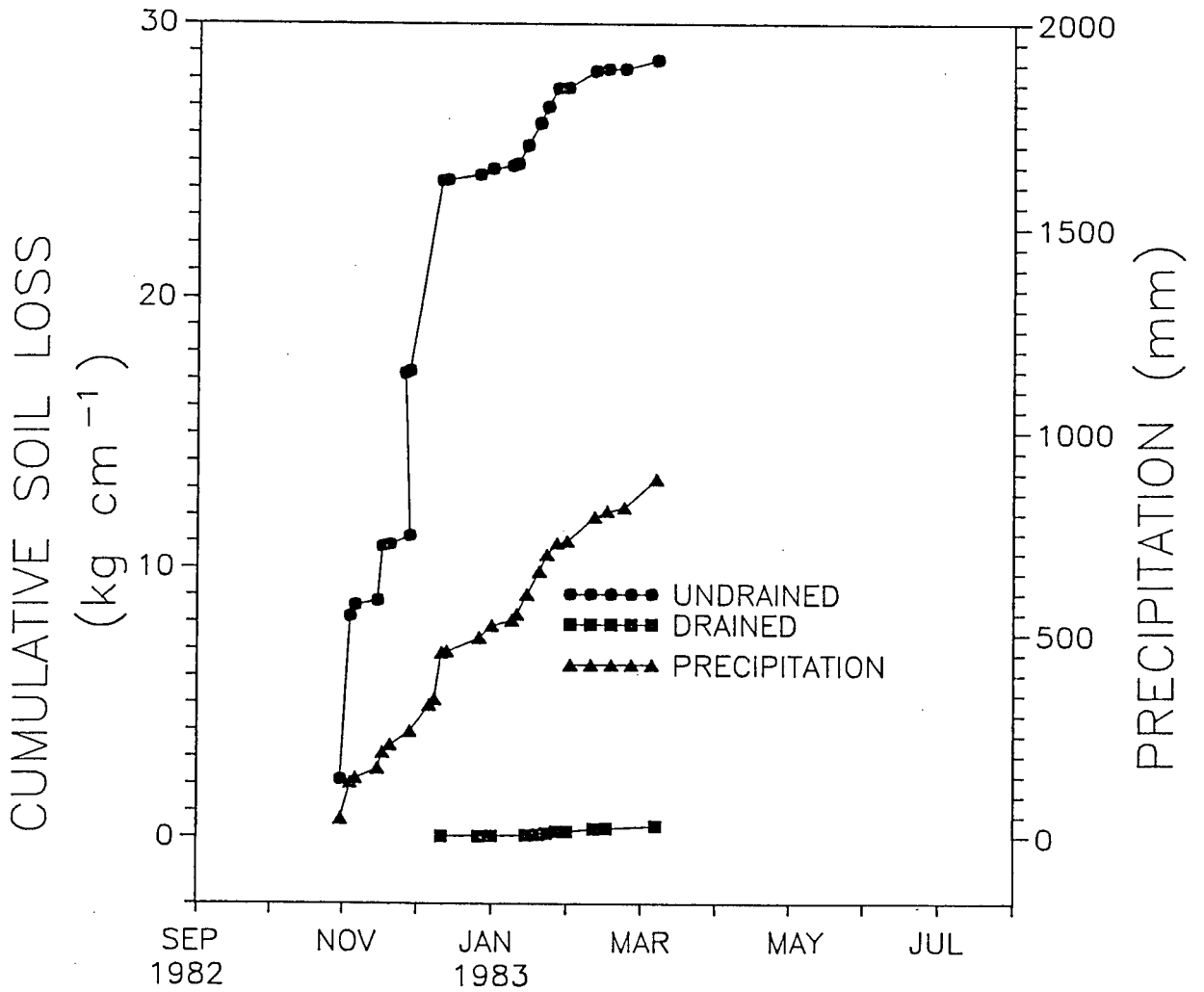
Figure 1.12: Cumulative soil erosion losses for the Wood (1983) plot study, 1982–1983.
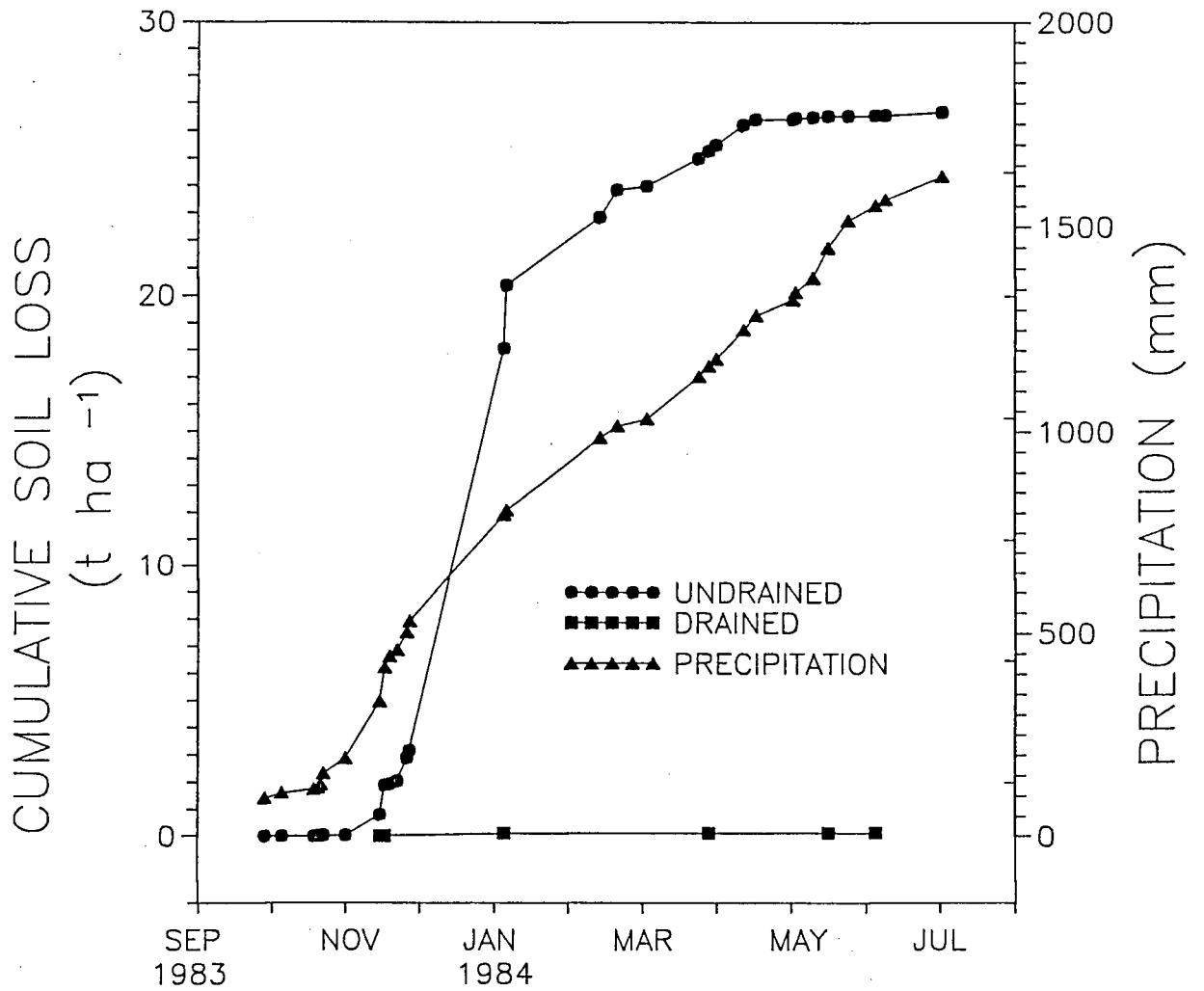
Figure 1.13: Cumulative soil erosion losses for the Wood (1984) plot study, 1983–1984.

Chapter 2

SOIL HYDRAULIC PROPERTIES AT THE MAHAL FARM

2.1 INTRODUCTION

Soil hydraulic properties can be limiting factors to rainfall infiltration, thereby determining the amount of runoff generated. The objective of this chapter is to report measurements of the hydraulic properties of a Whatcom soil in the uplands of the lower Fraser Valley. Additional measurements of cone penetration resistance, soil colour, texture, bulk density and porosity are used to characterize the site. Measurements of the sorptivity, wetting-front advance and satiated conductivity are made using a low tension absorption device. Constant-concentration absorption theory is used to calculate the soil-water diffusivity characteristic from these data. The measured soil-water diffusivity functions are compared to values predicted from the desorption soil-water retention curves and the satiated hydraulic conductivity. The measured hydraulic properties will be used to predict infiltration, runoff and drainage in Chapter 3.

2.2 THEORETICAL BACKGROUND

2.2.1 LOW TENSION ABSORPTION

A list of the symbols used in the text is given in appendix A. The soil is assumed to be homogeneous with a hydraulic diffusivity (D) given by (Gardner, 1959; Zachmann et al. , 1980)

$$D(\theta) = D_n \exp \left[\frac{\beta(\theta - \theta_n)}{(\theta_s - \theta_n)} \right] \tag{2.1}$$

21

where θ is the volumetric water content, θ_s and θ_n are two particular values of θ, generally the saturated value and the air-dry value respectively, D_n is $D(\theta_n)$ and β is an exponent. From (2.1) the differential function may be written as $D = b \exp(a\theta)$ where

$$a = \frac{\beta}{\theta_s - \theta_n} \tag{2.2}$$

and

$$b = \frac{D_n}{\exp\left(\frac{\beta\theta_n}{\theta_s - \theta_n}\right)} \tag{2.3}$$

According to Brutsaert (1979), dimensional considerations yield

$$D_n = \frac{\gamma S^2}{(\theta_s - \theta_n)^2} \tag{2.4}$$

where γ is a function of β and S is the sorptivity for the θ_s and θ_n values. Combining (2.1) and (2.4) gives (Clothier and White, 1981)

$$D(\theta) = \frac{\gamma S^2(\theta_s, \theta_n)}{(\theta_s - \theta_n)^2} \exp\left[\frac{\beta(\theta - \theta_n)}{(\theta_s - \theta_n)}\right] \tag{2.5}$$

For small time (t) and when θ_n is less than or equal to field capacity, gravity effects may be neglected (absorption). The soil-water flow equation governing $\theta(x, t)$ for absorption is given by (Childs and George, 1950)

$$\frac{\partial \theta}{\partial t} = \frac{\partial}{\partial x}\left(D\frac{\partial \theta}{\partial x}\right) \tag{2.6}$$

where x is the horizontal distance. Initially $(t = 0)$ the soil is assumed to be uniformly wet, i.e.

$$\theta(x, 0) = \theta_n \tag{2.7}$$

For a semi-infinite soil

$$\lim_{x \to \infty} \theta(x, t) = \theta_n \tag{2.8}$$

The constant-concentration surface boundary condition is given by

$$\theta(0, t) = \theta_s \tag{2.9}$$

i.e. θ at the surface is suddenly changed from θ_n to θ_s. For (2.6) subject to (2.7), (2.8) and (2.9) the Boltzman similarity variable (λ) and S are given by (Philip, 1957)

$$\lambda(\theta) = \frac{x}{t^{1/2}} \qquad (2.10)$$

and

$$S = \frac{i}{t^{1/2}} \qquad (2.11)$$

where i is the cumulative inflow. According to Philip (1973) and Philip and Knight (1974), if θ is a monotonic function of x, then the nondimensionalized solution of (2.6) subject to (2.7), (2.8) and (2.9) is given implicitly by

$$x = \frac{2t^{1/2}}{S} \int_{\theta}^{\theta_s} \frac{D(\theta)}{F(\Theta)} d\theta \qquad (2.12)$$

and

$$S^2 = 2 \int_{\theta_n}^{\theta_s} (\theta - \theta_n) \frac{D(\theta)}{F(\Theta)} d\theta \qquad (2.13)$$

where $F(\Theta)$ is the flux concentration function (Philip, 1973) and

$$\Theta = \frac{\theta - \theta_n}{\theta_s - \theta_n} \qquad (2.14)$$

Substituting (2.5) into (2.13) gives

$$\gamma = \frac{1}{\left[2 \int_0^1 \frac{\Theta \exp \beta(\Theta) d\Theta}{F(\Theta)}\right]} \qquad (2.15)$$

If θ^* is the volumetric water content at the wetting-front, then from (2.10) and (2.12)

$$\frac{\lambda}{\lambda^*} = \frac{\int_{\theta}^{\theta_s} \frac{D(\theta)}{F(\Theta)} d\theta}{\int_{\theta^*}^{\theta_s} \frac{D(\theta)}{F(\Theta)} d\theta} = \frac{\int_{\Theta}^1 \frac{D(\Theta)}{F(\Theta)} d\Theta}{\int_{\Theta^*}^1 \frac{D(\Theta)}{F(\Theta)} d\Theta} \qquad (2.16)$$

where λ^* is λ at the wetting-front. Defining

$$\phi = \frac{S}{\lambda^*(\theta_s - \theta_n)} \qquad (2.17)$$

and substituting λ^* from (2.12) and S from (2.13) with $\theta = \theta^*$ yields

$$\phi = \frac{\int_0^1 \frac{\Theta D(\Theta)}{F(\Theta)} d\Theta}{\int_{\Theta^*}^1 \frac{D(\Theta)}{F(\Theta)} d\Theta} \qquad (2.18)$$

Evidently the solution is completely specified when $F(\Theta)$ is known. By definition $F(\Theta) = q(x,t)/q(0,t)$, where $q(x,t)$ is the water flux density, so that $F(1) = 1$ and $F(0) = 0$. In general, $F = F(\Theta,t)$ but for the constant-concentration case $F = F(\Theta)$ (Philip and Knight, 1974). The lower bound to $F(\Theta)$ occurs for a delta function soil, and is given by (Philip and Knight, 1974)

$$F(\Theta) = \Theta \qquad (2.19)$$

The upper bound to $F(\Theta)$ occurs for the linear case (D constant and $\beta = 0$) which according to White et al. (1979) can be closely approximated by

$$F(\Theta) \simeq \sin\left[\frac{\pi}{2}\Theta^{\pi/4}\right] \qquad (2.20)$$

The flux concentration relations for delta function absorption and linear absorption provide bounds on $F(\Theta)$. $F(\Theta)$ for absorption in field soils will lie between (2.19) and (2.20). Data from repacked laboratory columns suggest $\beta = 8$ for a range of soil textures (Miller and Bresler, 1977; Reichardt et al., 1972). As the solution is relatively insensitive to the form of $F(\Theta)$ (Philip and Knight, 1974), for $\beta \geq 8$ the delta function flux concentration relation (2.19) is assumed. For $0 < \beta < 8$ the change in β is estimated by

$$F(\Theta) = \sin\left[\frac{\pi}{2}\Theta^{\pi/4}\right] \frac{8-\beta}{8} + \Theta\frac{\beta}{8} \qquad (2.21)$$

Substituting (2.21) and (2.5) into (2.18) gives an implicit solution for β when ϕ is known from measurements.

2.2.2 CALCULATING $D(\theta)$ FROM RETENTION CURVE DATA

The hydraulic conductivity (K) of an unsaturated soil may be calculated from (Mualem, 1976)

$$\frac{K(\theta)}{K_s} = \left(\frac{\theta - \theta_r}{\theta_s - \theta_r}\right)^{1/2} \left[\frac{\int_0^\theta \frac{d\theta}{h}}{\int_0^{\theta_s} \frac{d\theta}{h}}\right]^2 \qquad (2.22)$$

where K_s is the saturated conductivity, θ_s is the saturated moisture content and h is the tension. Therefore $K(\theta)$ can be calculated when $h(\theta)$, i.e. the retention curve, is known. Van Genuchten (1980) suggested representing retention data by

$$\theta = \theta_r + \frac{\theta_s - \theta_r}{[1 + (\alpha h)^n]^m} \qquad (2.23)$$

where α is a constant, n and m are exponents and θ_r is the residual water content. For the Mualem (1976) model

$$m = 1 - \frac{1}{n} \qquad (2.24)$$

Eq. (2.23) with (2.24) contains 4 independent parameters (θ_r, θ_s, α and m) which are determined by fitting to measured soil-water retention data. Solving (2.23) for h and substituting into (2.22) gives

$$K(\theta) = K_s \left(\frac{\theta - \theta_r}{\theta_s - \theta_r}\right)^{1/2} \left\{ 1 - \left(1 - \left[\frac{\theta - \theta_r}{\theta_s - \theta_r}\right]^{1/m}\right)^m\right\}^2 \qquad (2.25)$$

where $0 < m < 1$. The soil-water diffusivity is defined as

$$D(\theta) = K(\theta) \left|\frac{dh}{d\theta}\right| \qquad (2.26)$$

Differentiating (2.23) with respect to h gives

$$\left|\frac{d\theta}{dh}\right| = mn\alpha(\theta_s - \theta_r) \left(\frac{\theta - \theta_r}{\theta_s - \theta_r}\right)^{1+1/m} \left[\left(\frac{\theta - \theta_r}{\theta_s - \theta_r}\right)^{-1/m} - 1\right]^m \qquad (2.27)$$

Substituting (2.27) and (2.25) into (2.26) yields

$$D(\theta) = \frac{K_s \left(\frac{\theta - \theta_r}{\theta_s - \theta_r}\right)^{1/2} \left\{1 - \left[1 - \left(\frac{\theta - \theta_r}{\theta_s - \theta_r}\right)^{1/m}\right]^m\right\}^2}{mn\alpha(\theta_s - \theta_r) \left(\frac{\theta - \theta_r}{\theta_s - \theta_r}\right)^{1+1/m} \left[\left(\frac{\theta - \theta_r}{\theta_s - \theta_r}\right)^{-1/m} - 1\right]^m} \qquad (2.28)$$

2.3 METHODS

2.3.1 SAMPLING

Soil cores were sampled using a stratified random sampling scheme with slight modifications. The study area was divided into 17 sampling units (Fig. 2.1). The grid design

Figure 2.1: Sampling design for soil hydraulic properties.

corresponded to an earlier topographic survey at the Mahal site by Crudge (1987). Each sampling unit was approximately 2025 m². Unit 1 was included as free water was observed along the top of the field in the winter of 1985–1986. Unit 8 was included as the slope of the field concentrated water in unit 8 and rilling was observed in the winters of 1984–1985 and 1985–1986. Unit 17 was included as it was the location of an earlier erosion study by Wood (1983; 1984). Sampling was conducted at 2 levels of intensity. Grid representative samples consist of 1 site randomly located within each unit. Detailed grid samples include 5 additional sampling sites randomly located in unit 9 for comparison of within versus between site variability. The combined data set is made up of the grid representative and detailed grid samples.

Absorption cores were sampled to measure $D(\theta)$ and water retention cores were sampled to calculate $K(\theta)$. The volume of the water retention cores ranged from 60–69 cm³. The volume of the absorption cores (851–961 cm³) were based on the representative elementary volume of a loamy textured soil with small peds (Table 2.1).

Table 2.1: Hypothetical representative elementary volumes (REV) (Bouma, 1984).

Texture	Structure	REV [cm³]
Sandy Loamy Clayey	No peds	10^2
	Small peds	10^3
	Medium peds	
	Continuous macropores	10^4
Clayey	Large peds	
	Continuous macropores	10^5

At each site, soil profiles were sampled at two depths, corresponding to the A_p and a lower more compact horizon. The A_p horizon was sampled 1–2 cm below the surface to remove potential surface crusting effects and any weed or algae growth. The lower horizons were identified by soil colour and resistance to shovelling. At the time of sampling

all lower horizon cores were believed to be C horizon samples. The depth to the subsoil at each site was later verified by additional soil pits and cone penetrometer readings.

Soil samples were taken in April 1986 prior to ploughing. Cores were collected in, as near as possible, an undisturbed state. Water retention cores were gently hammered into the soil and dug out with a trowel. Absorption cores were collected in thin walled (0.5 mm) perspex tubes. The perspex was bevelled on the bottom to aid in penetration. The soil surrounding each core was removed with a putty knife before the core was pushed downwards to avoid compression (Fig. 2.2). The perspex tubes were pressed downwards until the soil surface was approximately 1 cm above the upper edge. The core was then dug out with a trowel and trimmed with a putty knife. All cores were then labelled and wrapped in sealed plastic bags to prevent drying. The cores were taken to the laboratory and stored in a refrigerator at approximately 5 deg C to suppress biological activity until the laboratory analysis could be done.

Figure 2.2: Absorption core sampling.

2.3.2 ADDITIONAL SITE PROPERTIES

The depth to the compact subsoil at each site was verified by additional soil pits and cone penetrometer readings (Davidson, 1965). At each sampling site, soil horizons were identified in soil pits and cone penetrometer measurements were taken with a 2.5 cm diameter cone.

The large, absorption cores were used in the determination of soil bulk density, porosity, texture, and colour, as their larger volume provides a more representative sample. After the completion of the low tension absorption measurements, the cores were dried to constant weight at 105 deg C. The bulk density (ρ_b) was calculated from the oven-dry mass divided by the volume of the core (Blake, 1965). The porosity (f) was calculated from

$$f = 1 - \frac{\rho_b}{\rho_s} \tag{2.29}$$

where ρ_s is the particle density. The particle density was calculated from

$$\rho_s = \frac{1}{\frac{f_m}{2650} + \frac{f_o}{1300}} \tag{2.30}$$

where f_m is the mass fraction of mineral soil, f_o is the mass fraction of organic soil, 2650 kg m^{-3} is the particle density of the mineral components and 1300 kg m^{-3} is the assumed particle density of the organic components. The organic matter content for the A_p horizon is approximately 6% (Harrop, 1987; Crudge, 1987, Brown and Morin, 1985) and for the lower horizons is approximately 3% (Brown and Morin, 1985) giving $\rho_s = 2495$ and 2570 kg m^{-3} respectively. Dry soil colour was based on the Munsell soil colour charts. The soil samples were divided into USDA particle-size classes by hand texturing.

Statistical analyses were carried out using SPSS/PC+ (Norusis, 1986). Histograms were used to display the distribution of the data. The skewness was used to indicate deviations from normality in the distribution. The mean, median and 50th percentile

were used to describe the central tendency of the data. The standard deviation (SD), minimum, maximum and range were used to measure dispersion. Linear associations were measured by the square of the Pearson correlation coefficient (r^2). Regression lines, fitted by the method of least squares, were used to summarize linear relationships. Differences between group means were determined by the Mann Whitney U test. A non-parametric test was used as the data distributions were not normal.

2.3.3 SORPTIVITY TUBE

A low tension absorption technique, described by Clothier and White (1981), was used to measure the hydraulic diffusivity characteristics of the undisturbed absorption cores. The sorptivity tube device of Clothier and White (1981) was modified according to Watson and Luxmore (1986). The sorptivity tube device (Fig. 2.3) consists of a perspex tube with an 80 μm nylon mesh base. The tube is sealed at the upper end by a rubber stopper. Once sealed, water can only move through the mesh if air enters the hypodermic needle located in the side of the tube. The tension at the base of the mesh is controlled by the height of the hypodermic since

$$h \approx l - \frac{2\sigma}{r_h \rho_w g} \qquad (2.31)$$

where h is the tension at the bottom of the mesh, l is the height of the hypodermic needle above the mesh, σ is the surface tension (7.26E-2 kg s^{-2} at 25 degC), r_h is the inside radius of the hypodermic (2.80E-4 m), ρ_w is the density of water (997 kg m^{-3}), and g is acceleration due to gravity (9.81 m s^{-2}). Eq.(2.31) is only approximate since it excludes pressure differences due to the vertical flow in the tube. The desired tension at the base of the mesh was selected to be -4 cm of water, so that the soil would be nearly saturated but water would not flow down gaps between the soil core and the perspex tube. To obtain a tension of -4 cm of water at the bottom of the mesh, the bottom of
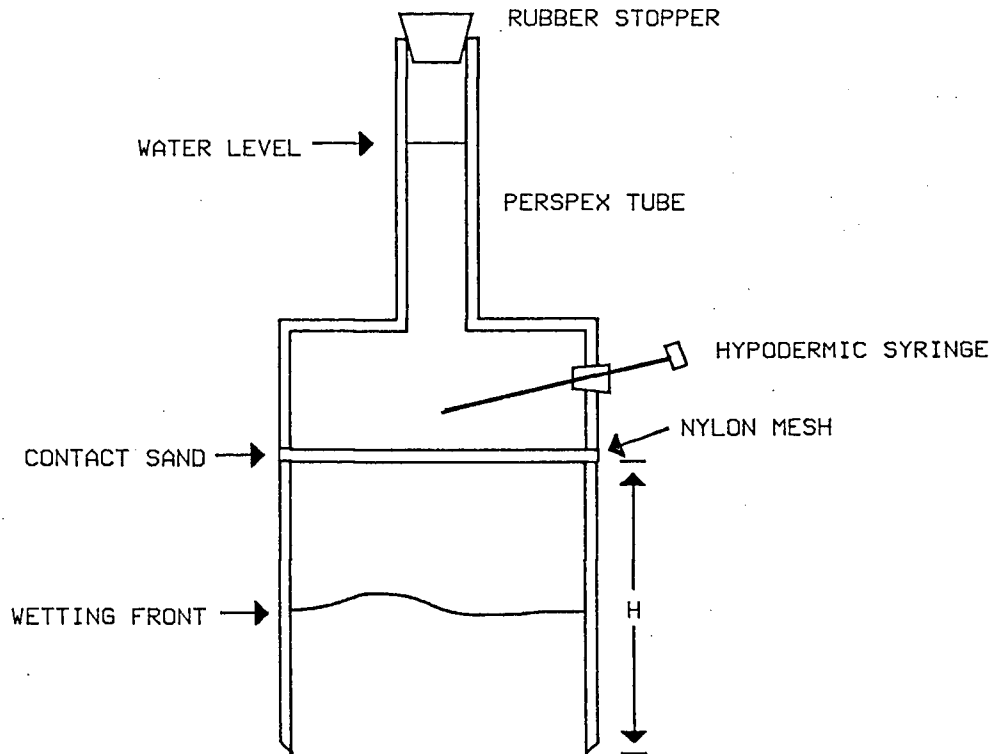
Figure 2.3: The unsaturated sorptivity tube device.

the hypodermic needle is positioned 1.3 cm above the mesh.

For $h = -4$ cm, the radius of the largest water filled pore (r_p) is given by

$$r_p = \frac{2\sigma}{\rho_w g h} \qquad (2.32)$$

For $h = -4$ cm, pores whose radii are greater than 0.37 mm will not influence the absorption of water from the sorptivity tube device. During the low tension absorption measurements no water flow in the gaps between the soil core and the perspex tube was observed.

Prior to the low tension absorption analysis, the ends of the absorption soil cores were wrapped in cheese cloth to add stability. The cores were dried under fans, at room temperature, for 10 days. After 10 days, θ and the change in θ with time were significantly lowered. For each low tension absorption run, the cheese cloth on the top of the core was

removed and the initial core weight was measured. The core was placed on a wire stand
and the upper edge was sealed with putty. A thin layer of air-dried, fine sand was placed
over the top of the core to ensure good contact with the nylon mesh of the sorptivity
tube device. The putty seal was used to stop sand from accumulating in and conducting
water along the core sides.

The sorptivity tube was filled with water, sealed and placed on the soil core. Ob-
servations of the wetting-front advance and water inflow over time were made using a
stop watch and metal rulers attached to the side of the sorptivity tube and the soil core.
The wetting front was defined by a sharp contrast in soil colour. For cores displaying
unevenness in the wetting-front advance, the distance to the wetting-front (x^*) was mea-
sured at 2–3 positions around the core. The transient measurements continued until
the wetting-front was within 2 cm of the bottom of the soil core or for times up to 1.5
hours. The -4 cm tension at the surface was then maintained until steady-state flow
was achieved. In this steady-state, the tension at the base of the soil was essentially 0
cm of water and the mean potential for the soil core was $h/2$ or -2 cm of water. The
steady-state outflow was measured using a stop watch and graduated cylinder. The final
core weight was then measured. The initial moisture content (θ_n) and the final moisture
content (θ_{-2}) were then calculated from the initial and final weights, the oven dry weight
and ρ_b of the absorption cores.

λ^* and S were determined from regression analysis of x^* and i versus $t^{1/2}$ based on
(2.10) and (2.11), respectively. For cores displaying uneven wetting-front advance, plots
of x^* versus $t^{1/2}$ were constructed for each lobe of the wetting-front. Values of λ^* were
determined by weighted averages of the slopes of the regression lines. D_n, β, a and
b were calculated as indicated in the theory of section 2.2.1 using a Fortran program
(appendix C) and the University of British Columbia main frame computer.

The hydraulic conductivity (K_{-2}) at a mean potential of -2 cm of water is given by

$$K_{-2} = \frac{QH}{At(H + h)} \tag{2.33}$$

where Q is the volumetric outflow, $A = 9.15\text{E-}3$ m^2 is the area of the base of the core, and H is the core height.

The constant-concentration absorption theory only applies when gravity effects are negligible. The maximum time (t_g) for gravity effects to be $< 10\%$ of the surface flux is estimated by (Talsma, 1969)

$$t_g \leq 0.0784 \left(\frac{S}{K_s} \right)^2 \tag{2.34}$$

Trial runs, using 4 A_p horizon cores sampled in late August, 1986, were conducted to determine t_g for field and air-dried moisture contents. The low tension absorption results are given in Table 2.2. S, λ^*, a and b are not reported for test cores T3 and T4 with field values of θ_n as the wetting-front advance was not visible due to their high moisture content. Variations in θ_{-2} and θ_n for a given test core should effect S and λ^* as they are dependent on θ_{-2} and θ_n. However, a and b should be constants for a particular test core. Changes in a and b for a given test core reflect measurement error and the effects of core drying. Variation in h due to changes in the positioning of the hypodermic needle would produce deviations in measured values of a and b. The positioning of the hypodermic needle above the mesh was approximately $l = 1.3 \pm 0.25$ cm yielding $h = -4.0 \pm 0.25$ cm. Core shrinkage due to drying may alter the pore size distribution, but these effects are most pronounced in clay soils (Baver, 1956).

Values of t_g for test cores T1 and T2 are given in Table 2.3. Average values of K_{-2} from Table 2.2 are used for K_s in the calculation of t_g. For field values of θ_n, gravity effects become important at times an order of magnitude less than when the samples are air-dried. For cores sampled at wetter field conditions (e.g. April, 1986), t_g will be less, necessitating core drying to meet the assumption of negligible gravity effects.

Table 2.2: Low tension absorption variables for field and air-dried values of θ_n.

Core	θ	θ_{-2}	θ_n	S [m s$^{-1/2}$]	λ [m s$^{-1/2}$]	K_{-2} [m s^{-1}]	a	b [m^{2}s^{-1}]
T1A	Field	0.49	0.24	2.69E-4	1.43E-3	8.09E-6	21.6	8.41E-11
T1A	Air-dry	0.46	0.06	7.32E-4	2.07E-3	1.26E-5	25.1	1.59E-10
T2A	Field	0.50	0.27	3.26E-4	1.96E-3	1.32E-5	21.1	1.37E-10
T2A	Air-dry	0.48	0.06	9.44E-4	2.56E-3	1.74E-5	23.0	3.89E-10
T3A	Field	0.50	0.29			6.25E-6		
T3A	Air-dry	0.48	0.09	8.48E-4	2.59E-3	6.85E-6	11.9	1.68E-8
T4A	Field	0.47	0.27			7.94E-6		
T4A	Air-dry	0.46	0.08	6.10E-4	1.99E-3	7.65E-6	10.1	2.27E-8

Table 2.3: The effect of core drying on t_g.

Core	θ	t_g [min]
T1A	Field	0.8
T1A	Air dry	6.6
T2A	Field	0.6
T2A	Air dry	5.0

A thin layer (≈ 1 mm) of 53–250 μm sand was placed over each soil core to ensure good contact with the sorptivity tube device. Fine grained sand has an air entry value of 35–70 cm of water tension (Bear, 1972) so the sand should remain saturated at a tension of -4 cm of water. The effect of hydraulic resistance of the sand is estimated from Darcy's Law, i.e.

$$\Delta h = \frac{q \Delta z}{K_s} \qquad (2.35)$$

where q is the flow, Δh is the change in potential due to the sand layer, and Δz is the thickness of the sand layer. K_s for loose, fine sand is approximately 10^{-4}m s^{-1} (Hillel, 1980; Freeze and Cherry, 1979; Bear, 1972). Over the first 60 s of absorption, the flow rates were high (1.7E-4 to 8.0E-4 m s^{-1}) and the hydraulic resistance of the sand was

estimated to cause h to be greater than -4 cm by $0.2-0.8$ cm. As the flow rate declined, the change in potential due to the sand layer became negligible and the tension at the soil surface underlying the sand approached to -4 cm.

2.3.4 WATER RETENTION

Water retention curves were determined using a pressure plate apparatus (Richards, 1965). The pressures used were 2.5, 5, 10, 33, 50, 100, 200, 400, 800 and 1500 kPa. Up to 9 cores were placed directly on each pressure plate and they were saturated between runs to ensure good hydraulic contact between the plate and the cores. After outflow from the apparatus ceased, the cores were quickly removed from the plate with a spatula and weighed. The measurements were done in order of increasing pressure and the measurement at 2.5 kPa was repeated after the 1500 kPa measurement. Following the completion of the water retention measurements, the cores were dried to constant weight at 105 deg C. The bulk density was calculated from the oven-dry mass divided by the core volume (Blake, 1965). The water contents measured on a mass basis were then calculated on a volume basis.

The parameters θ_s, θ_r, α and m in the Van Genuchten (1980) expression (2.23), were calculated from the observed soil-water retention data using a least squares curve-fitting technique. Calculations were done using the University of British Columbia mainframe computer and the Fortran curve-fitting subroutine NL2SNO (appendix D). For each core, θ_s, α and m were calculated for various assumed values of θ_r in the range from 0 to the measured θ at 1500 kPa. The 4 parameters giving the lowest sum of squared residuals $(\sum \zeta^2)$ determined the best fit curve for each sample.

2.4 RESULTS AND DISCUSSION

2.4.1 SITE CHARACTERISTICS

The raw data for the soil ρ_b, f, colour, and texture, and the depth to the subsoil are presented in appendix B, Tables B.1 and B.2.

The spatial distribution of the depth to the C horizon is shown in Fig. 2.4. The depth to the C horizon ranges from 7–65 cm, with a median depth of 26 cm. The depth to the C horizon is not consistently low near the top of the field and greater toward the base as expected in an erosional landscape.

The sampling depth was initially determined by soil colour and the resistance to shovelling. In verifying the depth to the subsoil, 5 of the lower horizon samples were identified as B horizon samples. Cone penetrometer resistance readings greater than 10 kg cm^{-2} were found to correspond with the C horizon and intermediate values correspond with the B horizon. Fig. 2.5 displays the separation of soil horizons by penetration resistance.

Soil colour was used to distinguish between the A_p and C horizons in the field. Table 2.4 lists the number of samples (n) in each horizon with a given Munsell soil colour. In general, the differences between the A$_p$ and C horizons are visually distinct (Fig. 2.6), but the same soil colours are found in the A$_p$, B and C horizons (Table 2.4).

The number of samples in each horizon in a given USDA particle size class are listed in Table 2.5. The texture ranges from coarse silty to fine loamy in the A$_p$ horizon, fine to coarse loamy in the B horizon, and fine silty to sandy in the C horizon.

Summary statistics for ρ_b and f are given in Table 2.6. The maximum and minimum values are found in the C horizon, and the SD is smallest in the A$_p$ horizon. Due to the effects of ploughing, the A$_p$ horizon is expected to be more homogeneous than the B or C horizons.
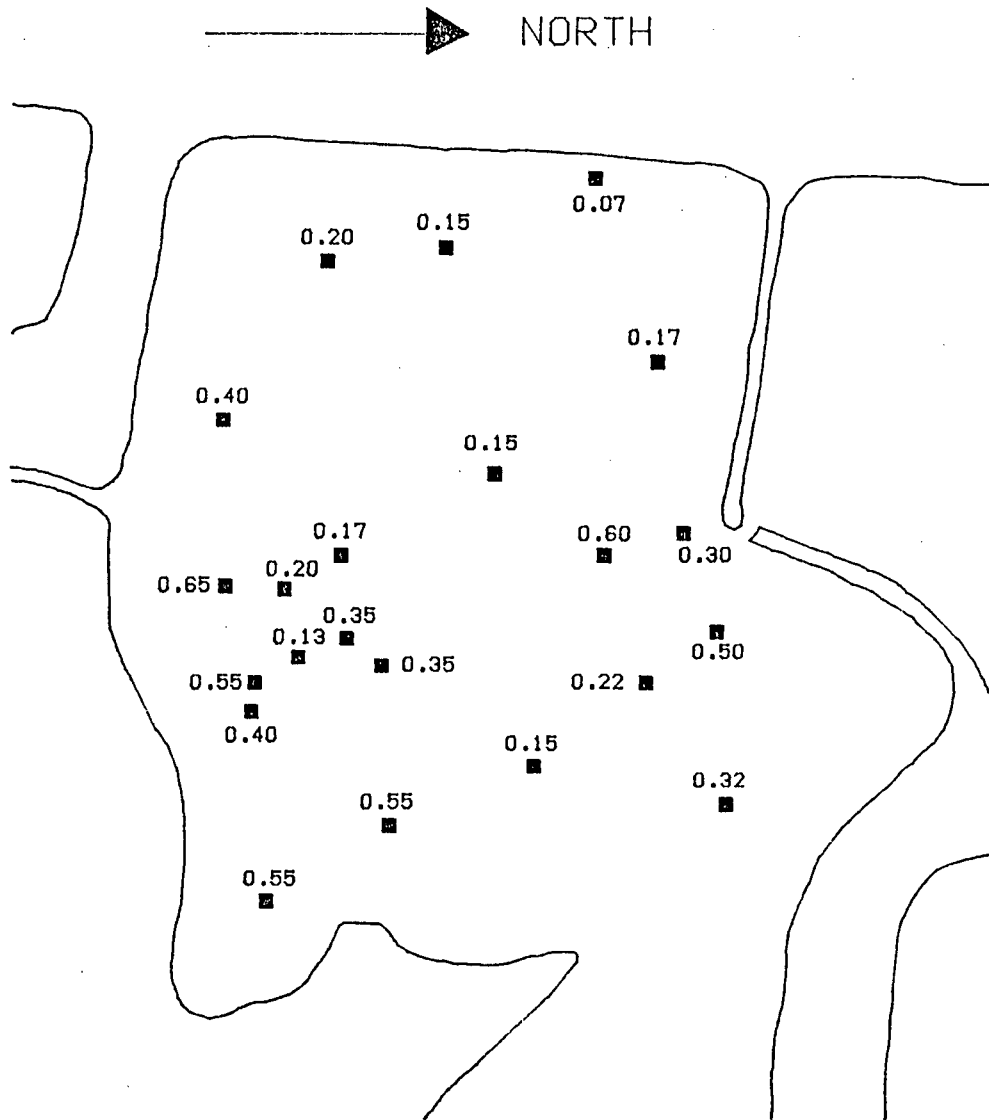
Figure 2.4: Spatial distribution of the depth to C horizon.
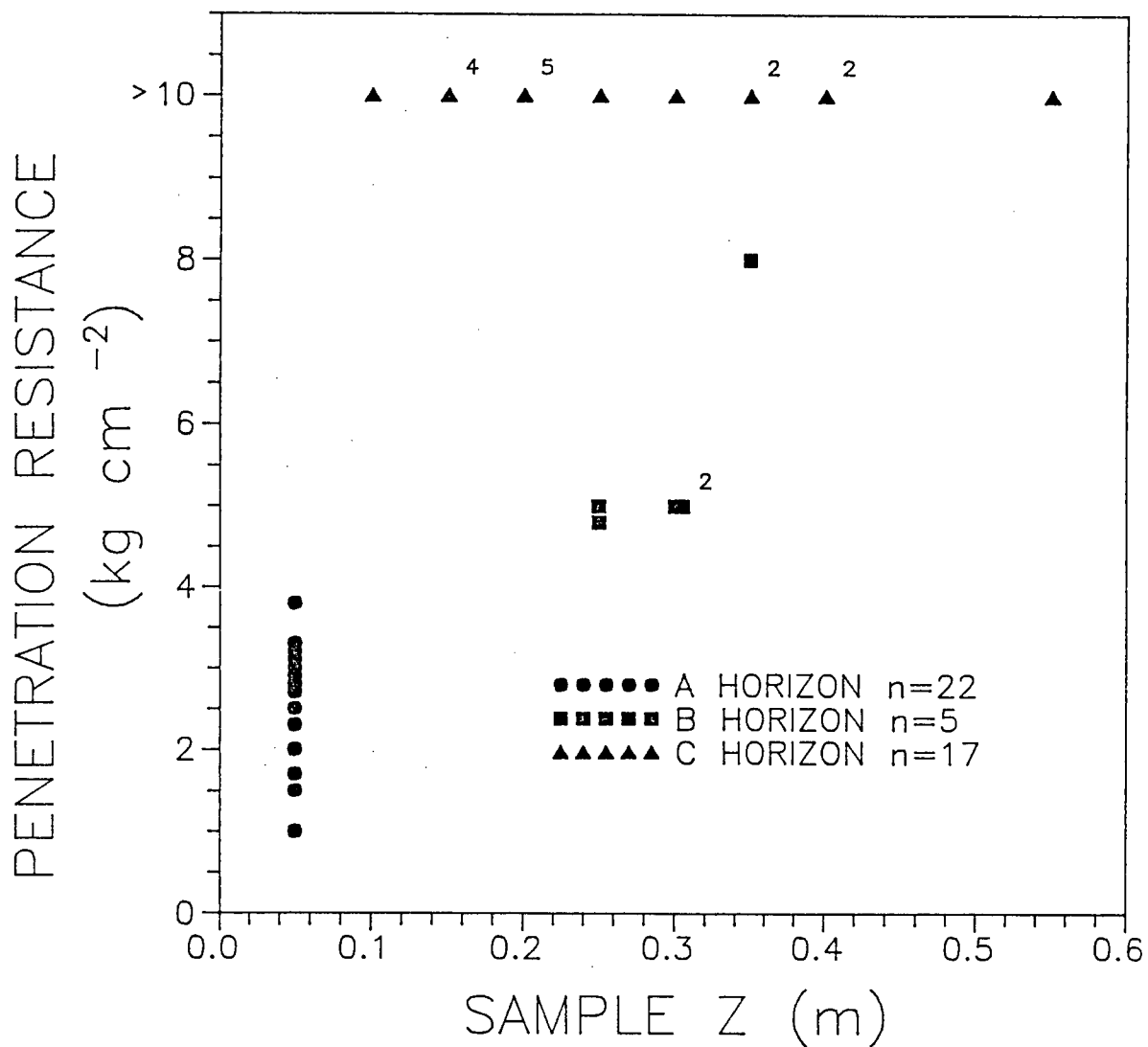
Figure 2.5: Soil horizon determination from cone penetration resistance.

Table 2.4: Munsell dry soil colour.

Horizon	Colour		n
A	2.5Y4/4	Olive Brown	2
	2.5Y5/4	Light Olive Brown	3
	10YR4/3	Brown Dark Brown	3
	10YR4/4	Dark Yellowish Brown	4
	10YR5/3	Brown	4
	10YR5/4	Yellowish Brown	6
B	2.5Y5/4	Light Olive Brown	1
	10YR4/3	Brown Dark Brown	1
	10YR5/3	Brown	3
C	2.5Y5/4	Light Olive Brown	1
	2.5Y6/2	Light Brownish Gray	1
	2.5Y6/4	Light Yellowish Brown	5
	2.5Y7/2	Light Gray	2
	10YR4/3	Brown Dark Brown	1
	10YR5/3	Brown	2
	10YR5/4	Yellowish Brown	1
	10YR6/3	Pale Brown	4

Table 2.5: Texture based on USDA particle size classes (textured by Dr. S.M. Smith).

Horizon	Texture	n
A_p	coarse silty	10
	fine loamy	12
B	fine loamy	4
	coarse loamy	1
C	fine silty	3
	coarse silty	5
	fine loamy	8
	sandy	1
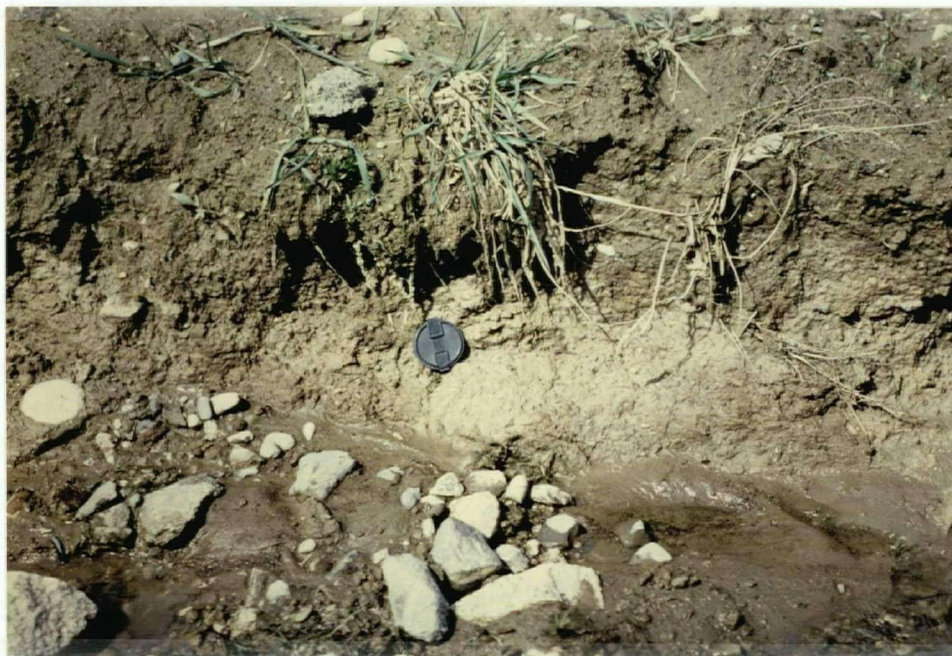
Figure 2.6: Rill erosion exposing the A_p horizon and the underlying C horizon

Table 2.6: Summary statistics for ρ_b and f.

Property	Horizon	n	Mean	Median	S.D.	Skew.	Max.	Min.	Range
ρ_b [kg m^{-3}]	A_p	22	1056	1051	90	0.410	1238	912	326
	B	5	1129	1121	156	-0.601	1304	901	403
	C	17	1260	1247	259	0.422	1734	861	873
f [m^{3}m^{-3}]	A	22	0.58	0.59	0.036	-0.411	0.64	0.51	0.13
	B	5	0.56	0.56	0.061	0.599	0.65	0.49	0.16
	C	17	0.51	0.51	0.100	-0.411	0.66	0.33	0.33

2.4.2 MEASURED $D(\theta)$

Example plots of the i and x^* versus $t^{1/2}$ relationships used to determine S and λ^* are shown in Fig. 2.7 and 2.8. All plots display strong $t^{1/2}$ relationships as expected from the constant-concentration absorption theory. Table 2.7 lists median values of the parameters from the regression analysis used to calculate S and λ^*. t_i and t_f are the initial and final times used in the regression. r^2 and intercept values are also given. i and x^* were typically measured over 20 minutes and the high r^2 values ($r^2 \geq 0.99$) confirm negligible gravity effects for $t < t_f$.

All A_p horizon cores displayed even wetting-front advance. One B horizon and 17 C horizon cores displayed unevenness in the wetting-front advance. Values of i and x^* display minor initial deviations from the $t^{1/2}$ relationship ($t < t_i$). Data points displaying deviations from the $t^{1/2}$ relationship are not included in the regression analysis used to determine S and λ^*. Typically, points over the first 20–84 seconds are excluded (Table 2.7). Minor, initial decreases in i and x^* are anticipated due to resistance and storage effects in the sand layer. Initial decreases in i and x^* are indicated by negative intercept values in Table 2.7. Minor increases in x^* were noted (positive intercepts) for some cores and presumably were due to the difficulty in measuring x^* accurately near $t = 0$.

Table 2.7: Median values of t_i, t_f, r^2 and intercept used in the calculation of S and λ^*.

Horizon	n	S				λ^*			
		t_i [s]	t_f [min]	r^2	Intercept [m]	t_i [s]	t_f [min]	r^2	Intercept [m]
A	22	20	20	0.999	-1.73E-3	45	20	0.995	1.51E-4
B	5	60	20	0.999	-2.10E-3	40	20	0.997	-2.12E-5
C	17	20	18	0.999	-1.53E-3	84	15	0.993	3.81E-3
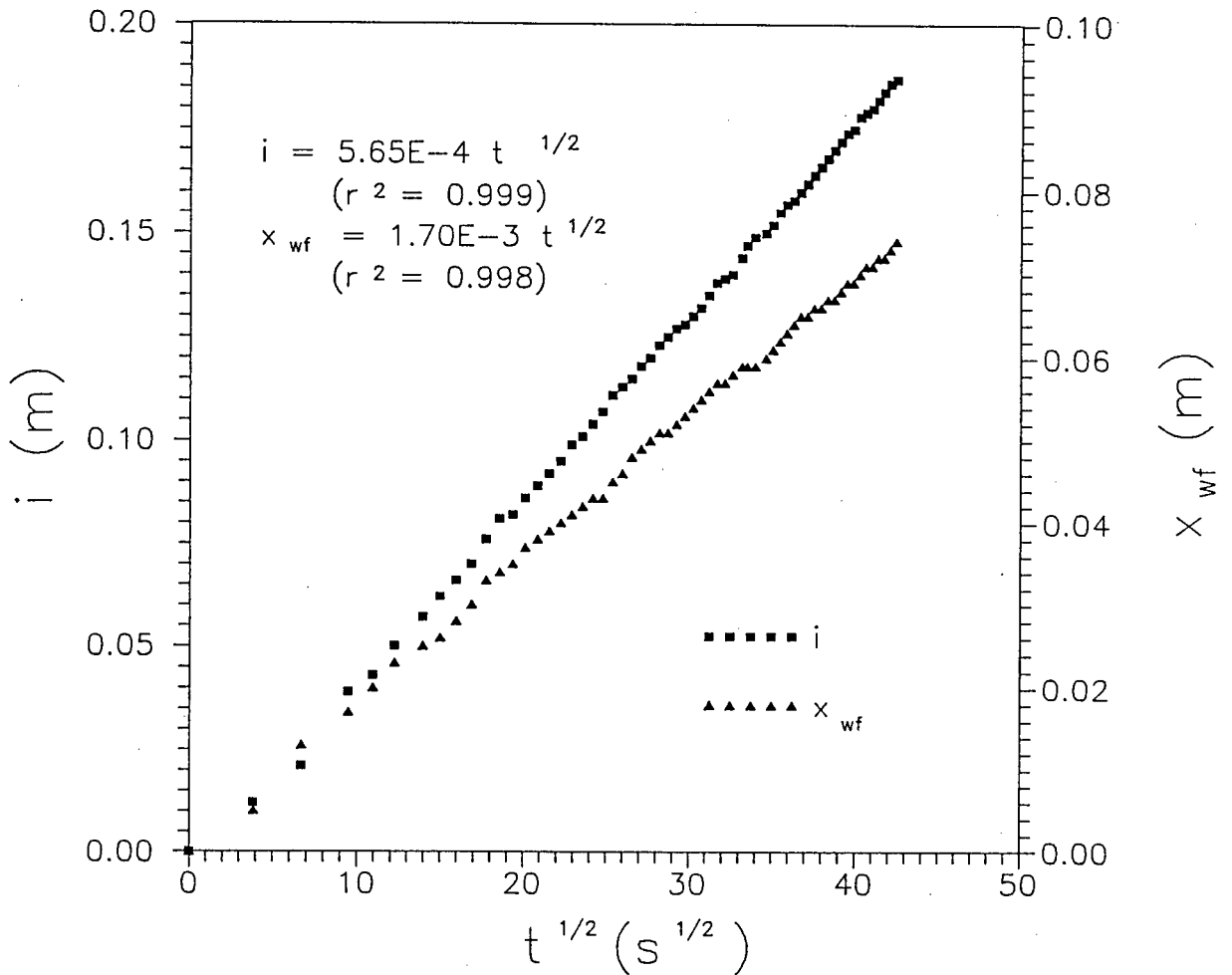
Figure 2.7: Example plots of water inflow (i) and wetting-front advance (x^*) versus $t^{1/2}$ for the A_p horizon.
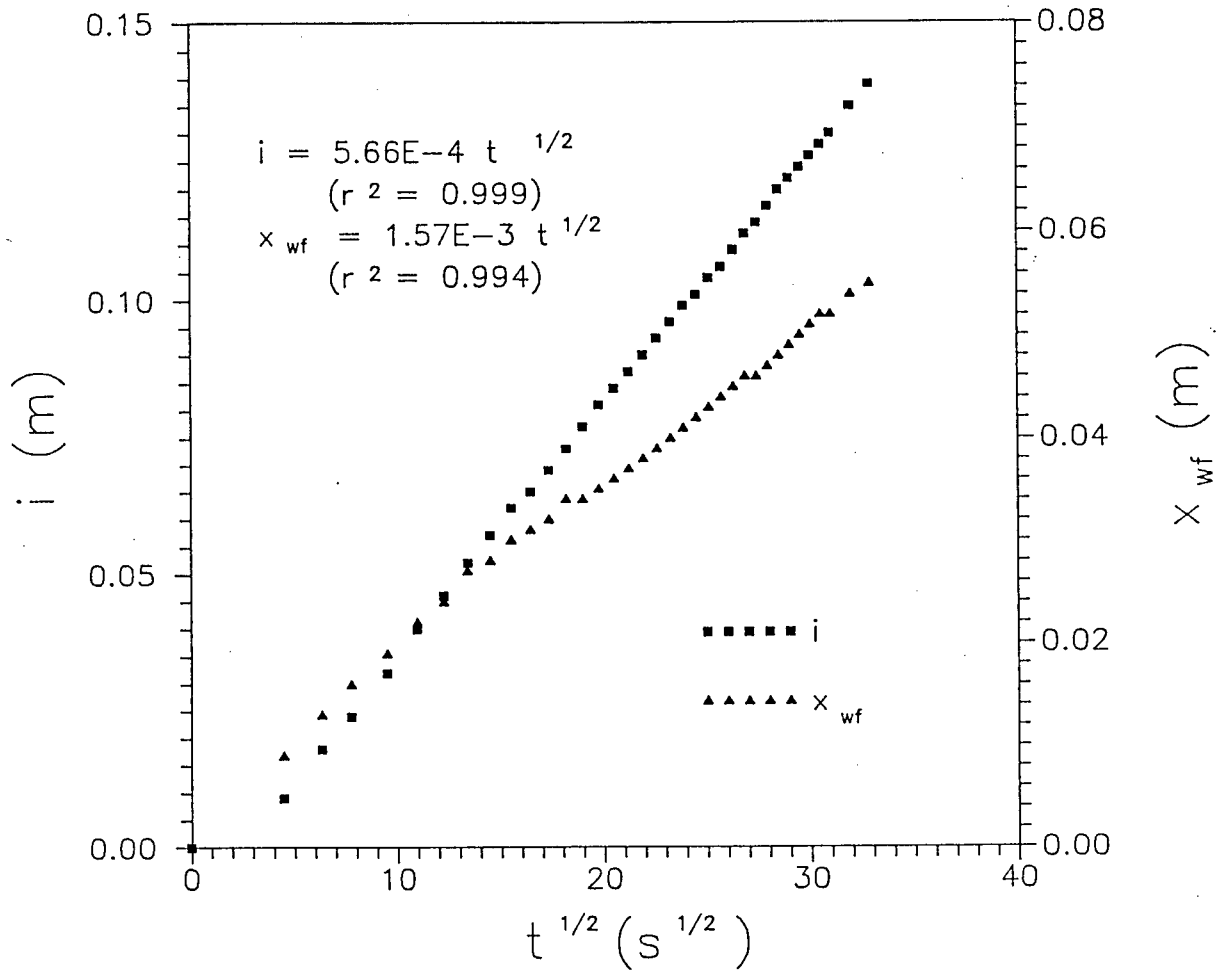
Figure 2.8: Example plots of water inflow (i) and wetting-front advance (x^*) versus $t^{1/2}$ for the C horizon.

An example moisture profile over time for constant-concentration absorption is shown in Fig. 2.9. The A_p and lower horizon cores required approximate 1.5–10 h and 2.5–68 h respectively to reach steady state outflow. Summary statistics for K_{-2} are given in Tables 2.8 to 2.10. Values are given for grid representative samples, detailed grid samples from unit 9 and for the combined data set.

Table 2.8: Summary statistics of K_{-2}, a and b for grid representative samples.

Variable	Horizon	n	Mean	Median	SD	Skew.	Max.	Min.
K_{-2}	A_p	17	4.70E-6	4.25E-6	8.28E-7	1.88	1.50E-5	1.53E-6
$(m\ s^{-1})$	B	3	1.36E-6	7.67E-7	1.33E-6	1.61	2.88E-6	4.33E-7
	C	14	4.70E-6	2.48E-6	5.84E-6	1.82	2.08E-7	2.50E-7
a	A_p	16	23.4	19.4	16.7	2.53	77.3	10.9
	B	3	19.7	16.7	5.9	1.70	26.6	15.9
	C	13	27.2	28.5	11.4	0.08	46.4	8.5
b	A_p	16	3.67E-9	8.51E-10	4.87E-9	1.28	1.51E-8	4.80E-22
$(m^2 s^{-1})$	B	3	1.12E-15	1.08E-15	1.14E-15	0.18	2.29E-15	5.32E-21
	C	13	6.63E-9	1.29E-10	5.82E-9	3.55	7.61E-8	1.57E-14

Table 2.9: Summary statistics of K_{-2}, a and b for detailed grid samples from unit 9.

Variable	Horizon	n	Mean	Median	SD	Skew.	Max.	Min.
K_{-2}	A_p	5	6.24E-6	5.95E-6	2.11E-6	1.28	9.65E-6	4.25E-6
$(m\ s^{-1})$	B	2	3.19E-6	3.19E-6	3.43E-6		5.62E-6	7.67E-7
	C	3	6.35E-6	2.48E-6	8.49E-6	1.22	1.61E-5	4.83E-7
a	A_p	5	17.4	13.6	9.0	1.89	32.9	11.4
	B	2	19.2	19.2	1.1		20.0	18.4
	C	3	21.7	12.0	26.2	1.22	51.3	1.7
b	A_p	5	1.03E-8	6.16E-9	1.15E-8	0.95	2.75E-8	8.47E-13
$(m^2 s^{-1})$	B	2	3.31E-17	3.31E-17	3.83E-17		6.04E-17	5.93E-18
	C	3	5.28E-8	1.82E-8	7.62E-8	1.22	1.40E-7	9.21E-15
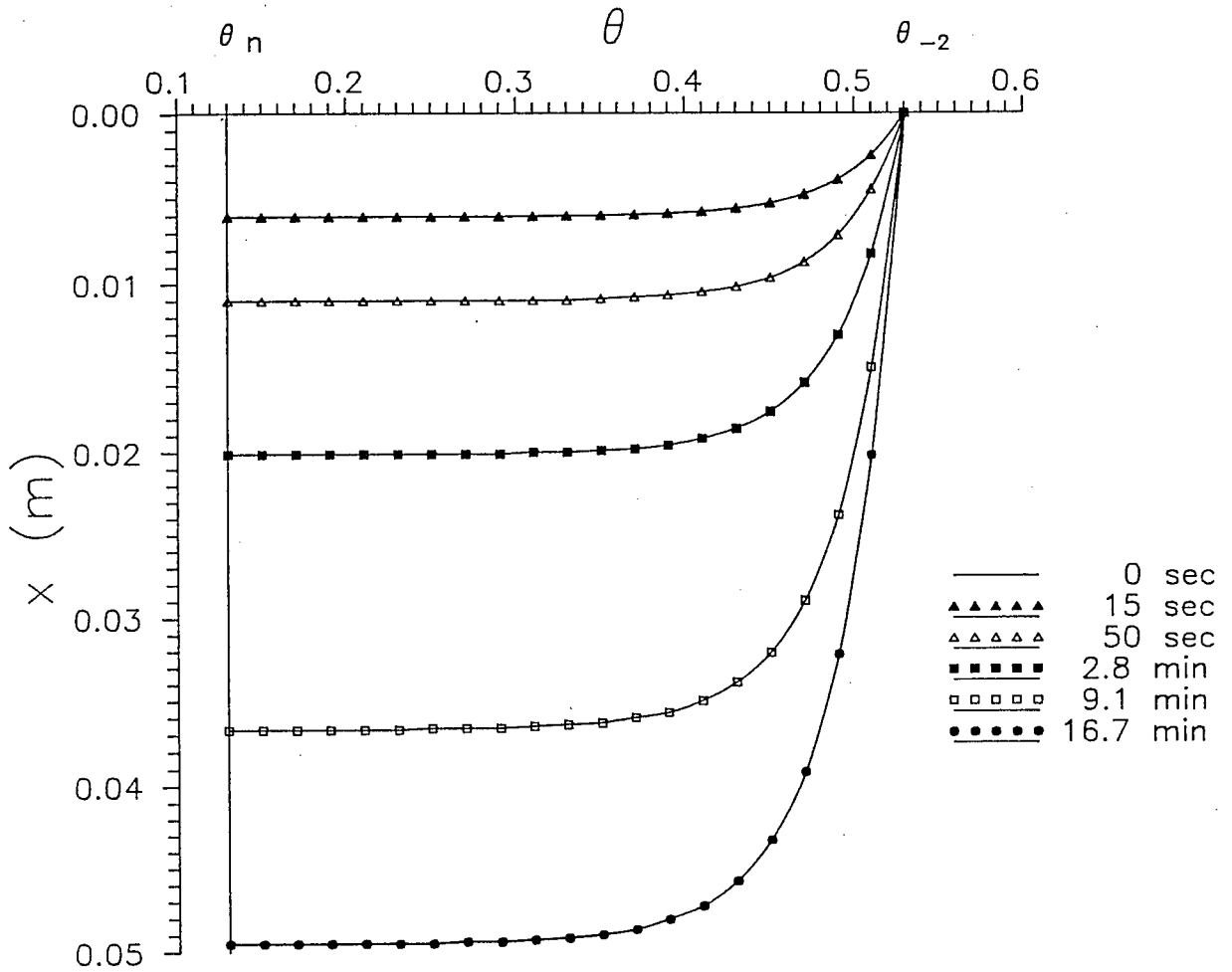
Figure 2.9: Example moisture profiles over time for constant-concentration absorption.

Table 2.10: Summary statistics of K_{-2}, a and b for the combined data set.

Variable	Horizon	n	Mean	Median	SD	Skew.	Max.	Min.
K_{-2}	A_p	22	5.05E-6	4.74E-6	3.19E-6	1.55	1.50E-5	1.53E-6
($m\ s^{-1}$)	B	5	2.09E-6	7.67E-7	2.20E-6	1.37	5.62E-6	4.33E-7
	C	17	4.99E-6	2.48E-6	6.09E-6	1.54	2.08E-5	2.50E-7
	Lower	22	4.33E-6	2.03E-6	5.54E-6	1.82	2.08E-5	2.50E-7
a	A_p	22	22.0	16.5	15.3	2.67	77.3	10.9
	B	5	19.5	18.4	4.2	1.53	26.6	15.9
	C	16	26.1	27.0	3.5	0.12	51.3	1.7
	Lower	21	24.56	21.33	2.78	0.46	51.313	1.68
b	A_p	22	5.17E-9	1.31E-9	7.16E-9	1.79	2.75E-8	4.80E-22
(m^2s^{-1})	B	5	6.86E-16	6.04E-17	1.01E-15	1.36	2.29E-15	5.32E-21
	C	16	1.53E-8	1.31E-10	9.58E-9	2.87	1.40E-7	9.21E-15
	Lower	21	1.16E-8	1.73E-11	7.39E-9	3.36	1.40E-7	5.32E-21

Values of t_g based on (2.34) are given in Table 2.11. Times are shown for samples with the minimum, 50th percentile and maximum values of t_g for the A_p, B and C horizons. The short time behaviour is limited to 2–8 minutes of constant-concentration absorption in the worst cases. Gravity effects are typically negligible in the A_p, B and C horizons at times less than 20, 44 and 62 minutes, respectively, supporting the $t^{1/2}$ behaviour displayed by i and x^* for $t < t_f$.

For absorption at $h = -4$ cm, $\theta_s = \theta_{-4}$ in section 2.2.1. However, θ_{-2} was measured. Measured water retention curves for absorption in sand and silt loams (Topp, 1971; Poulovassilis, 1970; Staple, 1965) indicate that θ_{-2} is very near θ_{-4} as $\theta(h)$ is relatively constant at these low tensions.

The data for the low tension absorption variables θ_{-2}, θ_n, S, λ^*, K_{-2}, D_n, β, a and b are presented in appendix B, Tables B.3 to B.6. Values of θ at the time of sampling (Apr. 1986) are also given. Values of S and λ^* are generally conservative, ranging from 10^{-3}–10^{-4} m s$^{-1/2}$. Summary statistics for a and b are given in Tables 2.8 to 2.10 respectively.

Table 2.11: The maximum time for gravity effects to be negligible.

Variable	Sample	tg [min]
$t_g$min	13A	4.6
t_g50	1A	19.3
$t_g$max	5A	147.6
$t_g$min	9-6B	7.5
t_g50	8B	62.2
$t_g$max	9-3B	72.4
$t_g$min	9-2C	1.6
t_g50	1C	43.8
$t_g$max	4C	937.3

Values are given for grid representative samples, detailed grid samples from unit 9 and for the combined data set.

For sample 11C β is > 100. The effects of forcing $\beta = 100$, 75, and 50 are given in Table 2.12. Sample 11C has the largest value of a, and smallest value of b, of the measured diffusivity functions. $K_{-2} = 3.5E - 7$ for core 11C is in the lower range of values measured at the Mahal farm (Table 2.10). Core 11C is an extreme case and due to the uncertainty in the diffusivity function, is not included in a and b of Tables 2.8 to 2.10 or in further calculations involving a or b.

Table 2.12: Values of D_n, a and b for core 11C with forced values of β.

β	D_n [m^{2}s^{-1}]	b [m^{2}s^{-1}]	a
100	3.16E-49	9.57E-72	370
75	1.71E-38	2.20E-55	278
50	8.19E-28	4.51E-29	185

The range of a, b and K_{-2} for grid representative samples and detailed grid samples from unit 9 are shown in Figs. 2.10 to 2.12. Figs. 2.10 to 2.12 and the SD values of
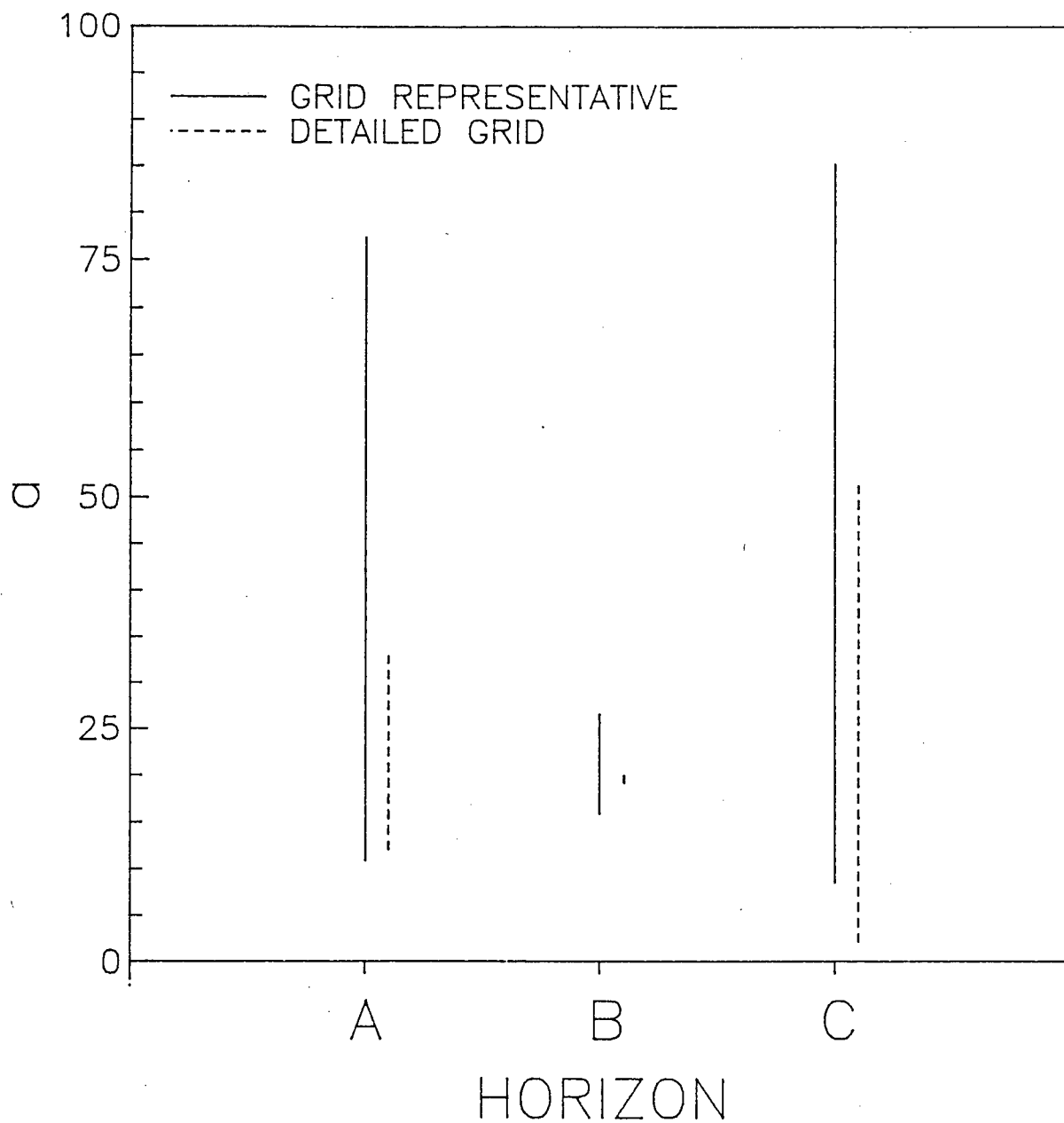
Figure 2.10:   The range of a for grid representative samples and detailed grid samples from unit 9.
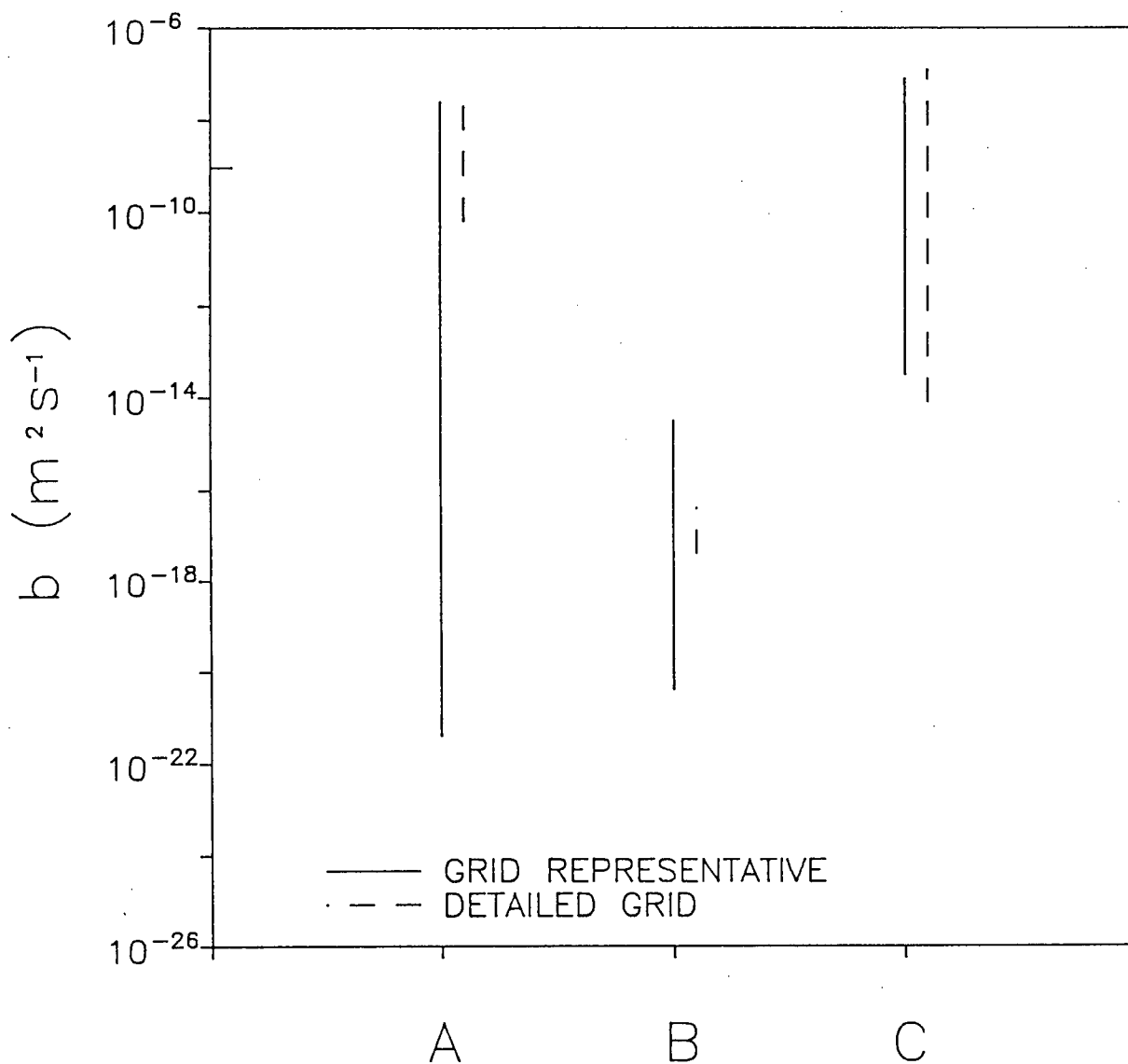
Figure 2.11: The range of b for grid representative samples and detailed grid samples from unit 9.
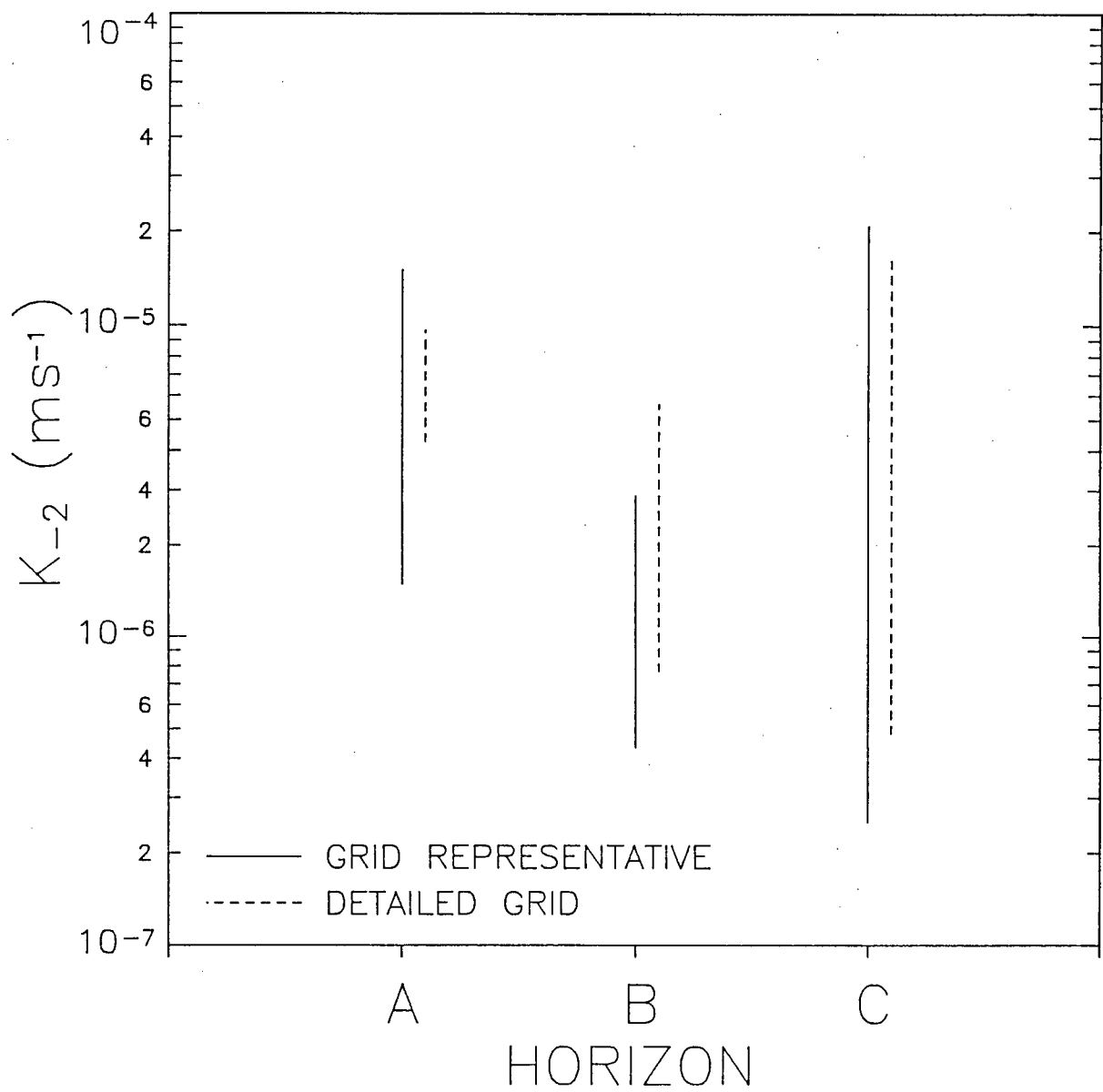
Figure 2.12: The range of K_{-2} for grid representative samples and detailed grid samples from unit 9.

Tables 2.8 and 2.9 indicate that the variability over shorter sampling distances (within unit 9) is of the same order of magnitude as between sampling units. The detailed grid samples from unit 9 are within the range of grid representative samples and are considered part of the same population. The combined data set is therefore used in following analyses.

Values of a and K_{-2} for the B horizon cores are within the range of values for the C horizon (Fig. 2.10 and 2.12). Values of b for the B horizon cores are generally smaller than the C horizon cores. Due to the small number of B horizon samples, there is some uncertainty in the median values of a, b and K_{-2}. For comparison with the overlying A_p horizon cores, the B and C horizon cores are combined and presented as the lower horizons.

The distributions of a and b for the A_p and lower horizons are shown in Figs. 2.13 to 2.16. The diffusivity characteristics (2.1) of the A_p and lower horizons are shown in Figs. 2.17 and 2.18. The diffusivity characteristics display high variability, typical of soil hydraulic properties (Warrick and Nielsen, 1980). The variability of the A_p horizon is less than the lower horizons, possibly due to the mixing effects of ploughing. There are strong negative correlations between a and $\ln b$. The inverse relationship between a and $\ln b$ is related to the conservative nature of S and λ^* as the process of absorption is determined by the integral behaviour of the diffusivity function (Eqs. 2.12 and 2.13).

To test the reproducibility of the sorptivity tube method, seven of the A_p horizon cores were re-dried and the low tension absorption repeated. Values of θ_{-2}, θ_n, S, λ^*, a and b are given in Table 2.13. Changes in a and b for a given sample indicate the magnitude of measurement errors, hysteresis and the effects of core redrying. As the texture of the A_p horizon samples are coarse silty to fine loamy (Table 2.5), drying effects are expected to be small. The changes in a and b for a given sample are relatively large, but a and b are sensitive to errors in the input variables. The effect of 5% increases in θ_s, θ_n, S and
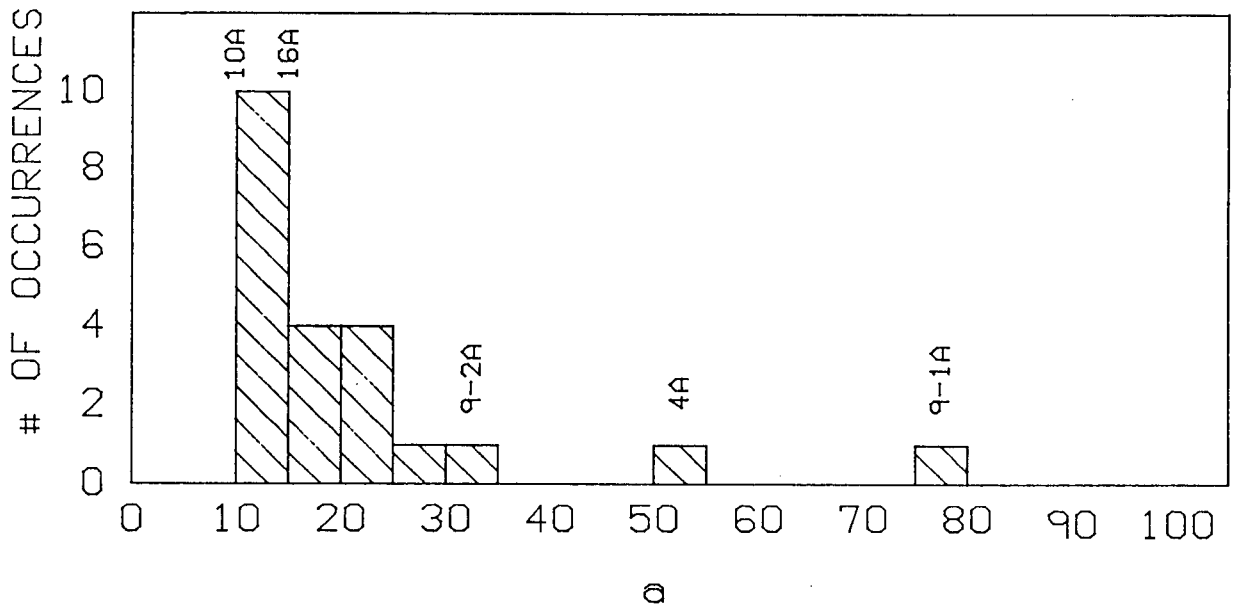
Figure 2.13: The distribution of a for the A_p horizon.
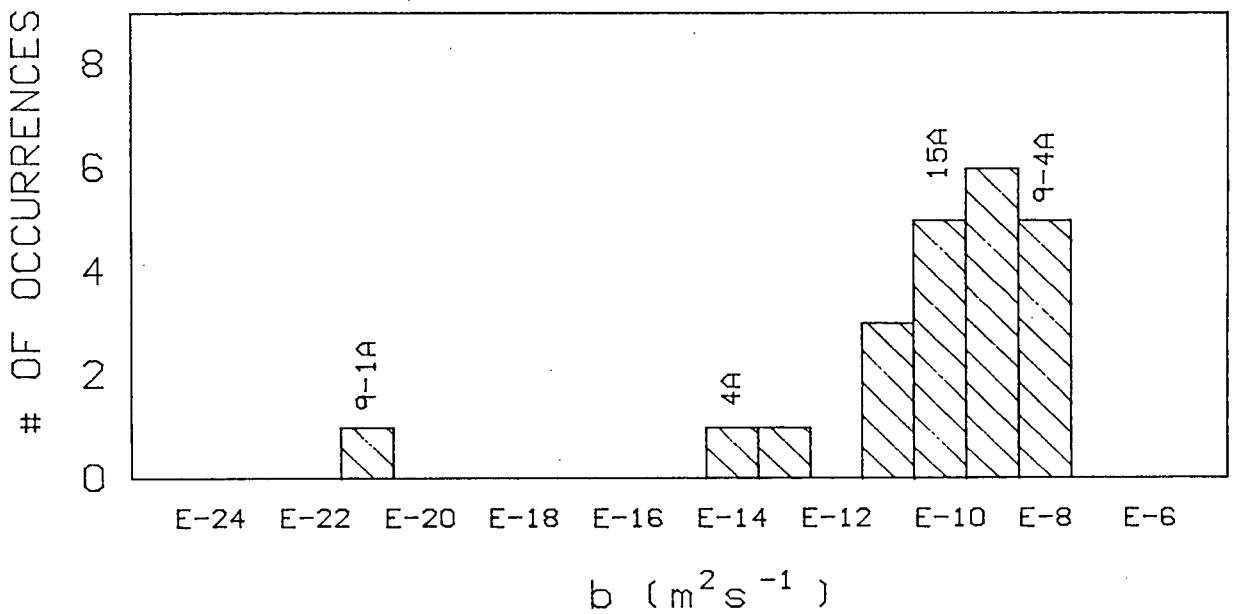
Figure 2.14: The distribution of b for the A_p horizon.
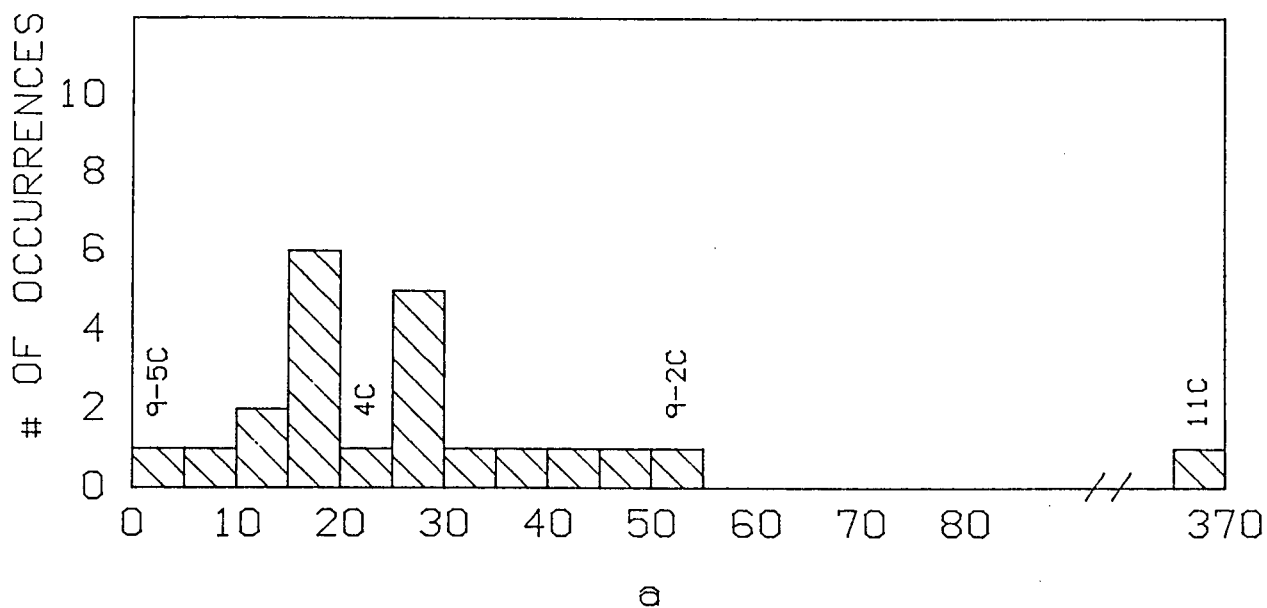
Figure 2.15: The distribution of *a* for the lower horizons.
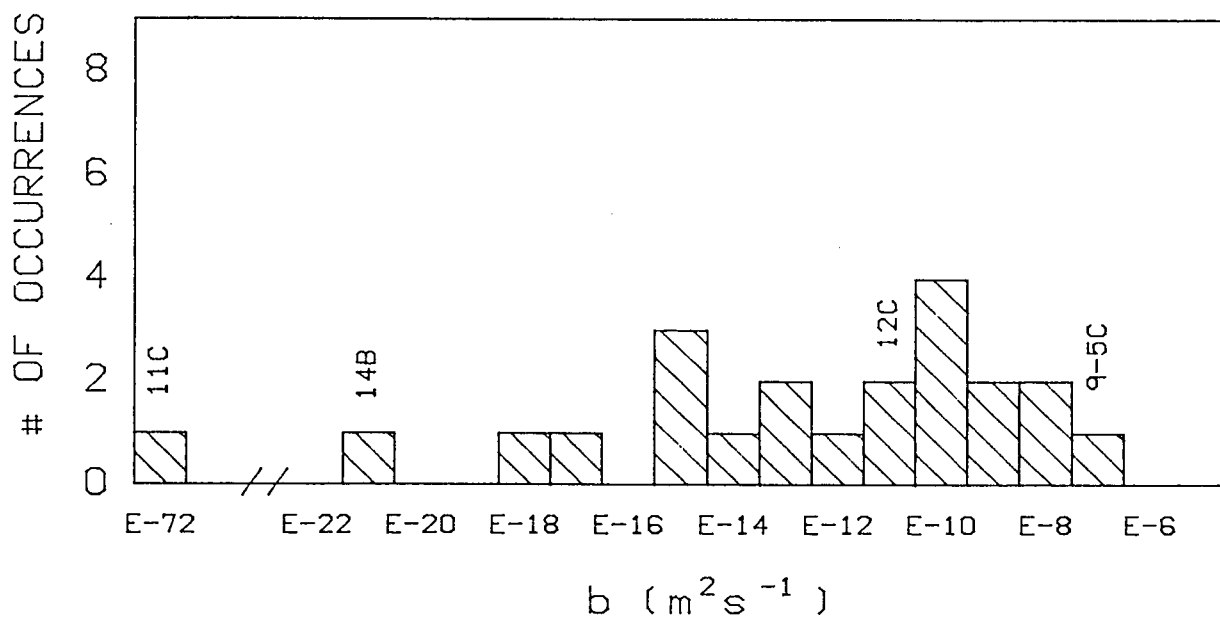
Figure 2.16: The distribution of *b* for the lower horizons.
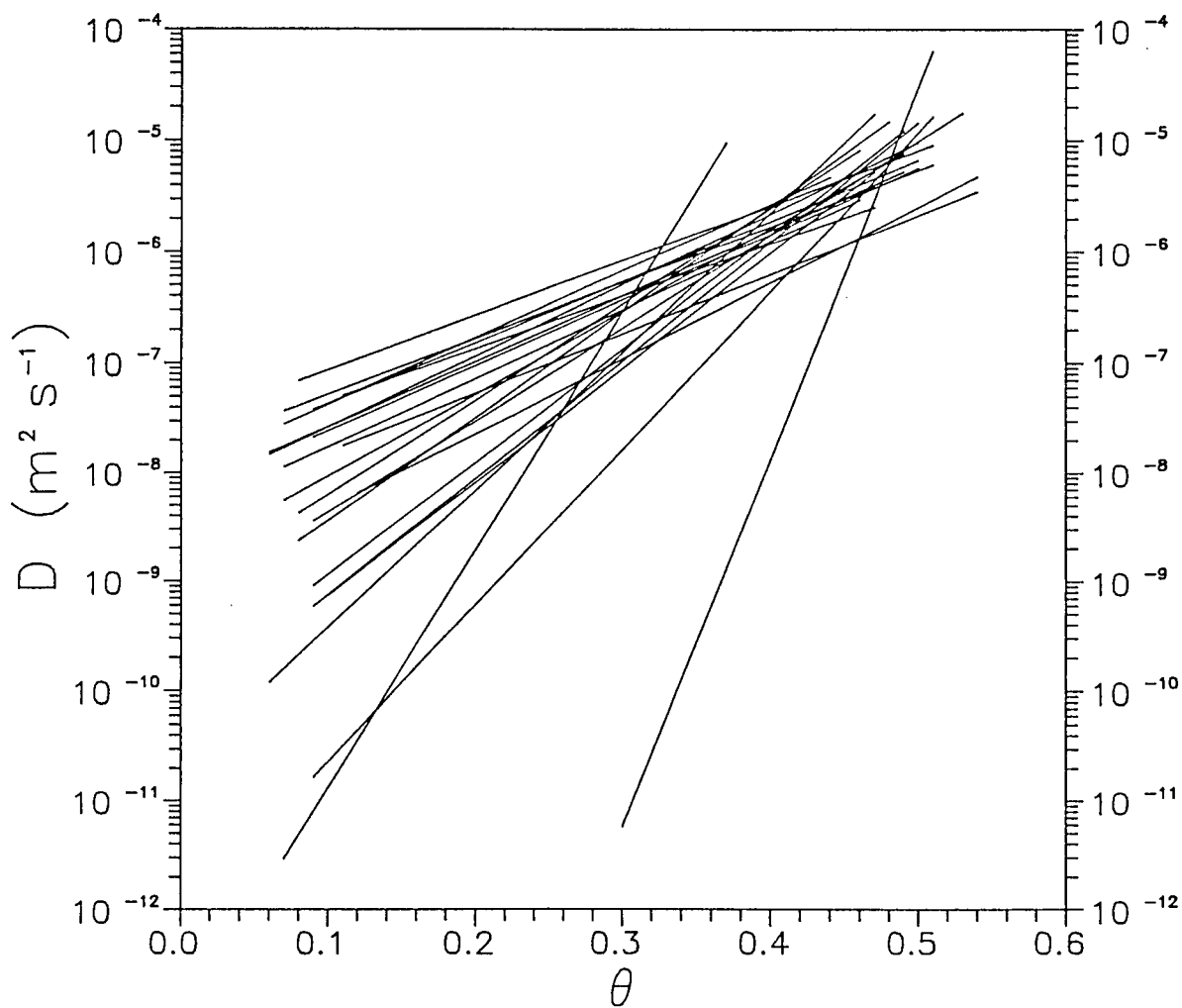
Figure 2.17: The diffusivity characteristics of the A_p horizon.
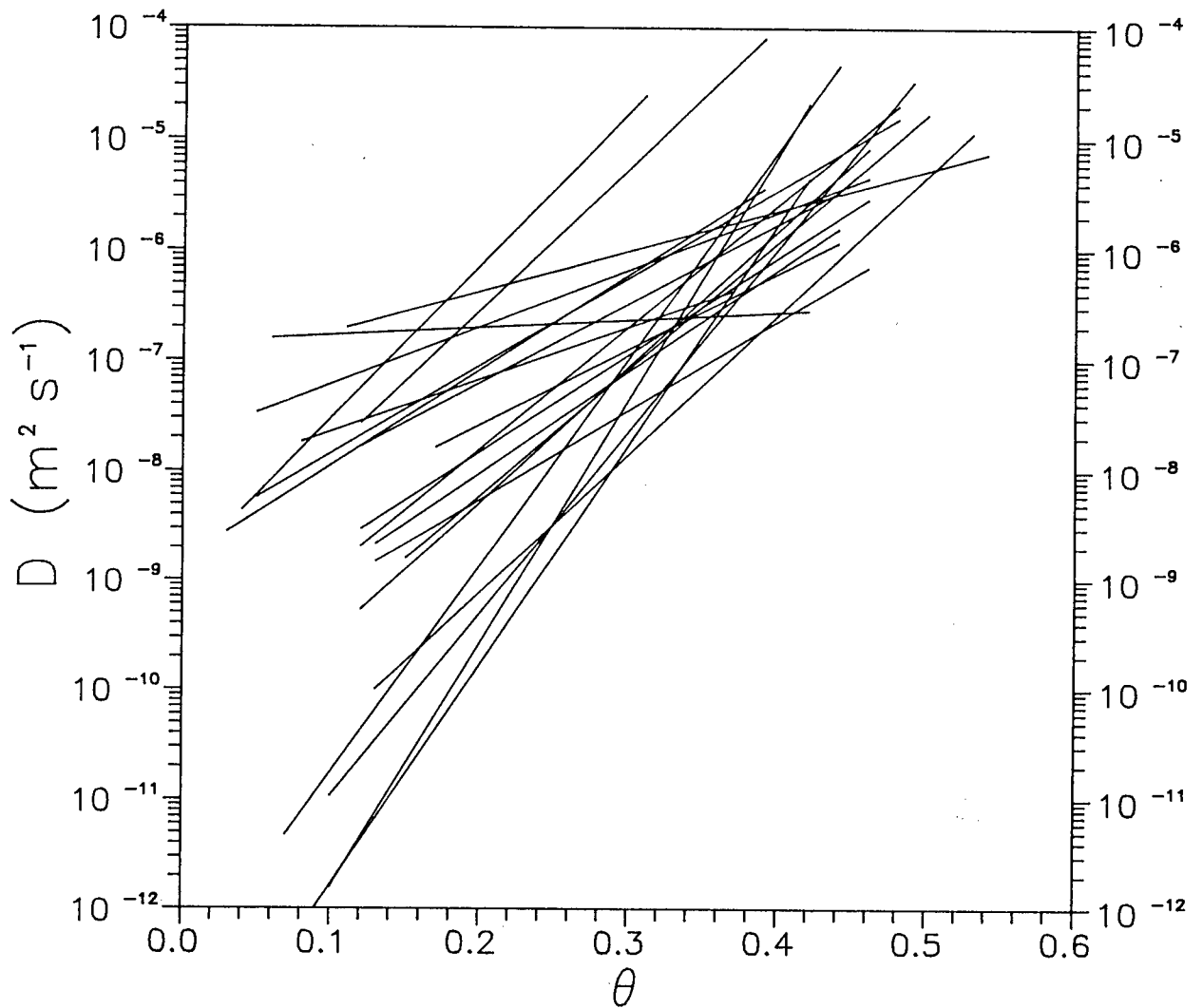
Figure 2.18: The diffusivity characteristics of the lower horizons.

λ^* on a and b are presented for core 1A in Table 2.14. Errors in the range of 5% would account for the observed differences in a and b between redried cores.

Table 2.13: The effects of core drying on constant- concentration absorption.

Sample	θ_s	θ_n	S [m s^{-1}]	λ [m s$^{-1/2}$]	K_{-2} [m s^{-1}]	a	b [m s$^{-1/2}$]
1-2A	0.47	0.03	5.08E-4	1.31E-3	2.41E-6	22.1	1.96E-10
1-2AR	0.46	0.14	4.24E-4	1.57E-3	2.60E-6	25.1	6.82E- 11
2A	0.46	0.07	3.91E-4	1.32E-3	1.53E-6	14.3	4.10E- 9
2AR	0.45	0.10	3.96E-4	1.30E-3	1.65E-6	17.2	1.58E- 9
3A	0.50	0.06	7.47E-4	2.13E-6	9.41E-6	14.8	6.03E- 9
3AR	0.50	0.10	6.01E-4	2.05E-3	5.46E-6	12.5	1.15E- 8
5A	0.50	0.09	6.94E-4	2.35E-3	2.06E-6	24.7	6.31E- 11
5AR	0.51	0.09	7.38E-4	1.94E-3	2.28E-6	28.4	9.60E- 12
8A	0.49	0.09	6.39E-4	1.82E-3	2.35E-6	23.8	1.06E- 10
8AR	0.50	0.11	5.53E-4	1.60E-3	2.90E-6	26.1	2.20E- 11
12-2A	0.53	0.05	6.48E-4	2.14E-3	2.80E-6	7.3	7.82E- 8
12-2AR	0.52	0.12	5.32E-4	1.87E-3	2.76E-6	11.6	1.06E-8
15A	0.47	0.06	6.96E-4	1.88E-3	6.38E-6	29.0	2.06E- 11
15AR	0.46	0.11	6.50E-4	2.06E-3	4.55E-6	32.8	5.53E- 12

Table 2.14: Sensitivity of a and b to input variables for sample 1A.

Input Variable	a	b [m^{2}s^{-1}]
Original	13.6	6.76E-7
5% ↑ θ_s	11.0	1.44E-6
5% ↑ θ_n	14.0	5.76E-7
5% ↑ S	16.0	2.65E-6
5% ↑ λ	11.9	1.43E-6

2.4.3 $D(\theta)$ CALCULATED FROM RETENTION CURVE DATA

The water retention characteristic curves are summarized using Van Genuchten's (1980) expression (2.23) relating θ to h. The transformed data for the water retention variables θ_s, θ_r, α, n, $\sum \zeta^2$ and ρ_b are presented in appendix B, Tables B.7 and B.8. Summary statistics for the water retention variables are given in Table 2.15. The histograms of θ_s, θ_r and n for the A_p and lower horizons display similar distributions, but values of α for the lower horizons are more variable than in the A_p horizon. Example plots of the water retention data and the corresponding curves from (2.23) are shown in Fig. 2.19. The good fit of (2.23) is indicated by the low $\sum \zeta^2$ in θ (Table 2.15). The magnitude of measurement error in the water retention measurements is indicated by the differences in the replicate θ at 2.5 kPa. Average differences in the replicate θ at 2.5 kPa are 0.04 and 0.01 m^{3}m^{-3} for the A_p and lower horizons respectively.

Example diffusivity characteristics calculated from (2.28) and the corresponding measured $D(\theta)$ functions are shown in Figs. 2.20 and 2.21 for samples with the 50th percentile values of a and b. The discrepancy between the measured and calculated values of $D(\theta)$ are 1–3 orders of magnitude. The calculated $D(\theta)$ functions are desorption curves, while the measured $D(\theta)$ functions are absorption curves. Additionally, in the calculation of $D(\theta)$, K_s in (2.28) is assumed equal to K_{-2} measured for absorption. By definition, the diffusivity function is given by

$$D(\theta) = K(\theta) h \frac{d(\ln h)}{d\theta} \qquad (2.36)$$

$K(\theta)$ measured for a range of soil textures show no noticeable hysteresis (Scotter and Clothier, 1983; Topp, 1971; Elrick and Bowman, 1964). Based on measured water retention curves from Scotter and Clothier (1983), Topp (1971), Poulovassilis (1970) and Elrick and Bowman (1964) $\frac{d(\ln h)}{d\theta}$ is similar for sorption and desorption cycles. Thus hysteresis in $D(\theta)$ can be estimated from differences in h between sorption and desorption

Table 2.15: Summary of the output from the water retention data.

Variable	Horizon	n	Mean	Median	SD	Skew	Max	Min
θ_s	A_p	22	0.52	0.52	0.039	0.67	0.63	0.47
	B	5	0.56	0.52	0.068	0.65	0.65	0.49
	C	17	0.51	0.52	0.067	-0.50	0.61	0.38
	Lower	22	0.52	0.52	0.069	-0.28	0.65	0.38
θ_r	A_p	22	0.04	0.03	0.040	0.55	0.12	0.00
	B	5	0.06	0.00	0.093	1.32	0.21	0.00
	C	17	0.02	0.00	0.46	2.60	0.16	0.00
	Lower	22	0.03	0.00	0.060	2.13	0.21	0.00
α	A_p	22	3.10E-3	3.14E-3	6.44E-3	0.29	4.62E-3	1.96E-3
	B	5	2.77E-3	2.80E-3	1.34E-3	-0.14	4.59E-3	8.72E-3
	C	17	2.57E-3	2.02E-3	2.54E-3	1.97	1.02E-2	2.59E-4
	Lower	22	2.62E-3	2.26E-3	2.29E-3	1.93	1.02E-2	2.59E-4
n	A_p	22	1.37	1.35	0.086	0.75	1.58	1.25
	B	5	1.35	1.31	0.128	2.03	1.58	1.26
	C	17	1.32	1.27	0.124	1.50	1.65	1.20
	Lower	22	1.33	1.30	0.123	1.42	1.65	1.20
$\sum \zeta^2$	A_p	22	6.46E-4	4.77E-4	4.27E-4	0.71	1.59E-3	9.57E-5
	B	5	1.04E-3	6.11E-4	6.20E-4	0.60	1.73E-3	5.52E-4
	C	17	7.85E-4	6.43E-4	5.27E-4	0.94	2.00E-3	2.07E-4
	Lower	22	8.43E-4	6.27E-4	5.45E-4	0.80	2.00E-3	2.07E-4
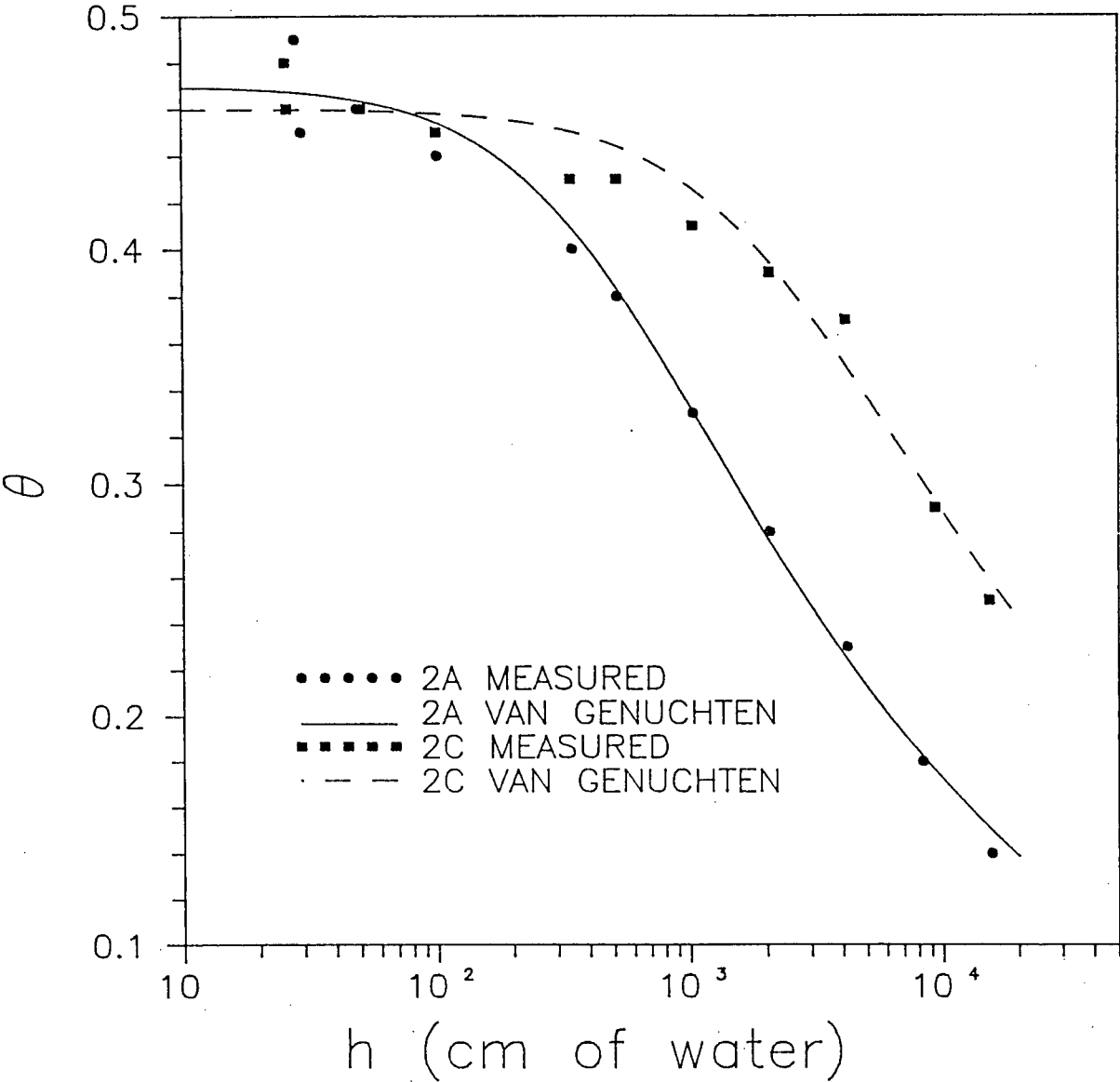
Figure 2.19: Example plots of the water retention characteristic curves.
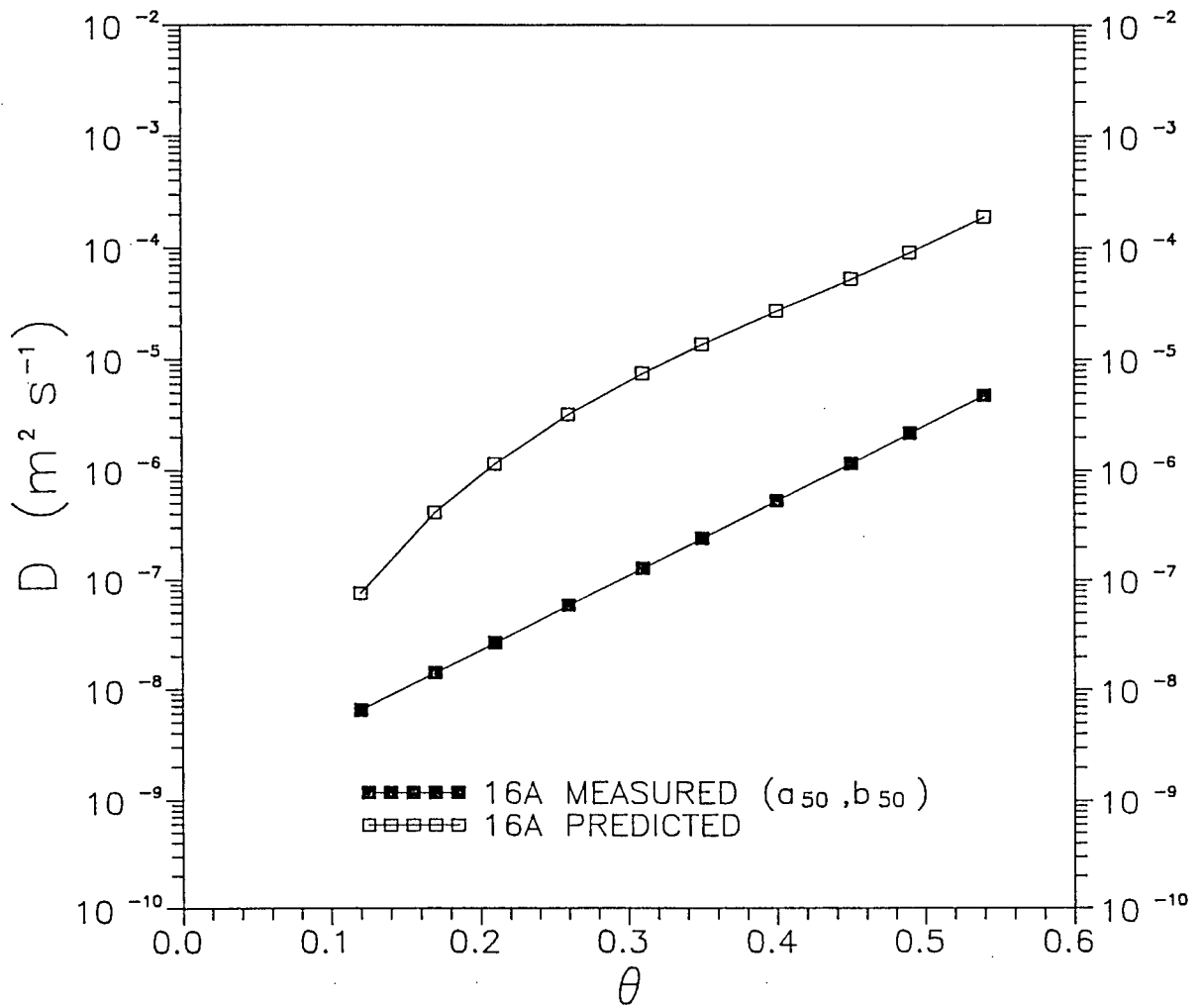
Figure 2.20: Measured and predicted $D(\theta)$ for 50th percentile values of a and b of the A_p horizon.
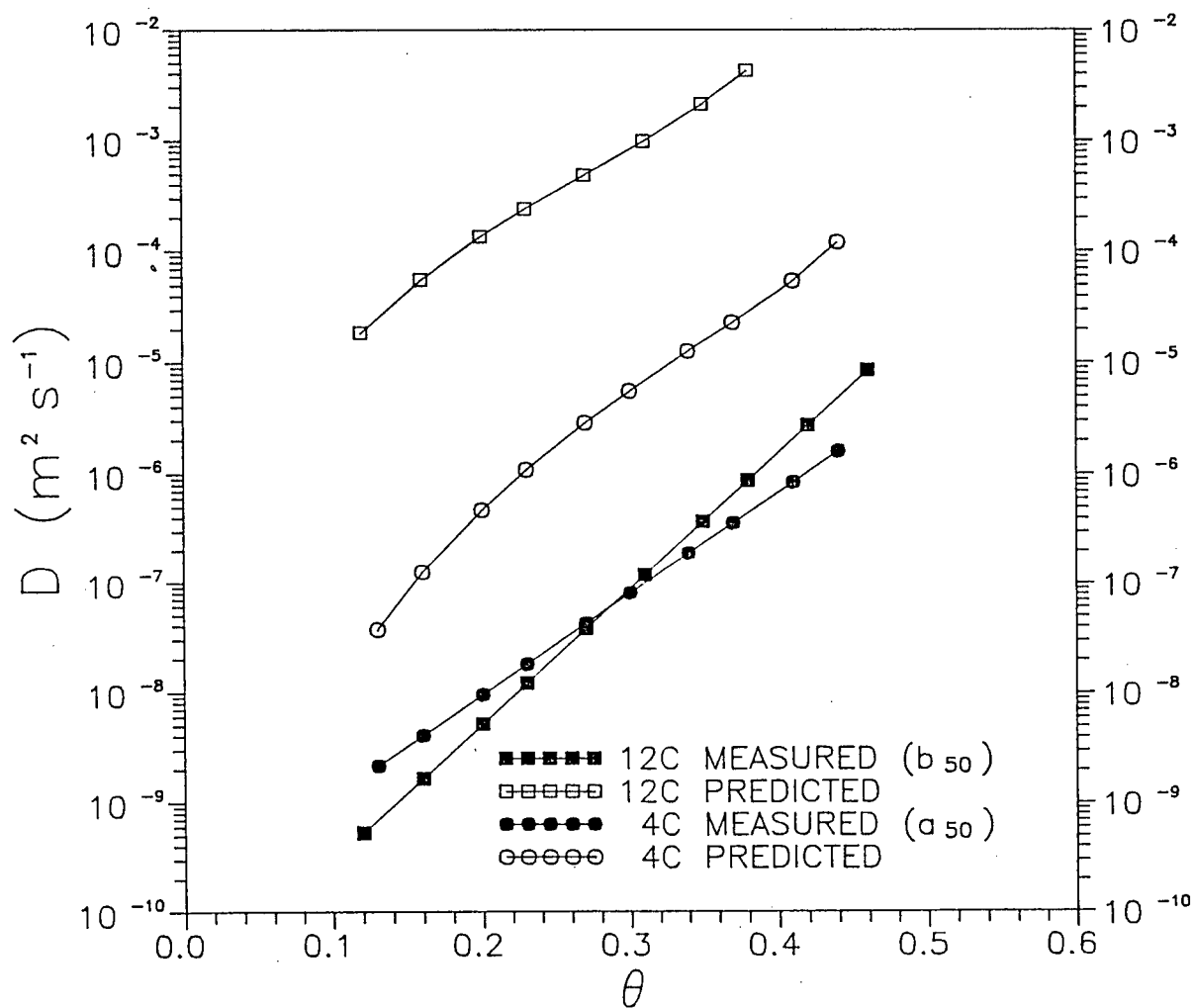
Figure 2.21: Measured and predicted $D(\theta)$ for 50th percentile values of a and b of the lower horizons.

cycles. Based on hysteretic water retention data from Scotter and Clothier (1983), Topp (1971), Staple (1965) and Elrick and Bowman (1964), $D(\theta)$ for desorption may be up to an order of magnitude greater than for sorption.

Additional differences between calculated and measured values of $D(\theta)$ may be due to errors in the input variables. For some samples (e.g. 1A) θ_{-2} is greater than θ_s. In order to calculate $K(\theta)$ over the range from θ_n to θ_{-2}, θ_s is set equal to θ_{-2}. The sensitivity of (2.25) to changes in the input variables is tested by increasing the input variables by 5% and recalculating $K(\theta)$. As an example, results for core 1A are presented in Table 2.16. $K(\theta)$ is calculated for θ at $h = 100$ kPa . The effects of increasing the input variables and of setting $\theta_s = \theta_{-2}$ on $K(\theta)$ are seen to be small.

Attributing an order of magnitude increase in the calculated $D(\theta)$ to hysteresis effects, the discrepancy between measured and calculated $D(\theta)$ is still large for some samples. The Mualem (1976) model for predicting $K(\theta)$ generally gives reliable predictions, but may overestimate $K(\theta)$ by up to 2 orders of magnitude for some soils (Mualem, 1976). The calculated $D(\theta)$ functions have similar slopes to measured $D(\theta)$ functions and if matching were done at $D(\theta_s)$ a good fit would be generated.

Table 2.16: Sensitivity analysis for $K(\theta)$ calculated from retention curve data.

Variable	$K(\theta)$
Original	6.57E-9
5% ↑ θ_r	6.57E-9
5% ↑ θ_s	4.10E-9
5% ↑ m	8.68E-9
5% ↑ K_{-2}	6.89E-9
$\theta_s = \theta_{-2}$	4.39E-9

2.5 CONCLUSIONS

The sorptivity tube device provides a simple method for obtaining S, λ^* and K_{-2}. Measured values of i and x^* depend on $t^{1/2}$ as expected from the constant-concentration absorption theory. However, core drying was necessary for gravity effects to be negligible. The $D(\theta)$ functions determined from constant-concentration absorption theory display high variability in a and b, especially in the lower horizons.

The Van Genuchten (1980) $\theta(h)$ expression provides a good fit to the water retention data. The $D(\theta)$ functions calculated from the Mualem model and the Van Genuchten (1980) water retention expression are at least 1–2 orders of magnitude greater than the measured functions. Hysteresis effects explain 1-order of magnitude increase in $D(\theta)$, but without matching at $D(\theta_s)$ the predictions are poor.

Chapter 3

RUNOFF GENERATION AT THE MAHAL FARM

3.1 INTRODUCTION

Runoff may be generated when the soil becomes saturated at the surface (Dunne runoff) or when the precipitation intensity is larger than the infiltrability of the soil (Hortonian runoff). The objective of this chapter is to determine whether typical rainfall events for the Lower Fraser Valley will generate runoff on a typical Whatcom soil. Constant-flux infiltration theory and the soil hydraulic properties determined in Chapter 2, are used to generate soil moisture profiles over time. Rainfall intensities, durations and return periods required to generate runoff for the sampled cores are compared to precipitation data for the Abbotsford airport and to storms known to cause runoff and soil loss at the Mahal farm. To evaluate soil moisture conditions between rainfall events, drainage for each core is estimated from a unit gradient model.

3.2 THEORETICAL BACKGROUND

3.2.1 CONSTANT-FLUX INFILTRATION

The soil water flow equation governing $z(\theta, t)$ for a homogeneous soil is given by (Philip, 1969)

$$-\frac{\partial z}{\partial t} = \frac{\partial}{\partial \theta}\left(\frac{D}{\frac{\partial z}{\partial \theta}}\right) - \frac{\partial K}{\partial \theta} \tag{3.1}$$

64

where z is the vertical distance. Initially $(t = 0)$ the soil is assumed to be uniformly wet, i.e.

$$\theta(z, 0) = \theta_n \tag{3.2}$$

For a semi-infinite soil

$$\lim_{\theta \to \theta_n} z(\theta, t) = \infty \tag{3.3}$$

The constant-flux surface boundary condition is given by

$$-\frac{D(\theta_0)}{\frac{\partial z}{\partial \theta}(\theta_0, t)} + K(\theta_0) = R \tag{3.4}$$

where $\theta_0 = \theta(0, t)$ and R is the constant flux. According to White (1979) the solution of (3.1) subject to (3.2), (3.3) and (3.4) can be written implicitly as

$$z = \int_\theta^{\theta_0(t)} \frac{D(\theta)}{F(\theta, t)\left[R - K(\theta_n)\right] - K(\theta) + K(\theta_n)} d\theta \tag{3.5}$$

and the time dependence of the surface moisture content is given by

$$[R - K(\theta_n)]t = \int_{\theta_n}^{\theta_0(t)} \frac{(\theta - \theta_n)D(\theta)}{F(\theta, t)[R - K(\theta_n)] - K(\theta) + K(\theta_n)} d\theta \tag{3.6}$$

The solution is not sensitive to F, so that we can assume $F(\theta, t) \approx F(\Theta)$, where

$$\Theta = (\theta - \theta_n)/(\theta_0(t) - \theta_n) \tag{3.7}$$

The dependence of F on t is then implicitly via $\theta_0(t)$ in Θ. According to White (1979), for large β at $t \to \infty$

$$F(\Theta) \approx \Theta \tag{3.8}$$

The upper bound to $F(\Theta)$ occurs with a linear soil (constant D) which according to White et al. (1979) can be closely approximated by

$$F(\Theta) \simeq \Theta^{2-4/\pi} \tag{3.9}$$

For $\beta = 0$, $F(\Theta)$ is given by (3.9). For $\beta \geq 8$, $F(\Theta)$ is assumed equal to (3.8). For $0 < \beta < 8$ the change in $F(\Theta)$ with β is estimated by

$$F(\Theta) = \Theta^{2-4/\pi}\left(\frac{8-\beta}{8}\right) + \Theta\frac{\beta}{8} \qquad (3.10)$$

Calculations of moisture profiles over time were done using a Fortran program (appendix E) and the University of British Columbia mainframe computer.

3.2.2 DRAINAGE CALCULATION

Assuming a unit gradient in the hydraulic head throughout the soil, the equation governing the one-dimensional flow of water is given by (Sisson et al., 1980)

$$\frac{\partial\theta}{\partial t} = -\frac{dK}{d\theta}\frac{\partial\theta}{\partial z} \qquad (3.11)$$

Considering only the drainage phase, (3.11) may be solved subject to the conditions

$$\theta(z,0) = \theta_s \qquad (3.12)$$

and
$$\theta(0,t) = \theta_m \qquad (3.13)$$

i.e. θ at $z = 0$ instantaneously declines to θ_m, where θ_m is the minimum obtainable θ and the soil is infinitely deep. The initial-value problem given by (3.11), (3.12) and (3.13) is a Cauchy-Riemann or characteristic-value problem (Sisson et al., 1980; Aris and Amundson, 1973; Lax, 1972). According to Sisson et al. (1980) the solution of (3.11) subject to (3.12) and (3.13) is

$$\theta = \theta_s \qquad t \leq \frac{z}{\frac{dK}{d\theta}(\theta_s)} \qquad (3.14)$$

$$\frac{z}{t} = \frac{dK}{d\theta}(\theta) \qquad \frac{z}{\frac{dK}{d\theta}(\theta_s)} \leq t \leq \frac{z}{\frac{dK}{d\theta}(\theta_m)} \qquad (3.15)$$

$$\theta = \theta_m \qquad t \geq \frac{z}{\frac{dK}{d\theta}(\theta_m)} \qquad (3.16)$$

where z is the depth of the draining front and

$$\frac{d^2 K}{d\theta^2} > 0 \tag{3.17}$$

$K(\theta)$ from 2.25 appears to satisfy 3.17. Substitution of the expression for $dK/d\theta$ from (2.25) into (3.15) yields

$$\frac{z}{t_d} = \frac{K_s}{\theta_s - \theta_m} \left\{ 2\Theta^{1/2}[1 - (1 - \Theta^{1/m})^m][(1 - \Theta^{1/m})^{m-1}][\Theta^{1/m-1}] + \frac{1}{2}[1 - (1 - \Theta^{1/m})^m]^2 \right\} \tag{3.18}$$

where t_d is the time required to drain a soil from θ_s to θ at a given z and

$$\Theta = \frac{\theta - \theta_m}{\theta_s - \theta_m} \tag{3.19}$$

A Fortran program (appendix F) and the University of British Columbia mainframe computer were used to calculate t_d.

3.3 RESULTS

3.3.1 FIELD MOISTURE CONDITIONS

In Chapter 1, it was shown that erosion rates at the Mahal farm are initially low in September and October, are high between November and January, and decline from January to March. Runoff coefficients increase when the moisture content of the soil prior to the rainfall event increases. The volumetric water content of the soil as determined at the study site on April 18, 1986, February 9, 14 and 25, March 31, and September 12, 1987 (Table 3.1). The April 18 values were determined for the infiltration cores collected in the A_p, B and C horizons. The moisture content for each core was calculated from the initial core weight, oven dry weight and bulk density. Moisture contents were measured gravimetrically at the 22 sampling sites from February to March, 1987 using moisture tins. In February, θ at depths greater than 15 cm were not measured. Walking on the

Table 3.1: Moisture conditions at the Mahal farm from September to April.

	Median θ [$m^3 m^{-3}$]	
	A_p	Lower
Apr. 18/86	0.42	0.40
Feb. 09/87	0.54 [a]	
Feb. 14/87	0.53[a]	
Feb. 25/87	0.52[a]	
Mar. 31/87	0.49	0.39
Sep. 12/87	0.36	0.40
f	0.59	0.53
θ_{-2}	0.49	0.45
$\theta_{-2} - \theta_{inSep}$	0.13	0.05

[a]possible sampling error

field was difficult due to the wet conditions and holes dug into the soil would fill with water making gravimetric sampling difficult. Free water was often sampled with the soil producing error in θ and unrealistic values as noted in Table 3.1. In March soil pits were dug at each site and gravimetric moisture contents were measured in the A_p, B and C horizons. In September, θ was determined gravimetrically at 11 locations scattered over the field, which do not correspond to the sampling sites.

In calculating runoff, a range of initial θ (θ_n) from dry to wet conditions are of interest. $\theta_n = \theta_{-2}$ is used to represent initially wet conditions. The lowest values of θ measured were in September and these are used to represent initially low values of θ_n. The median values of θ measured in September for the A_p and lower horizons may be greater than θ_{-2} for some of the soil cores. Therefore, for each core θ_n is estimated by subtracting the average difference between θ_{-2} and the September values of θ. The average differences for the A_p and lower horizons are 0.13 and 0.05 $m^3 m^{-3}$ respectively (Table 3.1).

Theoretically, when $\theta_0(t)$ reaches θ_s ponding will occur, and assuming negligible surface storage, runoff will be generated. In the constant-flux infiltration model, θ_s is assumed equal to θ_{-2}. The February values of θ are greater than θ_{-2} (Table 3.1). Some

of the difference may be accounted for by sampling error due to the wet field conditions. θ_{-2} is generally less than the calculated porosity (Tables B.1 to B.4). Poulovassilis (1970) found that for his wetting curves, $\theta_s \approx 0.85f$ due to air entrapment. Table 3.2 lists ρ_b, f and $0.85f$ for the minimum, 50th percentile and maximum values of θ_{-2}. The results show that for the Mahal soil, $\theta_{-2} \approx 0.85f$. Additionally, wetting scanning curves for sand and silt loams indicate that θ_{-2} is very near θ at 0 cm of water tension (Topp, 1971; Poulovassilis, 1970; Staple, 1965). Setting $\theta_s = \theta_{-2}$ in the constant-flux infiltration model is considered to be a good approximation, but runoff generation may be overestimated.

Table 3.2: Range in θ_{-2}, $0.85f$, ρ_b and f for the A_p and lower horizons.

Variable	Sample	θ_{-2}	$0.85f$	ρ_b [kg m^{-3}]	f
θ_{-2}min	4A	0.37	0.43	1238	0.51
θ_{-2}50	14A	0.50	0.50	1041	0.59
θ_{-2}max	17A	0.54	0.54	912	0.64
θ_{-2}min	16C	0.31	0.28	1734	0.33
θ_{-2}50	4C	0.44	0.41	1356	0.48
θ_{-2}max	10C	0.54	0.57	861	0.67

3.3.2 RUNOFF GENERATION

To estimate runoff generation at the Mahal site, infiltration into the A_p and lower horizons are considered separately. The hydraulic properties for each core are used to calculate hypothetical moisture content profiles over time for constant-flux infiltration. For the A_p horizon cores, no influence of the underlying soil is considered. For the lower horizon cores, the overlying soil is removed. Differences between infiltration into the hypothetical profiles are used to qualitatively assess the effects of layering on infiltration.

To determine if gravity effects were important for the moisture conditions measured

between September and April, the constant-flux infiltration solution was calculated with and without gravity terms. Excluding the gravity terms in the constant-flux infiltration model reduced the infiltration rate and the advance of the wetting-front. For θ measured in the field, even in September, gravity effects cannot be neglected and the $dK/d\theta$ term in (3.1) must be retained.

For runoff to be generated, $R > K_s$ is required. K_s is assumed equal to K_{-2}. As the actual K_s may be greater than K_{-2} due to macropores, the values of R that will generate runoff will be minimum values. The distributions of K_{-2} for the A_p and lower horizons are shown in Figs. 3.1 and 3.2. For a given R, the minimum storm duration (t_s) which will generate runoff is given by the time when $\theta_0(t) = \theta_{-2}$. A return period (T) for each storm is then calculated from

$$T = \left(\frac{It_s^{0.48}}{10.8}\right)^{3.6} \tag{3.20}$$

where I is the rainfall intensity [mm h^{-1}], T is the return period [yr] and t_s is the storm duration [h]. The parameters $10.8, 0.28$ and 0.48 were estimated directly from the 1977–1986 intensity-duration curves from the Abbotsford Airport.

Example moisture content profiles over time are shown in Fig. 3.3. For the September values of θ_n, the values of R, t_s, T and x^* for some rainfall events which generate runoff are shown in Table 3.3. Samples with the minimum, 50th percentile and maximum values of K_{-2} for the A_p and lower horizons are listed. Typically, high intensity, short duration storms with long return periods are required to generate runoff.

February values of θ (Table 3.1) suggest that θ remains near saturation over much of the winter. For saturated conditions runoff will be generated when $R > K_{-2}$ and the constant-flux infiltration model is not required to predict runoff. Whether runoff is generated at the Mahal farm for saturated conditions is dependent on the intensity of rainstorms in the region. Continuously recording rain gauge data at the Mahal site are
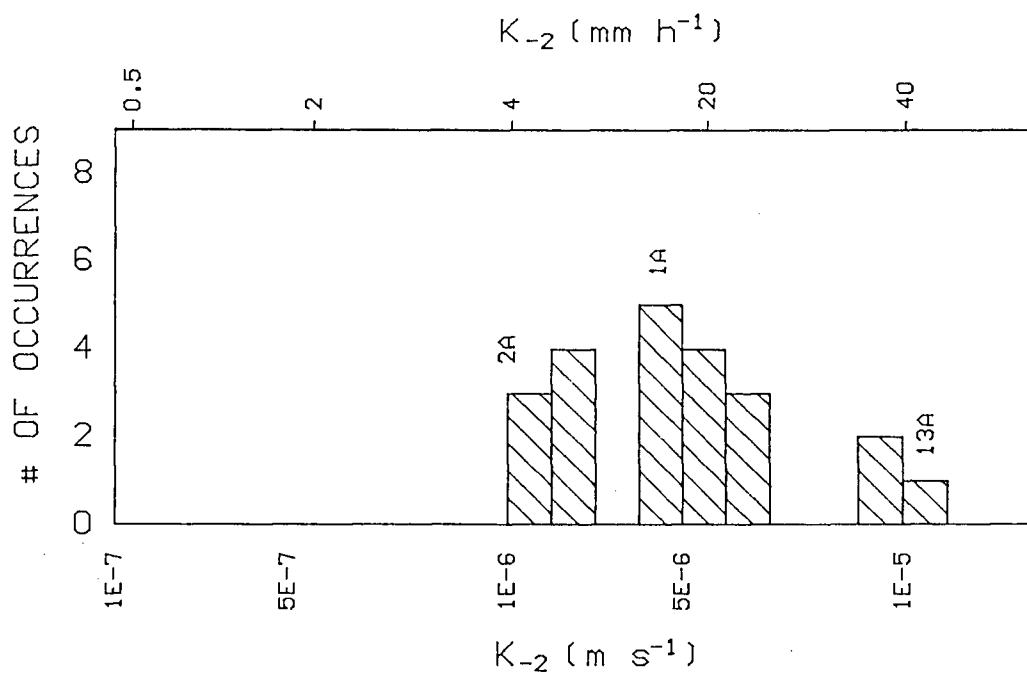
Figure 3.1: The distribution of K_{-2} for the A_p horizon.
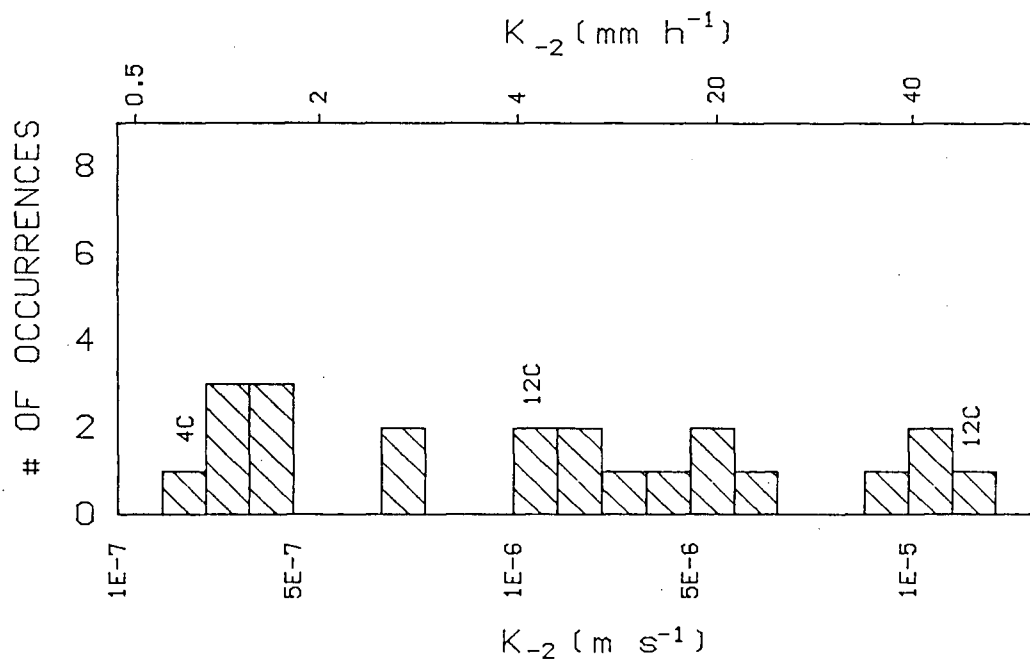
Figure 3.2: The distribution of K_{-2} for the lower horizons.
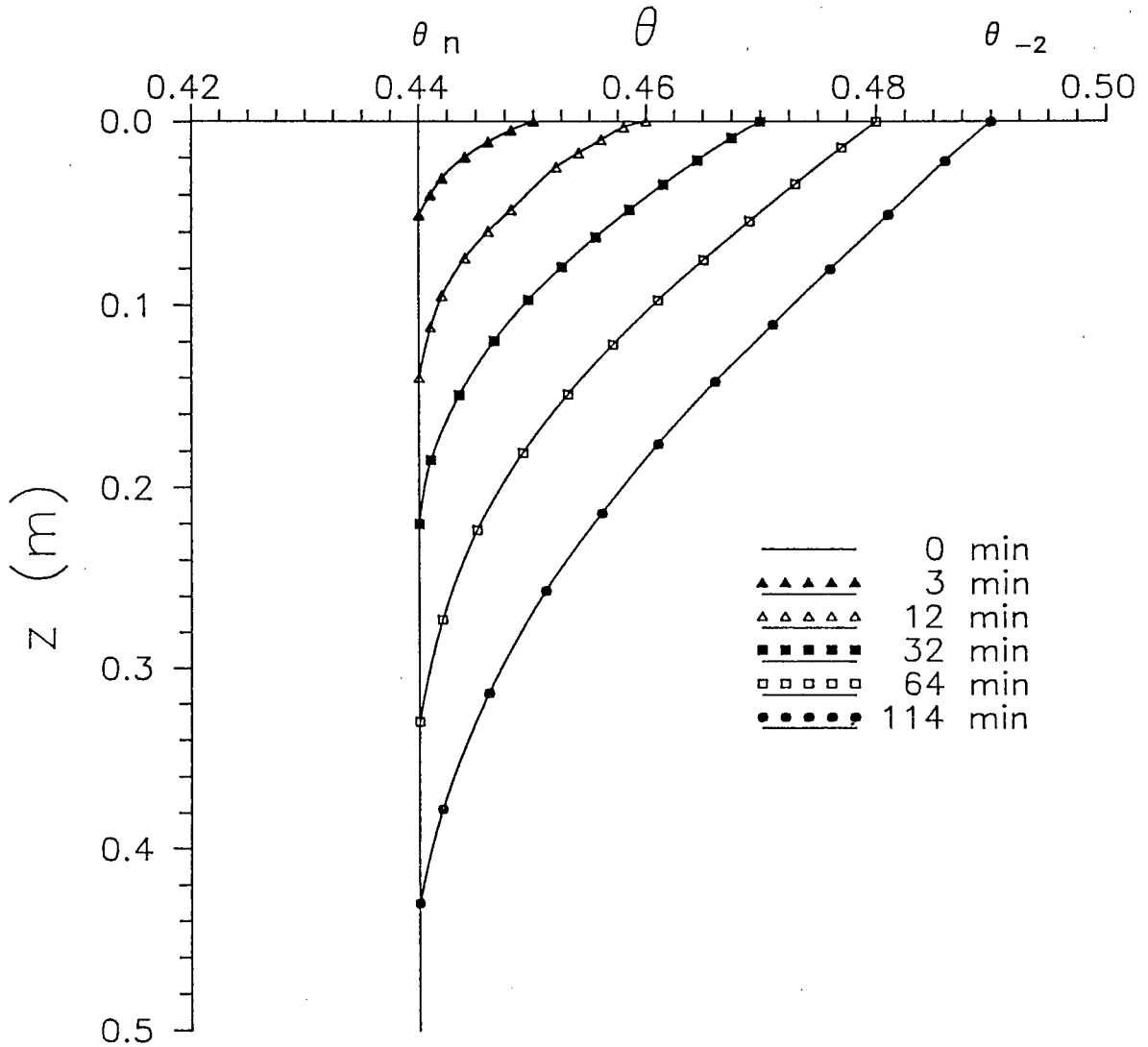
Figure 3.3: Example infiltration moisture content profiles over time for $R = 20$ mm h^{-1}.

Table 3.3: Rainfall intensity, duration and return periods generating runoff for September values of θ_n.

Variable	Sample	K_{-2} [mm h^{-1}]	R [mm h^{-1}]	t_s [min]	T [days]	x^* [m]
K_{-2}min	2A	5.5	6.6	1717	20255	1.03
			13.8	118	1262	0.22
K_{-2}50	1A	16.7	20.1	114	54745	0.45
K_{-2}max	13A	54.0	64.8	82	3.96E5	0.47
K_{-2}min	4C	0.9	1.08	9967	620	2.02
			2.25	513	24	0.42
			4.5	34	6	0.11
			9.0	7	4	0.05
K_{-2}50	12C	5.7	68.3	12	17245	0.14
			142.2	<1	620	0.03
			284.4	<1	155	0.01
K_{-2}max	17C	74.9	89.9	3200	7.09E8	47.19

available for September, 1983 to March 1984 (Wood, 1984) and are assumed to represent typical winter rainfall data at the study site. For the majority of storms I was < 5.5 mm h^{-1}, the minimum K_{-2} for the A$_p$ horizon, and only 4 storms were recorded with I > 5.5 mm h^{-1}. The maximum I recorded during a storm was 10 mm h^{-1} for a 0.5 h duration.

Some storm intensities and durations generating soil loss on the plot studies (Wood, 1984) from October 1983 to March 1984 are given in Table 3.4. In September and October, runoff and erosion are low, but some soil loss was measured for storms with maximum intensities less than 2.7 mm h^{-1}. For September values of θ_n, a 3.1 mm h^{-1}, 7.5 h duration storm will not generate runoff for any soil core; and a 4.5 mm h^{-1}, 2 h storm will generate runoff for only 6 lower horizon cores.

Runoff and erosion between November 1983 and March 1984 (Table 3.4) was measured for individual storms with maximum I as low as 2.3 mm h^{-1}. For saturated conditions and I < 2.3 mm h^{-1}, none of the A$_p$ core and only 7 lower horizon cores can potentially

Table 3.4: Storm intensities and durations generating soil loss for plot studies.

Date	# Storms	Max. I		Storm		Soil Loss
		I [mm h^{-1}]	t [h]	Ave. I [mm h^{-1}]	t [h]	[t ha^{-1}]
Oct. 17, 1983	1	2.7	1.5	1.5	9	0.001
Oct. 21	1	4.5	2	3.1	7.5	0.002
Nov. 14–16	1	5.0	1	1.8	43	1.091
Nov. 24–25	2	3.0	2	1.4	9	
		8.0	3	2.9	12	0.604
Nov. 26	1	2.3	6	1.5	18	0.260
Jan. 04, 1984	1	7.0	1	2.0	6	2.318
Feb. 14–20	3	3.5	1	1.2	10	
		1.2	6	1.2	6	
		2.7	6	1.3	34	0.999
Mar. 25	1	3.2	3	2.2	6	0.269
Mar. 28	1	10.0	0.5	1.6	10	0.217

generate runoff. For the storm with the maximum recorded I (10 mm h^{-1}) only 6 A$_p$ horizon cores and 13 lower horizon cores can potentially generate runoff (Figs. 3.1 and 3.2).

3.3.3 DRAINAGE CALCULATION

To estimate moisture contents between rainfall events at the Mahal site, drainage of the A$_p$ and lower horizons are considered separately, as in section 3.3.2 for infiltration. Differences between the times required to drain the hypothetical profiles are used to qualitatively assess the effects of layering on drainage.

The moisture content during drainage versus time for the A$_p$ and lower horizon samples corresponding to the minimum, 50th percentile and maximum values of K_{-2} are shown in Figs. 3.4 and 3.5. The residual moisture content at the surface is assumed equal to the air-dry moisture content. For comparative purposes, drainage at $z = 0.2$ m
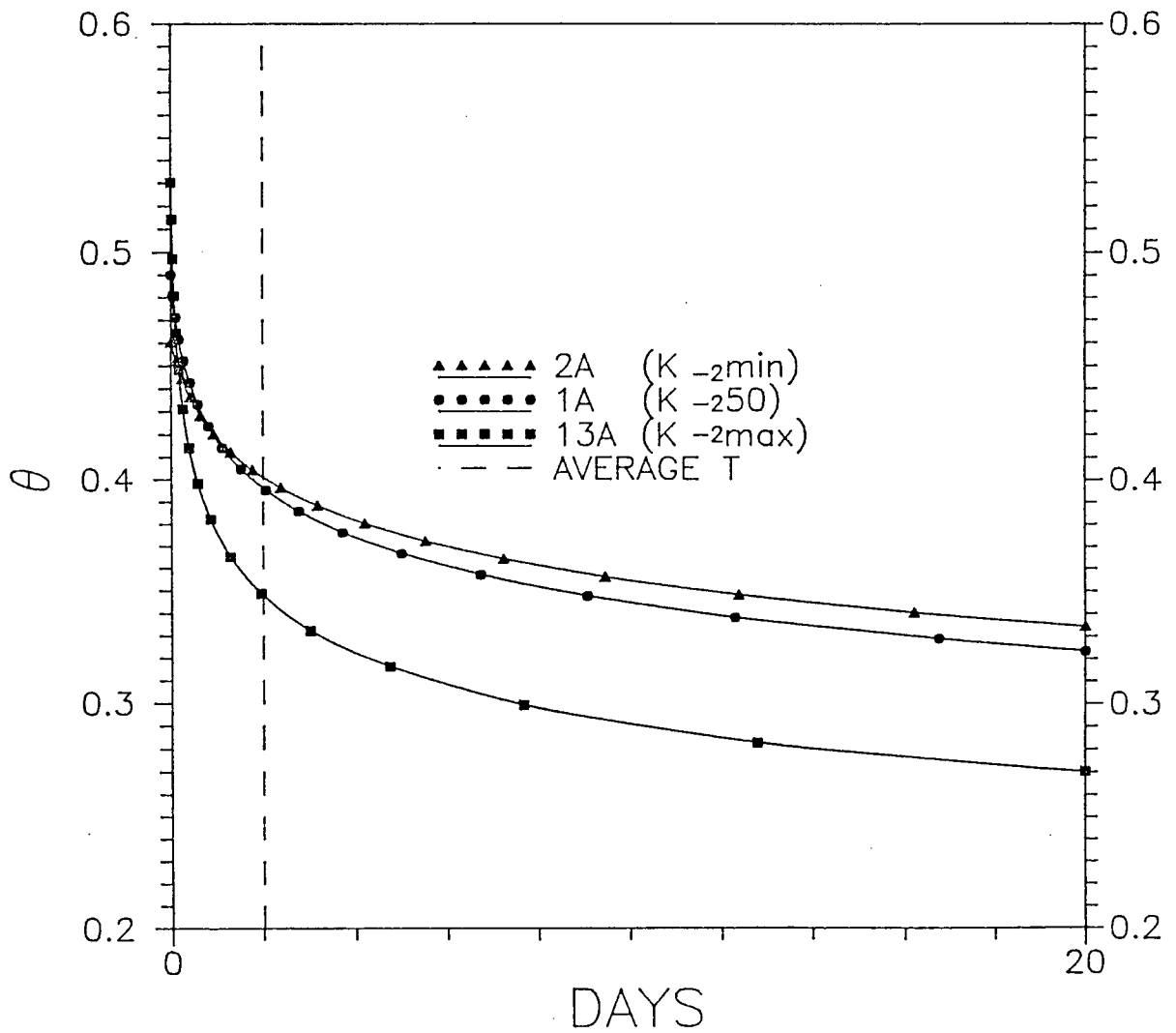
Figure 3.4: Soil drainage over time for the A_p horizon.
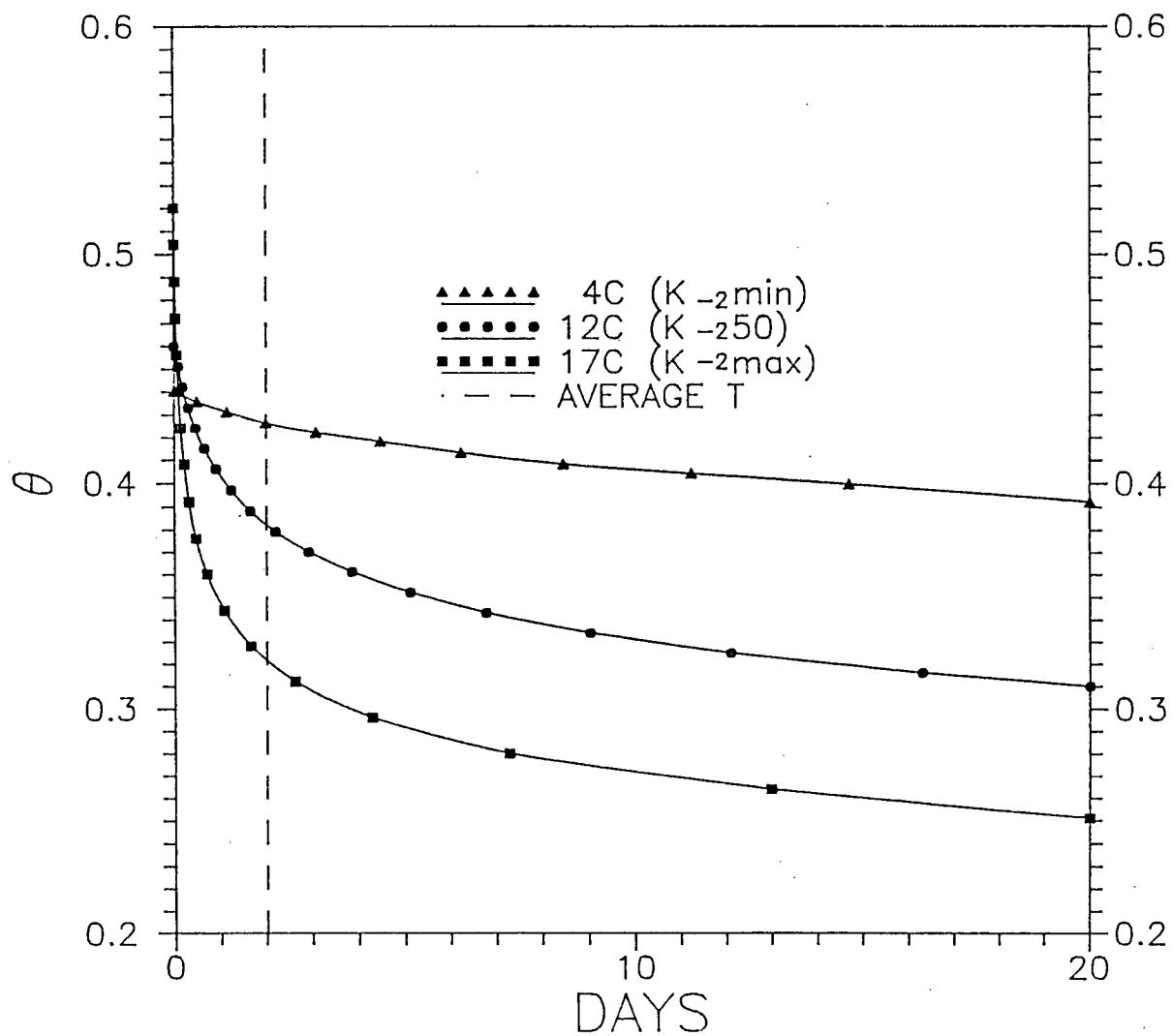
Figure 3.5: Soil drainage over time for the lower horizons.

is shown. The time required to drain cores 1A and 12C (typical A_p and lower horizon cores) from θ_{-2} to September values of θ are 5 and 0.5 days respectively.

The sensitivity of (3.18) to changes in the input variables is tested by increasing the input variables 5% and recalculating t_d. As an example, results for core 1A are presented in Table 3.5. In the original calculation, drainage at $z = 0.2$ m is shown with a residual moisture content equal to air-dried and a final moisture content of $\theta_s - 0.13$. θ_m is actually greater than the assumed air-dry value. The unit gradient drainage model is fairly sensitive to 5% increases in the input variables but drainage is still quite rapid.

Table 3.5: Sensitivity of the unit gradient drainage model to changes in input variables for sample 1A.

Variable	t_d [days]
Original	5.0
5% $\uparrow m$	3.1
5% $\uparrow K_{-2}$	4.8
5% $\uparrow z$	5.2
5% $\uparrow \theta$	2.9
5% $\uparrow \theta_s$	8.6
4% $\uparrow \theta_m$	4.4

The average time between rainfall events limits the time available for soil drainage. From the continuously recording rain gauge data at the Mahal farm (Wood, 1984) the average time between rainfall events from September until March is approximately 2 days. Values of θ predicted after two days of drainage are typically 0.40 and 0.38 for the A_p and lower horizons respectively. These moisture contents are near April values of θ (Table 3.1) and contradict values of $\theta \approx \theta_{-2}$ measured in February. In February the field was very muddy and walking was difficult while on April 19, the field was ploughed. The drainage calculation assumes unit gradient drainage at infinite depth. A water table or

a layer of restricted drainage at depth will slow drainage and θ would be increased.

3.4 DISCUSSION

Rainfall, runoff and soil loss measurements (Wood, 1984) indicate that runoff is low in September and October but considerable runoff and soil loss are generated from November to January. Most runoff appears to occur after the soil moisture content increases in the fall. Storms with relatively low intensities generate considerable erosion. For rainfall events known to cause runoff and erosion, runoff is not predicted for most A_p horizon cores. Infiltration may be restricted at some sites by the lower horizon, especially with high antecedent moisture contents, but runoff is not predicted at many sites.

Between rainfall events, the unit gradient drainage model predicts typical values of θ of 0.40 and 0.38 in the A_p and lower horizons respectively (3.4 and 3.5). Moisture contents measured at the Mahal farm suggest limited drainage between rainfall events. If θ predicted by the unit gradient drainage model is correct the constant-flux infiltration results indicate that runoff would be negligible. The rainfall, runoff and soil loss measurements suggest that factors other than those measured are contributing to the runoff observed in the field. Wheel compaction, surface sealing, topography, subsurface seepage and restricted soil-air movement may contribute to runoff in the field.

Wheel compaction may reduce infiltration on trafficked interrows by 30%–50% compared with rows and non-trafficked interrows (Cassel, 1983; Lindstrom and Voorhees, 1980). An increase in surface runoff is attributed to the reduced infiltration capacity of the compacted soil and the channelling effect of the wheeling (Bender, 1987; Martin, 1979). The effects of tractor wheelings on rill erosion are evident from the first year of cultivation. In 1981-1982, when strawberries were planted up and down the slope, rills occurred mainly in the trafficked interrows. In the 1985 growing season the Mahal site

was cultivated across the slope and cauliflower was left in the field to rot over the winter. Tillage was not precisely along the contour and gradients along interrows transported water to low spots. Rills formed in between rows along the secondary slope (Fig. 3.6), and along the main slope where water collected in low spots (Fig. 3.7). In the fall of 1986, the cauliflower crop was turned under parallel to the main slope. Rill spacing corresponds to the wheel tracks (Fig. 3.8) and rill direction follows the tractor wheelings (Fig. 3.9).

Figure 3.6: Rill formation in trafficked interrows along the secondary slope, 1985-1986.

In the fall of 1986 a cover crop of winter rye grass was planted at the Mahal farm. Cover crops are effective in reducing erosion (Meyer, 1985; Hussein and Laflen, 1982), but the vegetation should cover at least 70% of the ground surface to give adequate protection (Elwell and Stocking, 1976). An adequate cover crop was not achieved at the Mahal site (Fig. 1.2) and surface sealing was visually evident (Fig. 3.10). High intensity rainfalls (50–70 mm h^{-1}) are generally associated with the formation of soil crusts with

Figure 3.7: Rill formation along the main slope in low spots, 1985-1986.

reduced hydraulic conductivities (Morin et al., 1981; Hoogmoed and Stroosnijder, 1984; Morin and Benyamini, 1977; Hillel and Gardner, 1969). However, McIntyre (1958) noted crusting and reduced permeability of up to 1 order of magnitude in loam soils subjected to rainfalls of 2.6 mm h^{-1} in intensity. In the Abbotsford region, rainfall with intensities greater than 40 mm h^{-1} and durations longer than 30 minutes have return periods greater than 25 years (AES, 1987). However, storms with intensities of 2–10 mm h^{-1} occur frequently and may wash fines into interrows to form a surface seal with reduced infiltrability.

Figure 3.8: Rill spacing corresponding to wheel tracks, 1986-1987.

Figure 3.9: Rill direction affected by tractor wheelings, 1986-1987.

Figure 3.10: Surface sealing at the Mahal site.

Runoff and subsurface seepage from the farm upslope of the study area may transport additional water to the site and contribute to the wet field conditions observed over winter. The ditch between the 2 farms is poorly maintained and free water was observed in sampling unit 1 (Fig. 2.1) over much of the winter.

The low tension absorption procedure allows for the escape of soil-air. Restricted soil-air movement in the field may reduce infiltration by up to 55% (Suhr et al. 1984; Dixon and Linden, 1977). Field conditions usually prevent the free escape of soil-air. A restricting zone may be a layer or horizon of lower permeability or may be due to an increase in moisture content with depth (Youngs and Peck, 1964). Field values of θ for the lower horizons appear to be less than the A_p horizon except in the fall (Table 3.1). Median values of K_{-2} for the lower horizon cores are similar to the A_p horizon cores. Restricted soil-air movement is not expected to effect infiltration at the Mahal farm.

3.5 CONCLUSIONS

High field moisture contents necessitate the inclusion of gravity effects during infiltration modelling. For September moisture contents the rainfall intensities necessary to generate runoff are infrequent and low in volume. For saturated moisture conditions runoff generation is dependent on values of $R > K_{-2}$. The majority of storms measured at the Mahal farm have maximum $I < 5.5$ mm h^{-1}. For rainfall intensities known to cause runoff and erosion, runoff is not predicted for most A$_p$ horizon cores. Infiltration may be restricted at some sites by the lower horizon, especially at high antecedent moisture contents, but runoff is not predicted at many sites. The average time between rainfall events from September to March was approximately 2 days. A rapid decrease in θ between rainfall events is predicted by the unit gradient model, but θ measured at the Mahal farm suggests limited drainage between rainfall events. If the values of θ predicted by the unit gradient model are correct, negligible runoff is predicted for I measured at the site.

Rainfall, runoff and soil loss measurements suggest that factors other those measured are contributing to runoff observed in the field. The results of Wood (1983, 1984) indicate that relatively low runoff coefficients ($<26\%$) cause extensive erosion. Compaction, surface sealing and subsurface seepage may be factors influencing runoff and moisture conditions in the field. The high moisture contents observed in the field suggest the water table is perching on a layer with lower conductivity, which is consistent with Dunne runoff. However, the measured infiltrabilities suggest Hortonian runoff and the results of the thesis are not conclusive with respect the mechanism of runoff generation.

CONCLUDING REMARKS

This research was designed to investigate the processes by which runoff is generated on a Whatcom soil on an upland site in the Lower Fraser Valley. The objectives were to summarize water erosion measurements, to measure soil hydraulic properties and to determine the mechanism of runoff generation.

Water erosion occurs over most of the field in winter. Soil loss is dominated by rill erosion and erosion rates are greatest from November to January. Runoff coefficients are relatively low ($<26\%$), but erosion rates are considerable, ≈ 35 t ha^{-1}yr^{-1}.

For efficient erosion control and land management practices, an understanding of runoff generation is required. Soil hydraulic properties relative to the rainfall intensity determine the proportion of water which will runoff. Measurements of soil-water diffusivities were made using a low tension absorption technique (Clothier and White, 1981). The sorptivity tube device provides a simple method for obtaining S, λ^* and K_{-2}. Measured values of i and x^* depend on $t^{1/2}$ as expected from the constant-concentration absorption theory. Constant-concentration infiltration theory is used to determine the soil-water diffusivity. Measured $D(\theta)$ functions for the field display high variability in a and b especially for the lower horizons. The Van Genuchten $\theta(h)$ expression provides a good fit to the water retention data. $D(\theta)$ functions calculated from the soil-water retention curves and K_{-2} following Van Genuchten (1980) are at least 1–2 orders of magnitude greater than the measured functions. Hysteresis effects may explain 1 order of magnitude increase in $D(\theta)$, but the predictions are poor without matching at $D(\theta_s)$.

The measured hydraulic properties are used to predict infiltration, runoff and drainage. Constant-flux infiltration theory is used to model soil moisture profiles over time for various rainfall events. High field moisture contents necessitate the inclusion of gravity effects during infiltration. The rainfall, runoff and soil loss measurements at the Mahal farm indicate that rainfall intensities < 10 mm h^{-1} cause considerable runoff and erosion. For rainfall intensities known to cause runoff and erosion, runoff is not predicted for most A_p horizon cores. Infiltration may be restricted at some sites by the lower horizon, especially at high antecedent moisture contents, but runoff is not predicted at many sites. A rapid decrease in θ between rainfall events is predicted by the unit gradient model but θ measured at the Mahal farm suggests limited drainage between rainfall events.

Rainfall, runoff and soil loss measurements suggest that factors other than those measured are contributing to the runoff observed in the field. Compaction, surface sealing and subsurface seepage may be factors influencing runoff and moisture conditions in the field. The high moisture contents observed in the field suggest the water table is perching on a layer of lower conductivity which is consistent with Dunne runoff. However, the measured infiltrabilities suggest Hortonian runoff and the results of the thesis are not conclusive with respect to the mechanism of runoff generation.

Bibliography

[1] Aris, R., and N.R. Amundson. 1973. Mathematical Methods in Chemical Engineering. Volume 2. First Order Partial Differential Equations with Applications. Prentice-Hall. New Jersey.

[2] Atmospheric Environment Service (AES). 1987. Abbotsford Airport Climatic Data. Environment Canada.

[3] Baver, L.D. 1956. Soil Physics. John Wiley and Sons, Inc., New York. 489 pp.

[4] Bear, J. 1972. Dynamics of fluids in porous media, Elsevier, NY. 764pp.

[5] Bender, J. 1987. Large Farm Equipment and Soil Erosion. J. Soil and Water Cons. 42: 169-170.

[6] Blake, G.R. 1965. Bulk Density. *In* C.A. Black (ed.) Methods of Soil Analysis Part 1. Physical and Mineralogical Properties, Including Statistics of Measurement and Sampling. Amer. Soc. of Agronomy, Wisconsin. 374-390.

[7] Bolline, A. 1980. Splash Measurements in the Field. *In* M. DeBoodt and D. Gabriels (eds.) Assessment of Erosion. John Wiley and Sons, Toronto. 441-453.

[8] Bolline, A. 1978. Study of the Importance of Splash and Wash on Cultivated Loamy Sands of Hesbaye (Belgium). Earth Surface Processes and Landforms. 3: 71-84.

[9] Bouma, J. 1984. Soil Variabilitiy and Soil Survey. *In* D.R. Nielsen and J. Bouma (eds.) Soil Spatial Variability. 130-145.

[10] Brown, S.J. and F. Morin. 1985. Some Effects of Erosion on Soil Fertility. unpublished report, Dept. of Soil Sci., Univ. of British Columbia. 34 pp.

[11] Brutsaert, W. 1979. Universal Constants for Scaling the Exponential Soil Water Diffusivity? Water Resour. Res. 15(2): 481-483.

[12] Cassel, D.K. 1983. Spatial and Temporal Variability of Soil Physical Properties Following Tillage of Norfolk Loamy Soil. Soil Sci. Soc. Am. J. 47(2): 196-201.

[13] Childs, E.C., and N. Collis-George. 1950. The permeability of porous materials. Proc. Roy. Soc. A201, 392-405.

[14] Clothier, B.E. and I. White. 1981. Measurement of Sorptivity and Soil Water Diffusivity in the Field. Soil Sci. Soc. Amer. J. 45: 241-245.

[15] Crudge, S. 1987. Quantification of Rill Erosion Using Field Measurements and Remote Sensing Techniques. M.Sc. thesis, Dept. of Soil Sci., U.B.C. 154pp.

[16] Davidson, D.T. 1965. Penetrometer Measurements. *In* C.A. Black (ed.) Methods of Soil Analysis Part 1. Physical and Mineralogical Properties, Including Statistics of Measurement and Sampling. Amer. Soc. of Agronomy, Wisconsin. 472-484.

[17] De Ploey, J. 1969. L'erosion pluviale : experiences a l'aide de sables traceurs et bilans morphogenetiques. Acta Geographica Lovaniensia 7: 1-28. cited *in* Bolline 1980.

[18] Dixon, R.M. and D.R. Linden. 1977. Soil Air Pressure and Water Infiltration Under Border Irrigation. Soil Sci. Soc. Am. Proc. 36: 948-953.

[19] Elrick, D.E. and D.H. Bowman. 1964. Note on an Improved Apparatus for Soil Moisture Flow Measurements. Soil Sci. Soc. Proc. 28: 450-453.

[20] Elwell, H.A., and M.A. Stocking. 1976. Vegetal Cover to Estimate Soil Erosion Hazards in Rhodesia. Geoderma. 15:61-70.

[21] Freeze, R.A. and J.A. Cherry. 1979. Groundwater. Prentice-Hall, New Jersey. 604pp.

[22] Gardner, W.R. 1959. Solutions of the Flow Equation for the Drying of Soils and Other Porous Media. Soil Sci. Soc. Am. Proc. 23: 183-187.

[23] Harrop, G. 1987. A Study of the Usefulness of the Gupta-Larson Model in Predicting the Moisture Characteristics of Selected B.C. Soils. B.Sc. thesis, Dept. of Soil Sci., U.B.C. 44pp.

[24] Hillel, D. 1980. Fundamentals of Soil Physics. Academic Press, Toronto. 413pp.

[25] Hillel, D. and W.R. Gardner. 1969. Steady Infiltration into Crust-Topped Profiles. Soil Sci. 108: 137-142.

[26] Hoogmoed, W.B. and L. Stroosnijder. 1984. Crust Formation on Sandy Soils in the Sahel. I. Rainfall and Infiltration. Soil and Tillage Res. 4: 5-23.

[27] Hussein, M.H. and J.M. Laflen. 1982. Effects of Crop Canopy and Residue on Rill and Interril Soil Erosion. Trans. Am. Soc. Agric. Eng. 25: 1310-1315.

[28] Lax, P.D. 1972. The Formation and Decay of Shock Waves. Am. Math Monthly 79: 227-241.

[29] Lindstrom, M.J., and W.B. Voorhees. 1980. Planting Wheel Traffic Effects on Interrow Runoff and Infiltration. Soil Sci. Soc. Am. J. 44(1): 84-89.

[30] Luttmerding, H.A. 1980. Soils of the Langley-Vancouver Map Area, Vol. 1. Soil Map Mosaics and Legend, Lower Fraser Valley (scale 1:25,000). Report No. 15 of the British Columbia Soil Survey, RAB Bulletin 18. British Columbia Ministry of Environment, Kelowna British Columbia.

[31] Luttmerding, H.A. 1981. Soils of the Langley-Vancouver Map Area, Vol. 3. Description of the Soils. Report No. 15 of the British Columbia Soil Survey, RAB Bulletin 18. British Columbia Ministry of Environment, Kelowna British Columbia. 197-199.

[32] McCool, K.D., M.G. Dossett and S.J. Yecha. 1981. A Portable Rill Meter for Field Measurement of Soil Loss. *In* Erosion and Sediment Transport Measurement Symposium. IAHS-AISH Publication No. 133: 479-484.

[33] McIntrye, D.S. 1958. Permeability Measurements of Soil Crusts formed by Raindrop Impact. Soil Sci. 85: 185-189.

[34] Martin, L. 1979. Accelerated Soil Erosion from Tractor Wheelings: A Case Study in Mid-Bedfordshire England, *In* Proc. of Sem. on Agricultural Soil Erosion in Temperate Non Mediterranean Climate. Universite Louis Pasteur - Institut National de la Recherche Agronomique, Strasbourg. 157-161.

[35] Meyer, L.D. 1985. Interrill Erosion Rates and Sediment Characteristics *In* S.A. El-Swaify, W.C. Moldenhauer and A. Lo (eds.) Soil Erosion and Conservation. Soil Cons. Soc. Amer., Iowa. 167-177.

[36] Miller, R.D. and E. Bresler. 1977. A Quick Method for Estimating Soil-Water Diffusivity Functions. Soil Sci. Soc. Am. Proc. 41:1021-1022.

[37] Morin, J., and Y. Benyamini. 1977. Rainfall Infiltration into Bare Soils. Water Resources Res. 13: 813-817.

[38] Morin, J., Y. Benyamini and A. Michaeli. 1981. The Effect of Raindrop Impact on the Dynamics of Soil Surface Crusting and Water Movement in the Profile. J. of Hydrol. 52: 321-335.

[39] Mualem, Y. 1976. A New Model for Predicting the Hydraulic Conductivity of Unsaturated Porous Media. Water Resour. Res. 12(3): 513-522.

[40] Norusis, M.J. 1986. SPSS/PC+ for the IBM PC/XT/AT. SPSS Inc., Chicago.

[41] Novak, M.D. 1985. Soil Loss and Time to Equilibrium for Rill and Channel Erosion. Trans. Am. Soc. Agric. Eng. 28(6): 1790-1793.

[42] Philip, J.R. 1973. On Solving the Unsaturated Flow Equation: 1. The Flux Concentration Relation. Soil Sci. 116(5): 328-335.

[43] Philip, J.R. 1969. Theory of Infiltration. Advance. Hydrosci. 5: 215-290.

[44] Philip, J.R. 1957. The Theory of Infiltration: 4. Sorptivity and Algebraic Infiltration Equations. Soil Sci. 84:257-264.

[45] Philip, J.R. and J.H. Knight. 1974. On Solving the Unsaturated Flow Equation: 3. New Quasi-Analytical Technique. Soil Sci. 117(1): 1-13.

[46] Poulovassilis, A. 1970. The Effect of the Entrapped Air on the Hysteresis Curves of a Porous Body and its Hydraulic Conductivity. Soil Sci. 109(3): 154-162.

[47] Reichardt, K.D., D.R. Nielsen and J.W. Biggar. 1972. Scaling of Horizontal Infiltration in Homogeneous Soils. Soil Sci. Soc. Am. Proc. 36: 241-245.

[48] Richards, L.A. 1965. Physical Condition of Water in Soil. *In* C.A. Black (ed.) Methods of Soil Analysis Part 1. Physical and Mineralogical Properties, Including Statistics of Measurement and Sampling. Amer. Soc. of Agronomy, Wisconsin. 128-151.

[49] Scotter, D.R. and B.E. Clothier. 1983. A Transient Method for Measuring Soil Water Diffusivity and Unsaturated Hydraulic Conductivity. Soil Sci. Soc. Am. J. 47:1068-1072.

[50] Sisson, J.B., A.H. Ferguson and M. Th. Van Genuchten 1980. Simple Method for Predicting Drainage From Field Plots. Soil Sci. Soc. Am. J. 44: 1147-1152.

[51] Sparrow, H.O. 1984. Soil at Risk: Canada's Eroding Future. Standing Committee on Agriculture, Fisheries, and Forestry, to the Senate of Canada. 129pp.

[52] Staple, W.J. 1965. Moisture Tension, Diffusivity and Conductivity of a Loam Soil During Wetting and Drying. Can. J. of Soil Sci. 45: 76-86.

[53] Suhr, J.L., A.R. Jarrett, and J.R. Hoover. 1984. The Effect of Soil Air Entrapment on Erosion. Trans. Am. Soc. Agric. Eng. 93-98.

[54] Talsma, T. 1969. In Situ Measurement of Sorptivity. Aust. J. Soil Res. 7: 269-276.

[55] Topp, G.C. 1971. Soil Water Hysteresis in Silt Loam and Clay Loam Soils. Water Resour. Res. 7(4): 914-920.

[56] Troeh, F.R., J.A. Hobbs and R.L. Donahue. 1980. Soil and Water Conservation for Productivity and Environmental Protection. Prentice-Hall, Toronto. 83-114, 233-319.

[57] Van Genuchten, M. Th. 1980. A Closed-Form Equation For Predicting the Hydraulic Conductivity of Unsaturated Soils. Soil Sci. Soc. Am. J. 44: 892-898.

[58] Warrick, A.W. and D.R. Nielsen. 1980. Spatial Variability of Soil Physical Properties in the field. *In* D. Hillel (ed.) Applications of Soil Physics. Academic Press, Toronto. 319-355.

[59] Watson, K.W. and R.J. Luxmoore. 1986. Estimating Macroporosity in a Forest Watershed by Use of a Tension Infiltrometer. Soil Sci. Soc. Am. J. 50:578-582.

[60] White, I. 1979. Measured and Approximate Flux-Concentration Relations for Absorption of Water by Soil. Soil Sci. Soc. Am. J. 43: 1074-1080.

[61] White, I., D.E. Smiles and K.M. Perroux. 1979. Absorption of Water by Soil: The Constant-Flux Boundary Condition. Soil Sci. Soc. Am. J. 43: 659-664.

[62] Wood, C. 1983. Soil Erosion Control with Interceptor Drains: Project Specifications and Preliminary Data, B.C. Ministry of Agriculture and Food D.A.T.E. Project #106. 2pp.

[63] Wood, C. 1984. Annual Report. D.A.T.E. Project #106: Water Runoff and Soil Erosion Control Demonstration. Summary of Runoff and Erosion September, 1983 - July, 1984. B.C. Ministry of Agriculture and Food. 4pp.

[64] Youngs, E.G. and A.J. Peck. 1964. Moisture Profile Development and Air Compression during Water Uptake by Bounded Porous Bodies: 1. Theoretical Introduction. Soil Sci. 98: 290- 294.

[65] Zachmann, D.W., H.R. Gardner and P.C. DuChateau. 1980. A Mathematical Treatment of the Initial Stages of Drying of a Soil Column. Soil Sci. Soc. Am. J. 44: 235-237.

Appendix A

LIST OF SYMBOLS

α = parameter in Van Genuchten water retention function

β = exponent in exponential $D(\theta)$ function

γ = parameter in exponential $D(\theta)$ function

θ = volumetric moisture content [m^3 m^{-3}]

θ_m = minimum obtainable θ at $z = 0$

θ_n = initial volumetric moisture content

θ_r = residual volumetric moisture content

θ_s = saturated volumetric moisture content

θ_{-2} = θ at -2 cm of water tension

θ_0 = $\theta(0, t)$

θ^* = θ at the wetting-front

Θ = nondimensionalized volumetric moisture content

Θ^* = Θ at the wetting-front

λ = Boltzman similarity variable

λ^* = λ at the wetting-front

ρ = density

ρ_b = bulk density [kg m^{-3}]

ρ_s = particle density [kg m^{-3}]

ρ_w = density of water [kg m^{-3}]

σ = surface tension [kg s^{-1}]

ϕ = parameter in exponential $D(\theta)$ function

$\sum \zeta^2$ = sum of squared residuals

a = parameter in exponential $D(\theta)$ function

$$A \quad = \quad \text{area of absorption soil core}$$

$$\text{ave.} \quad = \quad \text{average}$$

$$b \quad = \quad \text{parameter in exponential } yD(\theta) \text{ function}$$

$$D \quad = \quad \text{hydraulic diffusivity } [\text{m}^2 \text{ s}^{-1}]$$

$$D_n \quad = \quad D(\theta_n)$$

$$f \quad = \quad \text{porosity}$$

$$f_m \quad = \quad \text{mass fraction of mineral soil}$$

$$f_o \quad = \quad \text{mass fraction of organic soil}$$

$$F \quad = \quad \text{flux concentration function}$$

$$g \quad = \quad \text{acceleration due to gravity}$$

$$h \quad = \quad \text{tension}$$

$$H \quad = \quad \text{height of absorption soil core } [\text{m}]$$

$$i \quad = \quad \text{cumulative water inflow } [\text{m}]$$

$$I \quad = \quad \text{rainfall intensity}$$

$$K \quad = \quad \text{hydraulic conductivity } [\text{m s}^{-1}]$$

$$K_s \quad = \quad \text{saturated hydraulic conductivity}$$

$$K_{-2} \quad = \quad K \text{ at an average tension of -2 cm of water tension}$$

$$l \quad = \quad \text{height of hypodermic above mesh}$$

$$m \quad = \quad \text{exponent in Van Genuchten water retention function}$$

$$\text{min} \quad = \quad \text{minimum}$$

$$\text{max} \quad = \quad \text{maximum}$$

$$\text{n} \quad = \quad \text{sample number}$$

$$n \quad = \quad \text{exponent in Van Genuchten water retention function}$$

$$q = \text{flux } [\text{m s}^{-1}]$$

$$Q = \text{volumetric water outflow } [\text{m}^3]$$

$$R = \text{constant-flux; constant rainfall rate}$$

$$r^2 = \text{Pearson's correlation coefficient}$$

$$r_h = \text{inside radius of hypodermic}$$

$$r_p = \text{pore radius}$$

$$\text{REV} = \text{representative elementary volume}$$

$$S = \text{sorptivity}$$

$$\text{SD} = \text{standard deviation}$$

$$\text{skew.} = \text{skewness}$$

$$t = \text{time}$$

$$t_s = \text{storm duration}$$

$$t_d = \text{drainage time}$$

$$t_f = \text{final time}$$

$$t_g = \text{maximum time for gravity effects to be negligible}$$

$$t_i = \text{initial time}$$

$$T = \text{return period}$$

$$x = \text{horizontal distance}$$

$$x^* = \text{depth to the wetting-front } [\text{m}]$$

$$z = \text{height below datum (ground surface)}$$

$$50 = \text{50th percentile value}$$

Appendix B

RAW DATA

Table B.1: A_p horizon site characteristics of infiltration cores.

Sample	ρ_b [kg m^{-3}]	f	Colour	Texture	z [m]
1A	1171	0.53	10YR5/4	coarse silty	0.07
2A	1186	0.53	10YR5/3	coarse silty	0.20
3A	1066	0.58	10YR5/3	fine loamy	0.15
4A	1238	0.51	2.5Y5/4	coarse silty	0.17
5A	1085	0.57	10YR5/4	fine loamy	0.40
6A	1130	0.55	10YR5/4	fine loamy	0.15
7A	1061	0.58	10YR5/3	coarse silty	0.60
8A	1092	0.57	2.5Y4/4	fine loamy	0.50
9-1A	965	0.62	10YR4/4	coarse silty	0.13
9-2A	948	0.62	10YR4/4	fine loamy	0.20
9-3A	998	0.60	10YR4/3	fine loamy	0.55
9-4A	986	0.61	10YR4/3	coarse silty	0.17
9-5A	1006	0.60	10YR5/3	coarse silty	0.20
9-6A	1024	0.59	10YR4/3	fine loamy	0.65
10A	1088	0.57	10YR4/4	fine loamy	0.35
11A	1096	0.56	2.5Y5/4	fine loamy	0.22
12A	1205	0.52	2.5Y5/4	fine loamy	0.30
13A	935	0.63	10YR4/4	coarse silty	0.40
14A	1041	0.59	2.5Y4/4	fine loamy	0.55
15A	1015	0.60	10YR5/4	fine loamy	0.15
16A	989	0.61	10YR5/4	coarse silty	0.32
17A	912	0.64	10YR5/4	coarse silty	0.55

Table B.2: Lower horizon site characteristics of infiltration cores.

Sample	ρ_b [kg m^{-3}]	f	Colour	Texture
1C	1535	0.40	2.5Y7/2	fine silty
2C	1432	0.44	2.5Y7/2	fine silty
3C	1345	0.48	2.5Y6/4	coarse silty
4C	1356	0.47	10YR5/3	fine loamy
5C	1171	0.54	2.5Y6/4	fine loamy
6C	1096	0.57	10YR6/3	coarse silty
7B	1304	0.49	10YR5/4	fine loamy
8B	1121	0.56	10YR4/3	fine loamy
9-1C	1006	0.61	2.5Y5/4	fine loamy
9-2C	1254	0.51	10YR6/3	fine loamy
9-3B	1239	0.52	10YR5/3	fine loamy
9-4C	1085	0.58	10YR4/3	fine loamy
9-5C	1136	0.56	10YR5/3	fine loamy
9-6B	901	0.65	10YR5/4	fine loamy
10C	861	0.66	10YR5/4	fine loamy
11C	1489	0.42	2.5Y6/2	fine silty
12C	1247	0.51	2.5Y6/4	coarse silty
13C	1716	0.33	2.5Y6/4	coarse silty
14B	1083	0.58	2.5Y5/4	coarse loamy
15C	988	0.62	2.5Y6/4	coarse silty
16C	1734	0.33	10YR6/3	sandy
17C	965	0.62	10YR6/3	fine loamy

Table B.3: A_p horizon measured variables for the low tension absorption.

Sample	Apr.'86 θ	θ_{-2}	θ_n	S $[\text{m s}^{-1/2}]$	λ^* $[\text{m s}^{-1/2}]$	K_{-2} $[\text{m s}^{-1}]$
1A	0.39	0.49	0.06	5.65E-04	1.70E-03	4.65E-06
2A	0.40	0.46	0.07	3.90E-04	1.32E-03	1.53E-06
3A	0.39	0.50	0.06	7.47E-04	2.13E-03	9.41E-06
4A	0.31	0.37	0.07	3.38E-04	1.21E-03	1.85E-06
5A	0.43	0.50	0.09	6.94E-04	1.91E-03	2.06E-06
6A	0.44	0.48	0.08	7.35E-04	2.13E-03	4.25E-06
7A	0.39	0.47	0.10	4.03E-04	1.26E-03	5.43E-06
8A	0.47	0.49	0.09	6.39E-04	1.83E-03	2.35E-06
9-1A	0.42	0.51	0.07	8.53E-04	2.00E-03	5.40E-06
9-2A	0.47	0.51	0.09	6.47E-04	1.67E-03	4.25E-06
9-3A	0.39	0.51	0.07	6.55E-04	2.02E-03	9.65E-06
9-4A	0.46	0.51	0.08	7.96E-04	2.55E-03	6.55E-06
9-5A	0.42	0.49	0.07	6.08E-04	1.76E-03	5.95E-06
9-6A	0.41	0.50	0.09	5.67E-04	1.81E-03	4.83E-06
10A	0.40	0.47	0.11	3.83E-04	1.61E-03	2.35E-06
11A	0.37	0.46	0.08	5.59E-04	1.77E-03	6.12E-06
12A	0.39	0.44	0.07	4.84E-04	1.77E-03	2.05E-06
13A	0.42	0.53	0.09	8.94E-04	2.38E-03	1.50E-05
14A	0.45	0.50	0.09	6.36E-04	2.09E-03	4.22E-06
15A	0.40	0.47	0.06	6.96E-04	1.88E-03	6.37E-06
16A	0.44	0.54	0.12	4.96E-04	1.47E-03	1.75E-06
17A	0.43	0.54	0.11	4.78E-04	1.49E-03	5.13E-06

Table B.4: Lower horizon measured variables for the low tension absorption.

Sample	Apr.'86 θ	θ_{-2}	θ_n	S [m s$^{-1/2}$]	λ^* [m s$^{-1/2}$]	K_{-2} [m s^{-1}]
1C	0.38	0.42	0.09	2.53E-04	8.26E-04	1.38E-06
2C	0.34	0.46	0.13	1.55E-04	5.98E-04	3.00E-07
3C	0.36	0.46	0.12	3.10E-04	1.12E-03	4.83E-07
4C	0.39	0.44	0.13	2.12E-04	8.51E-04	2.50E-07
5C	0.39	0.48	0.12	7.58E-04	2.42E-03	4.32E-06
6C	0.39	0.49	0.10	8.23E-04	2.27E-03	9.72E-06
7B	0.41	0.44	0.12	3.50E-04	1.46E-03	7.67E-07
8B	0.43	0.44	0.17	1.89E-04	1.02E-03	4.33E-07
9-1C	0.41	0.44	0.07	8.92E-04	2.58E-03	5.77E-06
9-2C	0.40	0.42	0.02	5.73E-04	1.51E-03	1.61E-05
9-3B	0.39	0.39	0.03	3.61E-04	1.22E-03	7.67E-07
9-4C	0.44	0.46	0.05	5.37E-04	1.80E-03	2.48E-06
9-5C	0.42	0.42	0.06	1.95E-04	1.48E-03	4.83E-07
9-6B	0.46	0.48	0.05	8.53E-04	2.36E-03	5.62E-06
10C	0.41	0.54	0.11	8.10E-04	2.93E-03	1.09E-05
11C	0.40	0.41	0.14	1.11E-04	3.14E-04	3.50E-07
12C	0.42	0.46	0.12	4.49E-04	1.50E-03	1.58E-06
13C	0.33	0.37	0.08	1.37E-04	7.86E-04	3.33E-07
14B	0.50	0.50	0.15	6.70E-04	2.20E-03	2.88E-06
15C	0.47	0.53	0.13	5.66E-04	1.57E-03	3.38E-06
16C	0.28	0.31	0.04	6.47E-04	2.79E-03	6.30E-06
17C	0.48	0.52	0.12	1.02E-03	2.81E-03	2.08E-05

Table B.5: A_p horizon low tension absorption variables.

Sample	D_n [m²s⁻¹]	β	a	b [m²s⁻¹]
1A	1.53E-08	5.85	13.6	6.77E-09
2A	1.12E-08	5.59	14.3	4.10E-09
3A	1.46E-08	6.50	14.8	6.03E-09
4A	2.91E-12	15.00	50.0	8.80E-14
5A	5.82E-10	10.12	24.7	6.31E-11
6A	2.31E-09	8.76	21.9	4.01E-10
7A	7.39E-10	8.87	24.0	6.71E-11
8A	9.01E-10	9.51	23.8	1.06E-10
9-1A	1.08E-19	34.02	77.3	4.80E-22
9-2A	1.64E-11	13.82	32.9	8.47E-13
9-3A	3.66E-08	5.12	11.6	1.62E-08
9-4A	6.83E-08	4.90	11.4	2.75E-08
9-5A	5.50E-09	7.25	17.3	1.64E-09
9-6A	2.11E-08	5.60	13.7	6.16E-09
10A	5.02E-08	3.93	10.9	1.51E-08
11A	4.20E-09	7.59	20.0	8.51E-10
12A	2.78E-08	5.14	13.9	1.05E-08
13A	3.54E-09	8.51	19.3	6.20E-10
14A	3.78E-08	5.18	12.6	1.21E-08
15A	1.18E-10	11.89	29.0	2.06E-11
16A	6.40E-09	6.61	15.7	9.69E-10
17A	1.76E-08	5.29	12.3	4.55E-09

Table B.6: Lower horizon low tension absorption variables.

Sample	D_n $[m^2s^{-1}]$	β	a	b $[m^2s^{-1}]$
1C	1.02E-12	15.30	46.4	1.57E-14
2C	1.47E-09	6.18	18.7	1.29E-10
3C	2.92E-09	6.92	20.3	2.54E-10
4C	2.14E-09	6.61	21.3	1.34E-10
5C	2.04E-09	9.21	25.6	9.48E-11
6C	1.06E-11	14.97	38.4	2.27E-13
7B	1.65E-08	5.33	16.7	1.08E-15
8B	1.61E-08	4.30	15.9	2.29E-15
9-1C	4.71E-12	16.11	43.5	2.24E-13 11
9-2C	2.57E-14	20.53	51.3	9.21E-15
9-3B	2.76E-09	7.20	20.0	5.93E-18
9-4C	3.31E-08	4.94	12.0	1.82E-08
9-5C	1.55E-07	0.61	16.8	1.40E-07
9-6B	5.70E-09	7.92	18.4	6.04E-17
10C	1.95E-07	3.67	85.3	7.61E-08
11C	3.16E-49	100.00	370.0	9.57E-72
12C	5.28E-10	9.68	28.5	1.73E-11
13C	1.80E-08	3.19	11.0	7.47E-09
14B	1.57E-09	9.30	26.6	5.32E-21
15C	9.95E-11	11.68	29.2	2.24E-12
16C	4.37E-09	8.65	32.0	1.21E-09
17C	2.66E-08	11.88	29.7	7.53E-10

Table B.7: A_p horizon water retention variables.

Sample	θ_s	θ_r	α	n	$\sum \zeta^2$	ρ_b [kg m^3]
1A	0.47	0.00	3.45E-03	1.303	7.39E-04	1092
2A	0.47	0.00	2.45E-03	1.313	5.94E-04	1157
3A	0.51	0.03	2.69E-03	1.352	7.00E-04	1092
4A	0.47	0.00	1.96E-03	1.299	1.84E-04	1279
5A	0.51	0.10	2.15E-03	1.585	3.25E-04	976
6A	0.52	0.09	3.31E-03	1.482	9.84E-04	1100
7A	0.48	0.03	2.88E-03	1.364	3.32E-04	1048
8A	0.51	0.02	4.12E-03	1.315	2.61E-04	1007
9-1A	0.52	0.08	3.79E-03	1.413	4.39E-04	840
9-2A	0.55	0.00	2.27E-03	1.268	1.22E-03	971
9-3A	0.54	0.00	2.94E-03	1.303	4.18E-04	991
9-4A	0.56	0.04	3.51E-03	1.399	3.64E-04	919
9-5A	0.54	0.00	3.38E-03	1.288	2.10E-04	1013
9-6A	0.54	0.00	4.62E-03	1.251	4.76E-04	977
10A	0.56	0.10	2.97E-03	1.505	9.57E-05	1112
11A	0.49	0.08	3.39E-03	1.411	9.99E-04	1095
12A	0.48	0.03	3.29E-03	1.352	1.04E-03	1174
13A	0.55	0.12	3.45E-03	1.451	1.29E-03	858
14A	0.56	0.03	2.99E-03	1.342	2.46E-04	1011
15A	0.51	0.08	3.43E-03	1.432	4.79E-04	942
16A	0.63	0.01	2.78E-03	1.330	1.59E-03	1020
17A	0.54	0.06	2.43E-03	1.473	1.22E-03	837

Table B.8: Lower horizon water retention variables.

Sample	θ_s	θ_r	α	n	$\sum \zeta^2$	ρ_b [kg m^3]
1C	0.61	0.00	2.02E-03	1.207	1.48E-03	1277
2C	0.46	0.00	5.09E-04	1.273	7.92E-04	1543
3C	0.59	0.04	4.43E-03	1.224	3.82E-04	1003
4C	0.48	0.00	9.82E-04	1.228	6.43E-04	1443
5C	0.53	0.00	1.02E-02	1.201	3.16E-04	1139
6C	0.51	0.00	2.71E-03	1.248	1.51E-03	1377
7B	0.52	0.00	2.44E-03	1.255	5.52E-04	1236
8B	0.49	0.00	8.72E-04	1.303	6.01E-04	1280
9-1C	0.56	0.11	6.51E-03	1.356	4.69E-04	1107
9-2C	0.58	0.00	2.35E-03	1.255	2.07E-04	1125
9-3B	0.61	0.10	2.80E-03	1.319	6.11E-04	946
9-4C	0.57	0.00	1.60E-03	1.242	2.00E-03	995
9-5C	0.52	0.00	2.17E-03	1.221	2.13E-04	1279
9-6B	0.65	0.21	4.59E-03	1.578	1.71E-03	873
10C	0.52	0.16	2.68E-03	1.646	3.80E-04	1076
11C	0.41	0.00	2.59E-04	1.295	4.03E-04	1510
12C	0.42	0.00	4.18E-04	1.450	9.52E-04	1570
13C	0.38	0.00	1.18E-03	1.398	4.31E-04	1654
14B	0.52	0.00	3.15E-03	1.307	1.73E-03	1124
15C	0.57	0.00	1.68E-03	1.342	9.44E-04	1218
16C	0.53	0.00	3.61E-03	1.297	8.88E-04	1273
17C	0.46	0.00	4.48E-04	1.524	1.33E-03	1303

Appendix C

CONSTANT-CONCENTRATION ABSORPTION PROGRAM

```
C DIMENSION AND DECLARE THE VARIABLES
      IMPLICIT REAL*8 (A-H,O-Z)
      DIMENSION T(20),W(20),CW(20),XWF(20),TG(20),X(20,20)
      EXTERNAL FN1,FN2,FN4
      LOGICAL LZ
      COMMON BETA,ALPHA
C INPUT PARAMETERS
C (A) GENERAL
      XWFMIN=1.0D-3
      XWFMAX=0.30D0
      THETAS=0.44D0
      THETAN=0.07D0
      THDSN=THETAS-THETAN
      MODE=1
C (B) MODE 1 - THE SORPTIVITY AND LAMBDA OF THE WETTING
C FRONT ARE KNOWN
      IF(MODE.EQ.2) GO TO 1
      S=6.49386D-4
      TLAMWF=2.14424D-3
      WRITE(1,96) S,TLAMWF
```

```
  96 FORMAT(' S, TLAMWF: '2G15.4)
     GO TO 2
C (C) MODE 2 - THE DIFFUSIVITY FUNCTION IS KNOWN
   1 DNM=9.2545D-7
     BETAM=7.091D0
     THNM=0.07
     THSM=0.44
     THDSNM=THSM=THNM
     B=BETAM/THDSNM
     A=DNM/DEXP(B*THNM)
     DN=A*DEXP(B*THETAN)
     BETA=B*THDSN
     GO TO 3
C CALCULATE ALPHA, BETA AND GAMMA AND THEN THE
C DIFFUSIVITY FOR MODE 1
   2 ALPHA=S/(TLAMWF*THDSN)
     BETA=0.D0
     BETAMX=100.D0
     WRITE(1,97) ALPHA,BETA,BETAMX
  97 FORMAT(' ALPHA, BETA, BETAMX: ',3G15.4)
     ERR=1.D-4
     CALL ZERO2(BETA,BETAMX,FN4,ERR,LZ)
     IF(.NOT.LZ) WRITE(1,4)
   4 FORMAT(' ZERO2 CANNOT FIND BETA')
     IF(.NOT.LZ) STOP
```

```
      GAMMA=1.D0/(2.D0*DCADRE(FN2,1.D-12,1.D0,0.D0,1.D-4,ERR))

      DN=GAMM*S**2/THDSN**2

      GO TO 5
C CALCULATE THE SORPTIVITY, LAMBDA AT THE WETTING-FRONT,
C ALPHA AND GAMMA FOR MODE 2
    3 GAMMA=1.D0/(2.D0*DCADRE(FN2,1.D-12,1.D0,0.D0,1.D-4,ERR))

      S=DSQRT(DN*THDSN**2/GAMMA)

      ALPHA=1.D0/(S.D0*GAMMA)

      ALPHA=ALPHA/DCADRE(FN1,1.D-2,1.D0,0.D0,1.D-4,ERR)

      TLAMWF=S/(ALPHA*THDSN)
C CALCULATE THE SURFACE FLUX, CUMULATIVE INFLOW,
C POSITION OF THE WETTING-FRONT, AND THE WATER
C CONTENT PROFILES AT SELECTED TIMES
    5 TMIN=(XWFMIN/TLAMWF)**2

      TMAX=(XWFMAX/TLAMWF)**2

      DT=(TMAX/TMIN)**(1.D0/19.D0)

      DO 6 NT=1,20

      T(NT)=TMIN*DT**(NT-1)

      SQT=DSQRT(T(NT))

      W(NT)=S/(2.D0*SQT)

      WC(NT)=S*SQT

      XWF(NT)=TLAMWF*SQT

      DO 6 NX=1,20

      THBG=1.D0-(NX-1)/20.D0

      TH(NX)=THETAN+THBG*THDSN
```

```
      DUM=2.D0*SN*THDSN*SQT/S
   6 X(NT,NX)=DUM*DCADRE(FN1,THBG,1.D0,0.D0,1.D-4,ERR)
C WRITE OUT RESULTS
      WRITE(1,20)
  20 FORMAT(' 12-2A ')
      WRITE(1,21) THNM,THSM,DNM,BETAM
  21 FORMAT(' THNMEAS, THSMEAS, DNMEAS, BETAMEAS: ',4G13.5)
      WRITE(1,22) A,B
  22 FORMAT('A B: ',2G13.5)
      WRITE(1,7) THETAN,THETAS,DN,BETA
   7 FORMAT(' THETAN, THETAS, DN, BETA: ',4G13.5)
      WRITE(1,8) S,TLAMWF,ALPHA,GAMMA
   8 FORMAT(' S, TLAMWF, ALPHA, GAMMA: ',4G13.5)
      DO 9 NO=1,20
      WRITE(1,10) T(NT),W(NT),CW(NT),XWF(NT)
  10 FORMAT(' T, W, CW, XWF: ',4G13.5)
      WRITE(1,11) (X(NT,NX),NX=1,20)
  11 FORMAT(' X:',10G11.3/4X,10G11.3)
   9 WRITE(1,12) (TH(NX),NX=1,20)
  12 FORMAT(' TH:',10G11.3/4X,10G11.3)
      STOP
      END
C FUNCTION SUBROUTINES
      FUNCTION FN1(X)
      IMPLICIT REAL*8 (A-H,O-Z)
```

```
COMMON BETA,ALPHA

FN1=DEXP(BETA*X)/FLXCNC(X)

RETURN

END

FUNCTION FN2

IMPLICIT REAL*8 (A-H,O-Z)

COMMON BETA,ALPHA

FN2=X*DEXP(BETA*X)/FLXCNC(X)

RETURN

END

FUNCTION FN4(X)

IMPLICIT REAL*8 (A-H,O-Z)

COMMON BETA,ALPHA

EXTERNAL FN1,FN2

BETA=X

FN4=DCADRE(FN2,1.D-12,1.D0,0.D0,1.D-4,ERR)

FN4=FN4/DCADRE(FN1,1.D-2,1.D0,0.D0,1.D-4,ERR)

FN4=ALPHA-FN4

RETURN

END

FUNCTION FLXCNC(X)

IMPLICIT REAL*8 (A-H,O-Z)

COMMON BETA,ALPHA

PI=3.1415926535897932D0

DUM1=DSIN(PI/2.D0*X**(PI/4.D0))
```

```
DUM2=X

FLXCNC=DUM1*(8.D0-BETA)/8.D0+DUM2*BETA/8.D0

IF(BETA.GT.8.D0) FLXCNC=DUM2

RETURN

END
```

Appendix D

VAN GENUCHTEN WATER RETENTION PROGRAM

```
C 3 PARAMETER (THETAS, ALPHA, N) EQUATION WITH NO CONSTRAINTS
      IMPLICIT REAL*8(A-H,O-Z)
      DIMENSION P(3),V(252),IV(63)
      EXTERNAL CALCR
      COMMON X(10),Y(10),RESID
      WRITE(6,40)
   40 FORMAT (' CORE 7C')
C SET INITIAL VALUES; READ IN AND LIST DATA
      RESID=0.D0
      N=10
      M=3
      P(1)=0.003D0
      P(2)=1.2D0
      P(3)=0.55D0
      WRITE(6,60) P(1),P(2),P(3)
   60 FORMAT ('P(1)=',G10.4,'P(2)=',G10.4,'P(3)=',G10.4)
      DELTAR=0.002D0
      WRITE (6,80) N,M
   80 FORMAT (' N=',I3,' M=',I3)
      READ(5,120) (X(I),Y(I),I=,N)
```

```
 120 FORMAT(2D15.9)

     WRITE(6,125)

 125 FORMAT('TENSION THETA')

     WRITE(6,130) (X(I),Y(I),I=1,N)

 130 FORMAT (2(D15.9,3X))
C LEAST SQUARED CURVE FITTING
   5 IV(1)=0.D0

     CALL NL2SNO (N,M,P,CALCR,IV,V,IPARM,RPARM,FPARM)
C WRITE OUT THE RESULTS
     WRITE(6,15) RESID

 150 FORMAT(' THETAR =',G10.4)

     WRITE(6,140) IV(1)

 140 FORMAT(' RETURN CODE=',I2)

     WRITE(6,160) (P(0),I=1,M),V(10)

 160 FORMAT(' SOLUTION:', 1P3G16.8/

   1        ' SUM OF SQUARES/2=', 1PG16.8)
C LOOP TO COVER POSSIBLE RANGE IN RESIDUAL THETA
     RESID=RESID+DELTAR

     IF(RESID.GT.0.200D0)GO TO 190

     GO TO 5

 190 STOP

     END
C SUBROUTINE
     SUBROUTINE CALCR(N,M,P,NF,R,IPARM,RPARM,FRARM)

     IMPLICIT REAL*8(A-H,O-Z)
```

```
      DIMENSION P(M),R(N)
      COMMON X(10),Y(10),RESID
C LIMITS ON VARIABLES
      IF(P(2).LE.1.DO) GO TO 180
      IF(P(1).LT.0.CO) GO TO 180
C RESIDUALS IN R
      DO 100 I=1,N
      DUM=P(1)*X(I)
      DEN=1.DO-1.DO/P(2)
      TM=1.DO-1.DO/P(2)
      TNUM=P(3)-RESID
      R(I)=(RESID+TNUM/DEN**TM)-Y(I)
  100 CONTINUE
      RETURN
  180 NF=0.DO
      RETURN
      END
```

Appendix E

CONSTANT-FLUX INFILTRATION PROGRAM

```
C DIMENSION AND DECLARE VARIABLES
      IMPLICIT REAL*8(A-H,O-Z)
      DIMENSION T(20),W(20),C2(20),XWF(20),TH(20,20),X(20,20)
      EXTERNAL FN1,FN2,FN3
      COMMON DN,BETA,THDSN,THETAN,THO,TKS,XM,R,THDSR,WRTHR
C INPUT PARAMTERS
      TKS=1.3833D-6
      XM-1.DO-1.DO/1.2074DO
      WRTHR=0.DO
      WRTHS=0.42DO
      THDSR=WRTHS-WRTHR
      THETAS=0.42DO
      THETAN=0.37DO
      THDSN=THETAS-THETAN
      THSM=0.42DO
      THNM=0.09DO
      THDSNM-THSM-THNM
      DNM=1.02079D-12
      BETAM=15.302DO
      A=BETAM/THDSNM
```

```
      B=DNM/DEXP(B*THNM)

      DN=B*DEXP(A*THETAN)

      BETA=A*THDSN

      R=1.2D0*TKS
C CALCULATE THE SURFACE FLUX, CUMULATIVE INFLOW,
C POSITION OF THE WETTING-FRONT, AND THE WATER
C CONTENT PROFILES AT SELECTED TIMES
      DUM1=THETAN+1.D-12

      DUM2=THETAN+0.01D0*THDSN

      DO 6 NT=1,20

      THO=THETAN+NT*THDSN/20.DO

      T(NT)=DCADRE(FN2,DUM1,THO,0.DO,1.D-4,ERR)/(R-FN3(THETAN))

      W(NT)=R

      XW(NT)=R*T(NT)

      XWF(NT)=DCADRE(FN1,DUM2,THO,0.DO,1.D-4,ERR)

      DO 6 NX=1,20

      TH(NT,NX)=THO-(NX-1)*(THO-THETAN)/20.DO

    6 X(NT,NX)=DCADRE(FN1,TH(NT,NX),THO,0.DO,1.D-4,ERR)
C WRITE OUT RESULTS
      WRITE(1,3)

   20 FORMAT(' 1C')

      WRITE(1,21) THNM,THSM,DNM,BETAM

   21 FORMAT(' THNMEAS, THSMEAS, DNMEAS, BETAMEAS: ',4G13.5)

      WRITE(1,22) A,B

   22 FORMAT(' A B: ',2G13.5)
```

```
      WRITE(1,7) THETAN,THETAS,DN,BETA
   7 FORMAT(' THETAN, THETAS, DN, BETA: ',4G13.5)
      WRITE(1,23) TKS,XM,WRTHR,WRTHS
  23 FORMAT(' TKS, XM, WRTHR, WRTHS: ',4G13.5)
      DO 9 NT=1,20
      WRITE(1,10) T(NT),W(NT),CS(NT),XWF(NT)
  10 FORMAT( 'T, W, CW, XWF: ',4G13.5)
      WRITE(1,11) (X,(NT,NX),NX=1,20)
  11 FORMAT(' X: ',10G11.3/4X,10G11.3)
   9 WRITE(1,12) (TH(NT,NX),NX=1,20)
  12 FORMAT(' TH: ', 10G11.3/3X,10G11.3)
      STOP
      END
C FUNCTION SUBROUTINES
      FUNCTION FN1(X)
      IMPLICIT REAL*8 (A-H,O-Z)
      COMMON DN,BETA,THDSN,THETAN,THO,TKS,XM,R,THDSR,WRTHR
      DUM=FN3(THETAN)
      FN1=DN*DEXP(BETA*(X-THETAN)/THDSN)/(FLXCNC(X)*(R-DUM)- FN3(X)+DUM)
      RETURN
      END
      FUNCTION FN2(X)
      IMPLICIT REAL*8 (A-H,O-Z)
      COMMON DN,BETA,THDSN,THETAN,THO,TKS,XM,R,THDSR,WRTHR
      DUM=FN3(THETAN)
```

```
DUMA=BETA*(X-THETAN)/THDSN

FN2=(X-THETAN)*DN*DEXP(DUMA)/(FLXCNC(X)*(R-DUM)-FN3(X)+DUM)

RETURN

END

FUNCTION FN3(X)

IMPLICIT REAL*8 (A-H,O-Z)

COMMON DN,BETA,THDSN,THETAN,THO,TKS,XM,R,THDSR,WRTHR

DUM=((X-WRTHR)/THDSR)**0.5D0

FN3=TKS*(DUM)*(1-(1-((X-WRTHR)/THDSR)**(1/XM))**XM)**2)

RETURN

END

FUNCTION FLXCNC(X)

IMPLICIT REAL*8 (A-H,O-Z)

COMMON DN,BETA,THDSN,THETAN,THO,TKS,XM,R,THDSR,WRTHR

PT=3.1415926535897932D0

DUM=(X-THETAN)/(THO-THETAN)

DUM1=DUM**(2.D0-4.D0/PI)

DUM2=DUM

FLXCNC=DUM1*(8.D0-BETA)/8.D0+DUM2*BETA/8.D0

IF(BETA.GT.8.D0) FLXCNC=DUM2

RETURN

END
```

Appendix F

SISSON DRAINAGE PROGRAM

```
C DIMENSION AND DECLARE THE VARIABLE
      IMPLICIT REAL*8 (A-H,O-Z)
      DIMENSION T(20),TH(20)
C INPUT PARAMETERS
      XM=0.3113D0
      TKS-1.5004E-6
      THETAM=0.19D0
      THETAS=0.53D0
      XMAX=0.30D0
      THETAN=0.40D0
C CALCULATE WATER CONTENT PROFILES AT SELECTED TIMES
      DO 6 NTH=1,19
      THBD=1.D0-NTH/20.D0
      THDSN=THETAS-THETAM
      TH(NTH)=THETAN+THBD*(THETAS-THETAN)
      DUMB=(TH(NTH)-THETAM)/THDSN
      DUMC=DUMB**(1.D0/XM)
      DUMD=1.D0-DUMC
      DUME=(1.D0/XM)-1.D0
      DUMF=XM-1.D0
```

```fortran
      DUMG=TKS/THDSN

      DUMH=1.D0-(DUMD**XM)

      DUMI=DUMD**DUMF

      DUMJ=DUMB**DUME

      DUMK=DUMH**2.D0

      DUML=DUMH*DUMI*DUMJ

      DUMM=1.D0/(1.D0*DUMB**0.5)

    6 T(NTH)=XMA/(DUMG*((2.D0*DUMB**0.5D0*DUML)+(DUMM*DUMK)))
C WRITE OUT THE RESULTS
      WRITE(1,20)

   20 FORMAT(' SISSON DRAINAGE MODEL ')

      WRITE(1,21) THETAM

   21 FORMAT(' CORE 13A THETAM=',G13.5)

      WRITE(1,23) XMAX

   23 FORMAT(' XMAX [m]=',G13.5)

      DO 9 NTH=1,19

      WRITE(1,24) TH(NTH)

   24 FORMAT(' TH:',G15.5)

    9 WRITE(1,25) T(NTH)

   25 FORMAT( ' T:',G11.5)

      STOP

      END
```